POWER CONSUMPTION ANALYSIS OF THE POWERTRAIN SYSTEM OF ELECTRIC BUS FOR THE CASE STUDY OF HIGH ALTITUDE ROADWAY

LWIN YAMON PHYO

A THESIS REPORT SUBMITTED IN PARTIAL FULFILLMENT

OF THE REQUIREMENTS FOR THE DEGREE OF

MASTER OF ENGINEERING IN AUTOMOTIVE ENGINEERING

SCHOOL OF ENGINEERING

KING MONGKUT'S INSTITUTE OF TECHNOLOGY LADKRABANG

2023

KMITL-2023-EN-M-037-046

POWER CONSUMPTION ANALYSIS OF THE POWERTRAIN SYSTEM OF ELECTRIC BUS FOR THE CASE STUDY OF HIGH ALTITUDE ROADWAY

LWIN YAMON PHYO

A THESIS REPORT SUBMITTED IN PARTIAL FULFILLMENT

OF THE REQUIREMENTS FOR THE DEGREE OF

MASTER OF ENGINEERING IN AUTOMOTIVE ENGINEERING

SCHOOL OF ENNGINEERING

KING MONGKUT'S INSTITUTE OF TECHNOLOGY LADKRABANG

ACADEMIC YEAR 2023

KMITL-202-EN-M-037-046

THESIS TITLE	Power consumption analysis of the powertrain system of electric bus for the case study of high altitude roadway
STUDENT NAME	Ms. Lwin Yamon Phyo
STUDENT ID	63601192
DEGREE	Master of Engineering
PROGRAM	Automotive Engineering
YEAR	2023
ADVISOR	Assoc. Prof. Dr. Nattawoot Depaiwa
CO-ADVISOR	Prof. Dr. Masaki Yamakita

ABSTRACT

The majority of the world's transportation systems are controlled by combustion vehicles that have a greater impact than the other types of vehicles on air pollution and greenhouse gas emissions. When the electricity power is generated from renewable resources, switching from convectional fuel cars to electric vehicles can reduce greenhouse gas emissions. In the energy transition, electric buses are anticipated to become even more significant. There are many challenges to manage the electric power consumption rate while operating on everyday routes, especially for the case of high altitude roadways. This thesis is mainly dealt with the power consumption analysis of the electric bus's powertrain system on many types of factors and numerous design variables, taking the slope of the roads into consideration. The basic parameters of 12 meter aluminum electric bus are used to prototype in the simulation model. The suitable electric motor and batterypack that are matched with the requirements of that electric bus are also selected. In this thesis, the sizing design calculation for each component is provided. Furthermore, the road test along the Samaedam bus depot and Samutprakan crocodile farm using bus line 142 is performed to get the data of geographic location and elevation of the roadways and the speed profile of the bus. Using these data as the inputs, the simulation model of the whole

system of electric bus's powertrain is built in MATLAB/Simulink environment. Different scenarios and design variables are settled to evaluate the power consumption rate analysis. The results of the simulated tests are compared and shown under various designs for the driving cycles, gear ratios, electric motors, batterypack and regenerative braking portions. The simulated outcomes demonstrate that regenerative braking cause an increase in power consumption when less electrical power is returned to the battery. Moreover, it is noticed that power output stays at its peak condition when the bus crosses on the RAMA IX bridge which is the highest altitude along the whole route.

Keywords: Power consumption rate, Altitude, Speed profile, Regenerative braking, MATLAB/Simulink

ACKNOWLEDGEMENT

Firstly, I am grateful to TAIST-Tokyo Tech committee for choosing as a full scholarship recipient and allowed me to study Master of Automotive Engineering at King Mongkut's Institute of Technology Ladkrabang.

I would like to express my deep and sincere gratitude to my research main advisor, Assoc. Prof. Dr. Nattawoot Depaiwa from King Mongkut's Institute of Technology Ladkrabang for giving me the opportunity to so research and providing invaluable guidance throughout this research.

I wish to extend sincere thanks to Dr- Ing Manob Masomtob from National Science and Technology Development Agency, Thailand who helped and gave me a lot of support throughout my research period. His experiences and skills guided me to get encouragement and his comprehensive advice and instructions lead me to improve my work.

I also would like to thank Prof. Dr. Masaki Yamakita from Tokyo Institute of Technology, Japan for his kindness and advice until this work came to existence. I offer my sincere appreciation to Dr. Burin Kerdsup from National Science and Technology Development Agency, Thailand for his kind endless help.

My completion of this project could not have been accomplished without the support of my seniors, Mr. Pera Tanateerapong and Ms. Swe Zin Win, who shared and guided me the work to carry out this research through the academic year. Also, I express my thanks to my friend, Hsu Myat Naing for sharing the useful information related to this work.

I would also like to express thanks to all the international friends from A2TE14 batch for their useful help and all those who were directly or indirectly involved in the successful completion of this research work. I would like to express my gratitude to National Science and Technology Development Agency (NSTDA), Thailand for providing me scholarship during these years.

Last but not least, my heart-felt and sincere gratitude goes to my parents who have nurtured a love of learning in me and allowed me to study in Thailand for making education accessible.

Lwin Yamon Phyo

TABLE OF CONTENTS

Chapter **Page**

LIST OF TABLES

Table **Page**

LIST OF FIGURES

Figure **Page**

LIST OF SYMBOLS

F_{tr}	Traction force of the vehicle
F_a	Inertial resistance
F_{aero}	Aerodynamic resistance
F_r	Rolling resistance
F_{grade}	Grade resistance
m_v	Mass of the vehicle
g	Gravitational acceleration, 9.81 ms^{-2}
ρ	Air density, 1.23 kgm^{-3}
c_d	Drag coefficient
c_r	Rolling resistance coefficient
A	Frontal area
θ	Road grade in degree
P_e	Rated motor power
P_i	Peak motor power
v_{max}	Maximum velocity of the vehicle
v_w	Average velocity of the vehicle
η	Efficiency
r_w	Wheel radius of the vehicle
P_{wheel}	Power demand of the vehicle
E_{Joule}	Energy consumption in Joule

E_{kWh}	Energy consumption in kWh
s_{total}	Total distance travelled
i	Gear ratio
T_{m_peak}	Peak motor torque
P_b	Power output of the batterypack
P_m	Power output of the motor
ω_m	Angular speed of the motor
V_b	Nominal voltage of the batterypack
V_c	Voltage of battery cell
V_{out}	Output voltage of the batterypack
R_{int}	Internal resistance of the battery cell
R_{ch}	Internal resistance, Charged
R_{dis}	Internal resistance, Discharged
C_b	Total capacity of the batterypack
C_c	Capacity of the battery cell
OCV	Open circuit voltage
I_{out}	Output current of the batterypack
N_{series}	Number of battery cells, connected in series
$N_{parallel}$	Number of battery cells, connected in parallel
SOC	Stage of charge
Q	Maximum capacity of the battery

LIST OF ABBREVIATIONS

EV	Electric Vehicle
EM	Electric Motor
ICE	Internal Combustion Engine
DC	Direct Current
AC	Alternative Current
PMM	Permanent Magnet Motor
IM	Induction Motor
DCM	Direct Current Motor
SRM	Switch Reluctance Motor
PMDCM	Permanent Magnet Direct Current Motor
PMSM	Permanent Magnet Synchronous Motor
PMBLDCM	Permanent Magnet Brushless DC motor
PM-HSM	Permanent Magnet Hybrid Excitation Motor
PI	Proportional and Integral
MPI	Moving Percentage
BPI	Braking Percentage
NEDC	New European Driving Cycle
WLTC	World Harmonized Light Vehicles Test Procedures
RB	Regenerative Braking
NF	Normal Braking Force
RF	Regenerative Braking Force
NT	Net Motor Torque
RMT	Negative Motor Torque

CHAPTER 1

INTRODUCTION

1.1 Research background

Nowadays, most people rely on their personal vehicles as more convenient mobility as a consequence of the growth in economics, the rapid expansion of population and suburbanization and the closure of certain public transportation systems [1] . Air pollutions and emissions become one of the effects of the sudden increase of different types of vehicles, which had negative effects on both environment and human health.

According to the WHO statement, around 7 million people die each year as a result of breathing uncleaned air which affects 90% of the world's population [2]. Air pollution, emissions and energy issues related to transportation are serious difficulties throughout the world. It is impossible to forgo transportation demands for environmental quality and public health. The Center for Transportation, Environment and Community Health (CTECH) conducts research and finds the new ways to facilitate the mobility system for people and to be sustainable environment, enhancing the public health [3].

Transportation system all over the world are mostly governed by combustion vehicles. These vehicles have more significant influence on air pollution and greenhouse gas emission than other types of vehicles [4]. Buses are one of the most significant public transport systems in many cities that is essential for the daily life of most citizens. In present days, it can be seen that diesel and compressed natural gas (CNG) have been taking a place in bus transportation system. The greenhouse gas emission and local air pollution, like nitrogen dioxide (NO_2) , carbon monoxide (CO), carbon dioxide (CO_2), ozone (O_3) and particulate matter (PM), can be affected in a high extent because of the excessive consumption of fossil fuel. Advanced development in the sector of various power sources needs to modify the public transportation systems for better environment. Shutting down the usage of convectional fuel vehicles for electric vehicles can give rise to minimize the greenhouse gas emissions when the electricity is induced by renewable resources [5]. The importance of electric buses in

the energy transition is expected to grow more. The UN and many governments are attempting to attain net zero emissions by 2050 in order to combat climate change [6].

There are several advantages that people can get support from the usage of electric buses. Electric buses do not produce the same number of emissions as less environmentally friendly buses since they don't consume any fossil fuels. Fast charging electric buses keep the air the environment cleaner and fresher by preventing air pollution. Also, buses powered by combustion and diesel engines tend to vibrate, although electric buses don't emit any noise. So, they can help to reduce noise pollution for the surrounding. Even though installing a large number of charging infrastructure and initial expenses of electric fleet are cost a lot, these expenditures can be mitigated over time by the reduced fuel and maintenance costs, and also, they can provide longer lifespan of electric buses. Hence, it can say that electric buses will cost more initially, but after a long time, they will end up being far less expensive. It is so crucial to encourage the use of more electric buses to be more environmentally friendly, in addition to significantly save in finance.

1.2 Statement of the problem

According to other studies, in Asian countries, although many manufactures are struggling to change the trend into producing electric buses, they are still lacked to consider some important factors such as the altitude, temperature, and other environmental conditions. When developing the electric bus, most manufacturers chose the standard flat route. High- altitude roadways need to be considered in some circumstances for practical reasons. Because standard driving cycles, such as NEDC, WLPT, and others, are meant to reflect the normal driving circumstances at sea level, and acceleration and deceleration patterns are standardized to test only for normal roads, they cannot be used to construct high altitudes. Furthermore, because of the lower air density, high altitude roadways can dramatically alter vehicle performance; as a result, employing typical driving cycles built for sea level circumstances may not effectively replicate driving conditions at high elevations. To account for high- altitude circumstances, unique driving cycles should be designed as well as an evaluation of

electricity usage. Besides, the cost of electricity will be increased since electricity consumption will go up. In addition, batterypack is the heart of the electric bus system because it is powered by electricity and the majority of storing the electricity is the batterypack where all electrical components are supplied from that. Buses will be necessary larger batteries to operate on the whole bus route. Energy system will be needed to adjust according to the area in which the bus operates. Currently, electric bus manufacturers are facing with the difficulties to control the high power demand and to reduce the consumption of the power. Accordingly, when the manufacturers build the electric buses, they need to consider a variety of statements about the power system.

1.3 Objectives

The main aim of this thesis is to analyze the power consumption rate of powertrain system for electric bus in the case of considering for the high altitude roadways. In order to achieve this main aim, this thesis is composed of the following sub- objectives:

- To build the simulation model of the powertrain system in MATLAB/ Simulink environment.
- To analyze the comparative performance of the powertrain system based on multiple scenarios and various design variables of each component.
- To compare the rate of power consumption when the different levels of regenerative braking is applied.

1.4 Scope of works

First and foremost, the parameters and specifications of the electric bus's powertrain components are determined depending on the sizing of the requirements of the selected electric bus. After selecting the suitable components, the simulation model of the powertrain system is built in MATLAB/ Simulink environment. It consists of a discrete number of sub- models and blocks. To get the input data for the model,

the road test with the bus line number 142 is performed on the route of Samaedam bus depot and Samut Prakan crocodile farm, including the RAMA IX bridge.

The driving cycle profiles are created with the elevation profile of the RAMA IX bridge based on many different scenarios, constant speed, speed reduction , and traffic conditions, to estimate the power demand and its consumption of the electric bus while operating the bus on that bridge. Moreover, the results of the simulation model are validated with the practical result of the electric bus and the result of commercial software. After validation, the real speed profiles collected on the whole route are simulated in the model and evaluated the performance of the whole powertrain system.

Furthermore, the power consumption rate is compared under different design variables of each component in powertrain. Two different gear ratios, 2.5 and 7, are chosen according to the design of gear ratios to analyze the performance of the electric bus. Then, the performance of two electric motors, switch- reluctance permanent magnet and asynchronous traction motor, with varying motor torque and power is compared. As the last, it focuses on the investigation of the electric bus batterypack's performance characteristics while employing two Li-ion battery types, LFP and NMC. In addition, three levels of regenerative braking are set to compare the power consumption rate on each battery type.

CHAPTER 2

LITERATURE REVIEW

2.1 Electric buses in Thailand

During these years, Thailand is now experiencing growth in the sectors of economy, tourism, and transportation, which causes the problems with increasing air pollution brought on by a variety of sources, including the emissions of internal combustion engines used in many applications [7]. In big cities, traffic congestion becomes worse, so emission of carbon dioxide worsens. The bus transportation system plays a key part of passenger public transportation in various sectors such as universities, shopping malls, government offices, the Provincial Electricity Authority in most cities of Thailand.

Government of Thailand has already submitted a plan to take over the convectional buses with hybrid or electric bus or fuel- cell bus to shorten the air pollution in metropolitan districts. All relevant policies and rules have been announced to Thai local car manufacturers for annual increase in production quantity. Most of the largest bus operators in Thailand are also trying for electric bus for the renewal of bus transportation system.

The Bangkok Mass Transit Authority (BMTA) implemented a strategy to encourage alternative clean technology by purchasing CNG buses and electric buses[8], [9]. According to the BMTA, assuming the plans to engage commercial operators is not postponed, new electric buses would probably start running in Bangkok in the early months of 2023 [10]. The demand of Bangkok bus commuters increased between 864,005- 1,062,947 person for a round per day from 2014- 2019. In Bangkok Metropolitan, the cumulative registration for all buses (16, 209 buses) in 2021 includes, 2,891 diesel buses, 6,630 CNG buses, and 119 battery electric buses, with year- over-year increases of -4.2 % percent, -7.5 percent, and 99.2 percent, respectively. The Ministry of Transport (MOT) has set the goals for the BMTA to replace 2,511 buses, Public- Private Partnership (PPP) operators to replace 1,500 buses, and the transport company limited to replace 401 vehicles for the substitution of 4,412 ICE buses in 2027[11]. There are a lot of local manufacturers in developing electric buses as Sakun.

C innovation Co.,Ltd, Electric Vehicles (Thailand) Co., Ltd (EVT), Thai Smile bus and so on as shown in figure 2.1. Together with MEA, PEA, BMTA, NSTDA AND Thai business owners, Electric Generating Authority of Thailand (EGAT) was researching the benefits of converting BMTA's old buses into electric buses and strengthening Thai business owner's abilities to develop and produce high- quality electric buses[12], [13].

Figure 2.1 Thailand electric buses [13]

2.2 Vehicle dynamic system [14]

The fundamentals of vehicle behavior can mathematically be represented depending on the general principles of mechanics during the vehicle movement. All the forces for propelling the bus fundamentally dictate its movement behavior considering the resistance forces that are against the driving wheels when the bus is trying to stop. Resistance forces, called forces opposing the bus motion, are defined as inertial resistance, aerodynamic resistance, rolling resistance and grade resistance, as described in figure 2.2. Required tractive force is evaluated by summation of these resistance forces , expressing in equation 2.1.

$$F_{tr} = F_a + F_{aero} + F_r + F_{grade} \quad (2.1)$$

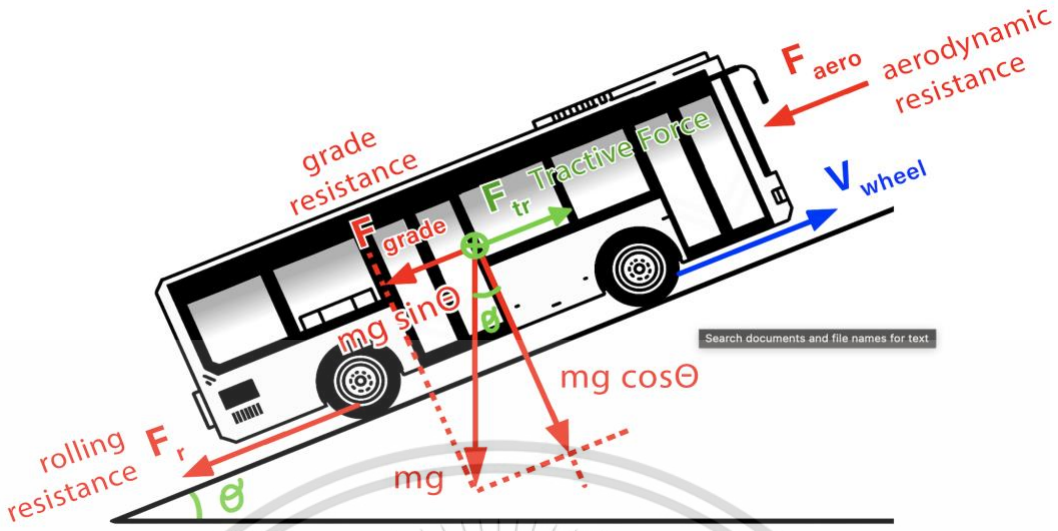

Figure 2.2 Vehicle dynamic system

2.2.1 Inertial resistance force F_a [15]

The Newton's law of motion states that as an object accelerates or decelerates, an inertial force is induced in the direction opposing the motion of the object. This encountered force during both positive and negative acceleration can be described as inertial resistance and this force is calculated by the following equation.

$$F_a = m_v * \frac{dv}{dt} \tag{2.2}$$

where m_v = mass of the vehicle, v = vehicle speed

2.2.2 Aerodynamic resistance force F_{aero} [14]

The friction of the bus body moving through the air is responsible for this portion of the force. This aerodynamic force depends on a number of different factors, including the frontal area, the body shape, side mirrors, ducts, and air tunnels, wind spoilers and other protrusions. The equation of this force is

$$F_{aero} = 0.5 * \rho * c_d * A * v^2 \tag{2.3}$$

where ρ is the density of the air, A is the frontal area and v is the bus velocity , c_d is constant value of drag coefficient. This drag coefficient value is varied according

to the design of the vehicle. There is more potential to vary c_d in the design, provided upon the less requirement for cooling air ducting and pipes and flexibility of the placement of major components. For sedan cars, a typical value for c_d is 0.3. even though other vehicles, like motors and buses have figured out larger values, around 0.7.

2.2.3 Rolling resistance force F_r [14], [16]

The hysteresis losses in the driving wheels are the major cause of the rolling resistance. Both the gearing system and bearing friction also contribute to the main factors of this resistance. The output of the rolling resistance is roughly constant and scarcely changes with the speed of the vehicle, however, it is directly related to the weight of the vehicle. The formula is

$$F_r = m_v * g * c_r * cos(\theta) \quad (2.4)$$

where c_r = rolling resistance coefficient, influenced by air pressure inside the vehicle tire and the structure of road surface. The coefficient value depending on the surface of road is described in table 2.1.

Table 2.1 Rolling resistance coefficient on different kinds of road [16]

Type of road surface	Value of rolling resistance coefficient
Concrete or Asphalt	0.013
Gravel	0.02
Macadam	0.025
Soil	0.1-0.35

2.2.4 Grade resistance force F_g[14]

It is the force that is required to move the vehicle up a slope. It is also the components of the weight of the vehicle acting along the slope in the downward direction when the vehicle goes up or down a slope. The upgrading and downgrading operations are considered in the vehicle dynamic model. This force is called the grade resistance, expressed by equation (2.5).

$$F_g = m_v * g * sin\,(\theta) \tag{2.5}$$

where θ is road grade in degree.

2.3 Electric Vehicle Powertrain Architecture [17]

In terms of electric vehicle architecture, the powertrain gives new freedom, but it also creates new criteria that must be met. The compositions of electric vehicle's energy source and other components of drive train are referred as its architecture. An EV's configuration is more adaptable as compared to an internal combustion engine's because there is no need for complicated engine setup, clutch, manual transmission, exhaust pipe, fuel tank, etc. The EV architecture is so crucial because it provides an understanding of how an EV works from start to finish and its performance and cost must be balanced when constructing a vehicle.

It is required to employ modeling and simulation tools while creating the architecture for electric vehicle, paying attention to its powertrain components such as battery, power electronics , electric motors, sensors, and control units (inverter and DC-DC converter). Its structure needs considerable adoptions in order to incorporate the battery securely. Figure 2.3 depicts the detailed framework of an electric vehicle's powertrain system and how it connects to various components.

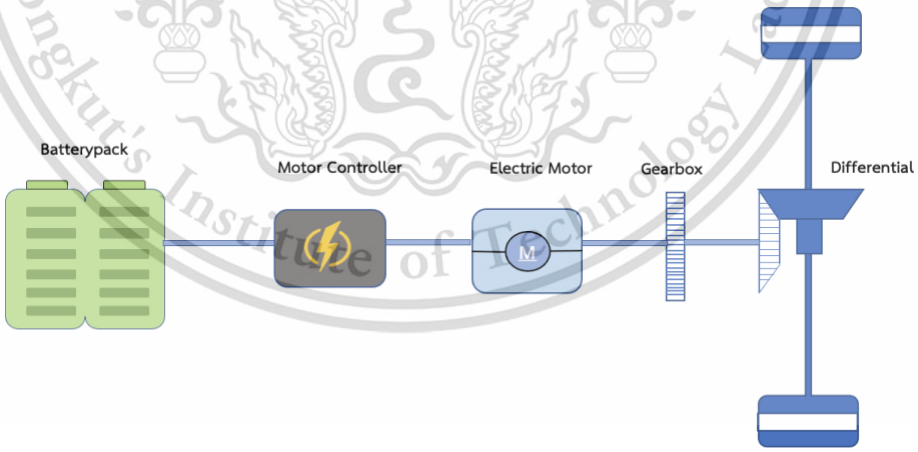

Figure 2.3 The architecture of electric vehicle's powertrain

The driver applies force to the accelerator and brake, then the vehicle gets the required input. Electric motors use electromagnetic fields and energy from batteries to provide torque to the vehicle, and the torque is adjusted by changing current flow/ In comparison to an ICE engine, electric motor offers more than 90% efficiency. It produces torque at zero speed, allowing a vehicle to have a single gear ratio between the motor and tires rather than a multispeed gearbox. The batterypack is the energy storage component, which receives and supplies electricity to the electric motor. Direct current us produced by these batterypack. The batteries need to charge for restoring the power. Power electronics also collaborate with the battery charging system to regulate charging behavior and keep track of the usage of batterypack. DC to AC conversion as well as the torque control functionality are provided by the motor inverter, Power is reduced from the batterypack voltage to 12 volts using a DC- DC converter, for instance wipers, infotainment system, mirror control.

2.4 Electric motor system [14], [17]

Electric motor is one of the important parts in electric vehicle's architecture. It makes use of the energy source that comes from batterypack. Also, it utilizes as the conversion of mechanical energy from electrical energy. This electric motor requires additional controllers to work as a single unit to propel the electric vehicles.

This electric machine is employed in electric vehicle to supply the transaxle with power and torque. So, the propulsion of electric vehicles is provided by electric motor. As an addition, it can say that its efficiency at converting energy to mechanical work is better than that of ICE vehicles because it offers greater torque characteristics at low speed, providing high torque and high power density, and instantaneous power ratings with two or three times the motor's rated power. It is used as a generator while processing as the negative power as a result of the reverse turn of electric motors, so called regenerative braking. There are different types of electric motors as shown in figure 2.4, considering the development of electric vehicles : direct current motor (DCM), induction motor (IM), permanent magnet motor (PMM) and switch reluctance motor (SRM). Focusing on permanent magnet motors, they can be additionally

separated into four classes: PM brushed DC motor (PMDCM), PM synchronous motor (PMSM), PM brushless DC motor (PM-BLDCM) and PM hybrid excitation motor (PM-HEM) [18]. The use of these motors implies that each of them have their own benefits and drawbacks that make them appealing for use in various designs. Hence, some of these types are discussed in the following of this section.

2.4.1 Direct current motor (DCM) [19]

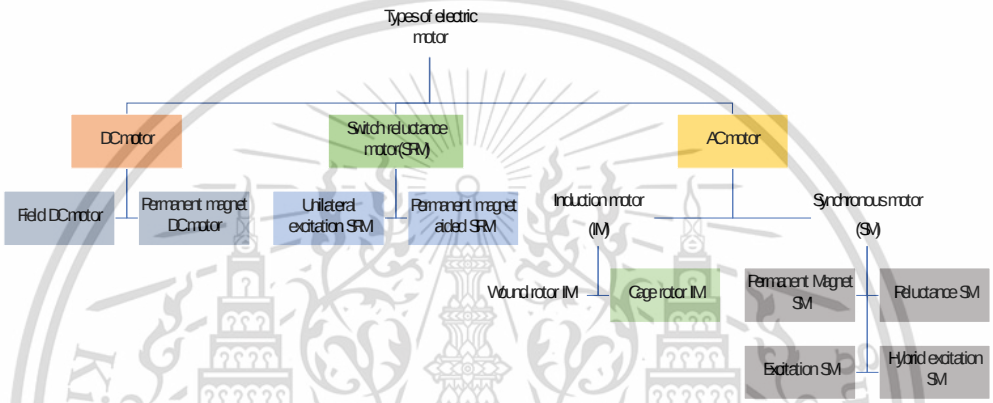

Figure 2.4 Different types of electric motor [16]

Due to its straightforward regulation of the speed, DCM has been utilized as electric traction motor in EVs since the late nineteenth century. However, their constructions having brushes and rings cause the maintenance problems. It becomes no longer appropriate for high-speed EVs because of their low efficiency, high mass, and poor reliability. The appeal of DCM in traction applications decreased as the vector control for AC motors like synchronous and induction motors grew. They are exclusively utilized in low- speed EVs, like as shuttle buses in scenic locations and carts for carrying logistic items inside plants.

2.4.2 Induction motor [20]

Along with the DCMs, induction motors with squirrel-cage rotors are among the most technologically advanced motors. They provide high power density and greater

efficiency than DCMs, however, when compared to PMSMs, it is lower than PMSM's efficiency and power density. IMs are distinguished by their simple and robust construction, low price, good reliability, minimal torque ripple, minimal noise, lack of maintenance and the ability to work in hostile environment. IMs have a large constant power range and can comfortably run at high speeds above 15,000 rpm.

2.4.3 Switch reluctance motor[21]

Although the SRM's basic idea has been known for a while, its use was delayed by the development of power electronics. Similar to the IM, the SRMs offering great power density and efficiency and simple control become its advantages. Although it lacks a rotor winding and has concentrated stator windings, its basic construction gives it a superior thermal characteristic. Their robustness, cost-effectiveness, and ability to operate in high- speed range are other benefits of SRMs. However, its uses in EVs are seriously hindered by torque variation, noise, and vibration.

2.4.4 Permanent magnet motor [19]

(1) Permanent magnet direct current motor (PM-DCM)

A PM-DCM is created when the magnetic poles and field windings of ordinary DCMS are switched out for PMs. However, due to the commutator and brush mechanism, PM-DCMs have limited life, torque fluctuation and greater maintenance requirements. These issues must be resolved for EV applications.

(2) Permanent magnet synchronous motor (PMSM)

Permanent magnets in the rotor provide the magnetic excitation for PMSM. This motor benefits from the magnets' high energy density since the permanent magnet excitation only takes up a little amount of area. In a PMSM, the excitation winding of conventional synchronous motors is replaced by a PM, while the stator's three phase windings are identical to or similar to those of an IM or synchronous motor. The PMSM has a high overall efficiency in the range of nominal speed since no excitation current is needed. High reluctance torque, good efficiency , high power density, low heat, simple and rigid design, and low noise are the characteristics of well- designed PMSMs.

They have dominated traction motor applications since the emergence of power electronics control methods. In addition, they have minimal wind friction losses and low windy noise due to the totally enclosed structure, which is free in maintenance.

(3) Permanent magnet brushless DC motor (PM- BLDCM)

In terms of structure and theory, PM- BLDCM is a unique PMSM, but its windings are generally concentrated, and the stator current waveform is trapezoidal as opposed to sinusoidal as in PMSM. There is no need for the commutator- brush mechanism. However, noise and torque ripple are present during electrical commutation, making it challenging to reach speeds that are higher than double of the base speed.

(4) Permanent magnet hybrid excitation motor (PH-HEM)

The motor can have both the PMs and excitation windings and become a hybrid excited motor, or PM-HEM, by adding excitation windings to PMSM. This motor has good torque- speed characteristics, little flux leakage, high flux density in the air gap, and high power density, but its topology and control are rather complicated because of two distinct excitations.

2.4.5 Characteristics of electric motor

Electric motor has the optimal characteristics that mainly indicates the variables such as motor speed, power, and torque. Figure 2.5 represents the behavioral characteristics of the electric motor used in electric vehicles. The base- speed, below which the motor torque is constant and above which the power is constant, serves as the identification of torque-speed characteristics of electric motor. The speed ratio, which is defined as the ratio of the motor's highest speed to its base speed, is used to determine the motor speed [22]. At zero speed, motor torque is at highest value and keeps constant at rated value until rated speed is attained. The torque will drop proportionally with the speed once it has exceeded the motor's rated speed, producing a constant power (rated power) output.

By choosing a lower motor speed in the constant power region, the maximum torque of the motor can be increased. However, each motor type's intrinsic characteristics have a maximum speed ratio that is restricted. For instance, permanent magnet motor has a small ratio because of the limitation of magnetic field weakening, whereas a switch reluctance motor's speed ratio is more than 6 and induction motor's is roughly 4 [23].

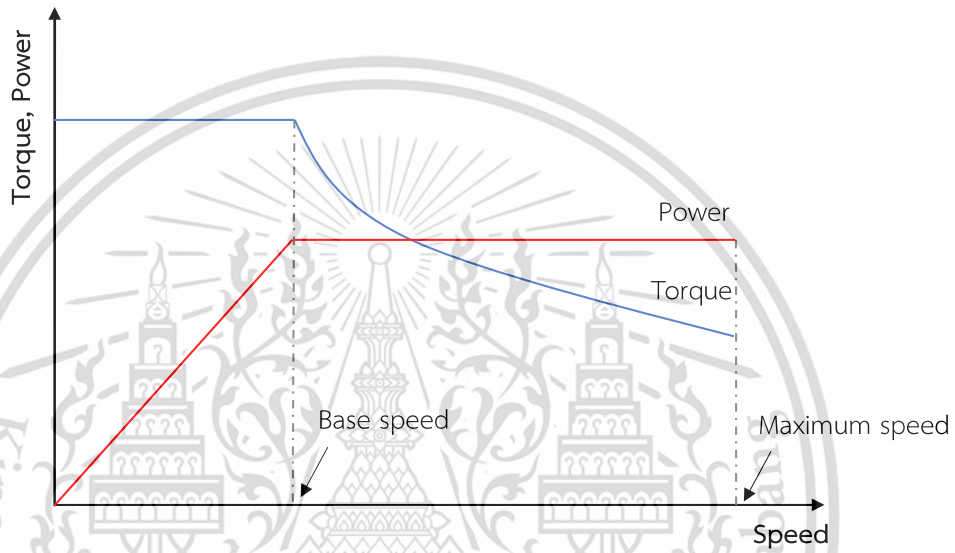

Figure 2.5 The behavioral characteristics of an electric motor

2.4.6 Motor efficiency

It is obvious that every application should select a motor that is as efficient as feasible. Although it is assumed that the selected type of motor would play a significant role, in fact it is not. It is not as easy to gauge and explain an electric motor's efficiency as one might think. There is an issue that is subjected to significant alteration under various circumstances. Generally, the greater size of the motor helps to boost the efficiency of the motor. The speed of a motor is the second aspect that affects efficiency more than the motor type. So, it can be said that the efficiency of motors increases with speed. At higher speed motors, it is found out that motor efficiency is greater than the lower ones. This is because, for a given amount of power, one of a motor's most significant losses is related to torque rather than to power, therefore a

motor operating at a lower speed will experience higher torque and, hence, larger losses.

As a comparison of the motor's efficiency based on the different types of motors, induction motor provides the greatest overall motor efficiency over a wide speed range, but its highest efficiency falls short of PMSM levels while the optimum maximum efficiency in a specific speed range is provided by PMSM, also SRM is comparable in efficiency with the IM. The efficiency maps of these three motor types are shown in Figure. The lines, which circle the range of an efficiency> 85%, are equipotential lines. The IM are SRM are more efficient at greater speeds and throughout a larger speed range, but the PMSM is most efficient at lower speeds. The PMSM would be the greatest option in the situation of low speed range, however the IM should be favored if the majority of the operating points occur at higher speeds or across a large speed range.

2.5 Battery system

Batteries in electric vehicles are currently used for the purpose of reliable electric energy storage system. In selecting these suitable energy storage systems, energy and power density, battery lifetime and cost are played as important roles. For these reasons, these systems must meet the electric vehicle's design requirements as although the battery is solely utilized for starting, ignition and lights in combustion vehicles. Moreover, the battery in EVs is built in supplying the vehicle a sizable all-electric range even when it is in charge depleting mode. Another point is that the battery in these vehicles undergoes deep charge and discharge cycles that negatively impact on its longevity. Accordingly, the demanded power, energy and battery life cycle become the critical aspects of battery system [24].

Although the battery technology is being improved in these days, the consumers are still expressing the concerns about the battery price, and they are worrying about the range limitation due to the out of charge on the roadways [25] . Additionally, owing to the shortage of charging station, high electricity price and long charging time, battery system becomes the main issue of designing the electric vehicles. While comparing to combustion cars, people can refill the fuels easily and quickly, so

there is no range limitation, and they can travel as much as they want. Consequently, battery management system (BMS) is developed as a crucial role for the battery and the good performance of the whole vehicle. In reality, the BMS must adapt to dynamic power needs that rely on driving style, tire pressure, and electrical accessories. Also, BMS is also in charge of maintaining cell safety. So, the key responsibilities of BMS are accurate SOC prediction, correct control of current and temperature, and cell potential balancing. However, the accuracy of the battery model that is integrated into a BMS has a significant impact on its efficiency.

2.5.1 Battery Glossary [26]

2.5.1.1 Battery management system

The main part of the battery system that controls how the battery cells are used is called BMS. By monitoring the characteristics like voltage, current and temperature of each battery cell in the whole batterypack, the BMS regulates how the battery cells are used. As an addition, it computes crucial variables like state of charge (SOC) and battery's charge and discharger power limitations. The vehicle control unit (VCU) receives these data from the BMS together with other signals and as a result, it is able to regulate the vehicle's propulsion in an effective manner without harming the batterypack.

2.5.1.2 State of charge (SOC)

The amount of remaining charge in the battery is represented by the state of charge (SOC). Typically, the SOC is shown as a percentage from 0 to 100. In applications involving electric vehicles, the SOC is viewed as vehicle's fuel gauge; its function is similar to the fuel gauge found on the dashboard of cars with internal combustion engines.

2.5.1.3 C- rate

The nominal capacity of a cell as indicated by the manufacturer at reference circumstances is scaled to the C-rate, which is a metric for the current of a battery cell. The capacity of the battery determines the maximum current level at which a battery cell may discharge. A battery cell is optimally charged or discharged at a current of 1C

in an hour, C/2 in two hours, and 2C in 30 minutes. Hence, 80A is equal to 0.5C of current for a cell with a nominal capacity of 160Ah.

2.5.1.4 Cell capacity

The amount of charge that might hypothetically be removed from a fully charged cell with an indefinitely small current for a specific minimum cell voltage, resulting in a voltage drop across the internal resistance that is almost zero, is known as the usable capacity. The actual capacity, which serves as a benchmark for determining capacity fading, is the usable capacity at reference temperature. The 1C capacity is typically used to gauge capacity fading and is measured with a 1C C-rate under reference circumstances.

2.5.1.5 Open circuit voltage (OCV)

The battery voltage under equilibrium, or the value when no current is flowing into or out of the battery and, consequently, no reactions are taking place inside the battery, is known as the open- circuit voltage (OCV). OCV is a function of state of charge and is anticipated to keep constant for the time of the battery's life. OCV can be utilized as an estimate approach because it has a substantial influence on SOC for the majority of batteries. It is not practicable for real- time or continuous estimate since the battery has to be at rest for several hours for being calculated.

2.5.1.6 Internal resistance

The internal resistance is occasionally taken with the cell's ohmic resistance, which is the direct voltage change resulting from applying a current step to an equilibrium cell. The maximum potential voltage drops in the cell, which is another way to define the internal resistance as the sum of ohmic, activation, and diffusion polarization resistances. In spite of this, the entire voltage drop will cause power to be lost as heat.

2.5.2 Battery types

The batteries come in two different types: high energy density and high power density. The amount of energy in relation to kilograms or liters is known as energy

density. Power density gives a proper indication of how much energy may be discharged at a particular time in terms of kilograms or liters. When a longer driving distance is required, a high energy density battery can be advantageous. A short but intense power pulse is needed, making a high power density battery suitable [27].

Lead- acid batteries were utilized in the first electrical vehicles (EVs) that were created in the 1990s. Since lead- acid batteries have poor energy density and the range was only around 100 kilometers, various chemistries were utilized in the following years. EVs began using nickel metal hydrate (NiMH) due to its better life cycle, greater power and energy density. Due to its lower cost, NiMH batteries are still utilized in hybrid electric vehicles (HEVs) and plug-in hybrid electric vehicles (PHEV) today. However, these batteries are inappropriate for EVs due to their fast self- discharge, constrained SOC operation range, and low energy density. Lithium- ion batteries are now the preferred option for electric vehicles owing to its better energy density, power density, minimal self- discharge, and good life cycle. The high pricing and safety concerns are additional drawbacks of Li- ion batteries. The different types under the development of Li-ion batteries are shown in table 2.2 .

Table 2.2 Different Li-ion batteries used in EVs [28]

Manufacturer	Types of Li-ion Battery	Vehicles
A123	Lithium nano phosphate	Fisker- Karma Vue PHEV
Panasonic	Lithium Nickel Cobalt	Toyota- PHEV
JCI-Saft	Aluminum oxide	S400- HEV
Hitachi	Lithium cobalt oxide	GM-HEV
Altair Nanotechnologies	Lithium titanate spinel	Phoenix electric
EnerDel	Lithium Manganese Titanate	Think
Compact(LG)	Manganese spinel	Volt- EV
NEC		Nissan- EV

2.6 Regenerative braking System

Most hybrid and electric vehicles have a regenerative braking system that transforms the kinetic energy from braking into electrical power to charge the high voltage of electric car's battery. Regenerative braking helps conventional braking by slowing the vehicle down as well because the wheels of the vehicles use energy as they turn the shaft in electric motor. In electric vehicles, the powertrain automatically activates the regenerative braking system to replace the energy lost during deceleration and transfer the energy back to the motor, which serves as the generator to recharge the battery at the instant of stopping the vehicle accelerating. Thoroughly, the regenerative braking capabilities of EV can help in recuperating and storing the energy while braking as contrast to conventional vehicles, which lose brake energy as heat [29]–[31].

To optimize EV and HEV regenerative braking, many different techniques have been put forth in the literatures. Reference [32] conducted an experiment to report the downshift braking strategy to account for the efficient energy of an EV while the vehicle is downgrading even though regenerative braking energy giving the EV on downgrading is uncommon to analyze. Regression models are also created to assess the variations in two types of power consumption in the event of downgrading and no grading, and it demonstrated an improvement in the result of consumption reduction with regenerative braking [33] The majority of literature assessments claim that regenerative braking systems can cause low- level of electrical energy consumption and emissions, although it should be noted that modeling regenerative energy still has some significant limitations [34].

2.7 Factors influencing on power consumption of electric bus

To assess the electric bus as a widespread public transportation system, demanded power and its consumption is modeled for daily operations. Energy consumption is estimated by computing the wheel and motor torque, rotational wheel speed, motor speed and transmission losses [35]–[37]. In reference[38] , electrical energy that is required to supply power an electric vehicle is evaluated for multiple transmission schemes providing differential maximal speed over various standard

driving cycles by vehicle dynamic simulation. Numerous simulation tools can be used for the estimation of consumption, occupying the analysis of each vehicle's components like motors and batteries[39]. Reference [40] submitted the model for fuel consumption rate for diesel and hybrid buses by formulating consumption rate with regression model in terms of vehicle power . Simulink is also used to represent the complex models in setting up vehicle components to forecast the energy consumption in simulation [41].

There are many factors that affect the driving conditions of the bus. Gradient of the road is one of the most important factors that should be considered for influencing on energy consumption [42]–[44]. The geographical dissimilarities in driving configurations that are dealt with road geography, traffic situations and other regional features are also affected on the efficiency of electrical energy in plug- in hybrid electric vehicles [45]. The major influences of energy performance of the electric buses encountered by most of the drivers involve length of the driving cycle[46] , driving style[47], weather and temperature [48], wind exposure and traffic conditions [49]. Moreover, energy consumption of the vehicle can be risen by using air conditioning on driving [50]. So the necessities of the energy in using heater, ventilator and air conditioner are mainly depended on the outside weather conditions [51]. In any case of modelling approach, bus parameters such as total weight of the bus including other components[52], cross sectional area[53], drag coefficient [54] and time of operation [55]. In addition, speed limit of the bus and number of stops per distance are also mentioned in reference [56]-[58] as the parts of the dominant factors on consumption.

For consideration of road topology, the consumed energy of battery electric buses with and without road gradient are calculated for each driving cycle, considering the driving behavior of the drivers in acceleration and decelerating driving style or aggressive driving style. It has been approved that higher road gradient leads to consume more energy is directly affected by the driving performance, especially in aggressive [56].

CHAPTER 3
ELECTRIC BUS PARAMETERS, SPECIFICATIONS AND REQUIREMENTS

3.1 Introduction

For the requirements of electric bus powertrain design specifications, matching and selecting the suitable parameters of the electric motor and battery were performed. The components of powertrain were scaled in accordance with the bus parameters and power requirements. These components were chosen for the simulation model based on the needs and specifications of each one after matching the parameters. The electric motor is sized to meet for specified acceleration or climbing high grades such as steep roads or bridges. Also, to accommodate the performance of motor's torque requirements, gear ratios are designed. Besides, batteries are constructed using the number of series or parallel battery cells to meet the power's requirements. The basic components will be discussed along with how to compute for the matching of the requirements of the electric bus powertrain.

3.2 Electric bus powertrain parameters matching

Choosing suitable power parameters and maximizing the performance of each device based on the target specifications of high speed and maximum grades, are crucial during the development phase of an electric bus since the power consumption of the electric bus is still so high and the buses cannot run further mileage due to the issues of their size and weight. The fundamental components of the powertrain will be gone through the parameters matching to meet the specifications of the electric bus.

3.2.1 Electric bus

The basic parameters of the electric bus used are based on the 12- meter A Bus EV, manufactured by Sakun C company. Aluminum body and steel chassis are used in electric bus to make a sturdy body structure and upgrade its ageing The A bus EV is 12 meter long and has the capacity of 45 passenger seats. The 12 meter A bus EV is shown in figure 3.1 and the overall bus parameter is shown in Table 3.1.

Table 3.1 Specifications of electric bus

Bus parameters & specifications	Values
Vehicle type	High floor
Model	120BH195/260
Dimensions	11,850 x 2,550 x 3,620 mm^2
Mass of the bus	14,075 kg
Air density	1.23 kg/m^3
Drag force coefficient	0.5
Rolling resistance coefficient	0.01
Maximum speed	100 km/h
Maximum gradient	8%
Tire	295/80R22.5 (Radial)

Figure 3.1 Sakun C aluminium electric bus

3.2.2 Electric Motor

Three important motor parameters such as rated power, peak power and peak torque are needed to consider for the sizing of electric motor. This chapter is firstly analyzed the demand of vehicle traction power because the selection of motor's performance characteristics is mainly taken the vehicle dynamic performance into account.

Maximum vehicle speed and maximum climbing gradient are used to limit the motor rated power and peak power. Normally, the power consumption of a vehicle rises with speed, and the vehicle's actual running speed is often lower than the specified top speed, allowing it to have adequate backup power. The criteria of rated power P_e meeting with the constant top speed (v_{max} *=100 km/h*) are satisfied by equation(3.1)

$$P_e \geq \frac{v_{max}}{\eta}\left(m_v g c_r + \frac{1}{2}\rho c_d A {v_{max}}^2\right) \tag{3.1}$$

At the top speed of 100km/h, the required power of the motor is calculated around 91kW. When the electric bus inclines the highest climbing slope at a certain constant speed *v*, the power generated by the resistance of inertial acceleration is neglected for the estimation of driving motor power. Equation (3.2) is presented in calculation of motor peak power P_i according to the maximum climbing gradient θ.

$$P_i \geq \frac{v}{\eta}\left(m_v g c_r \cos(\theta) + m_v g \sin(\theta) + \frac{1}{2}\rho c_d A v^2\right) \tag{3.2}$$

As a result, the required peak power of electric power is calculated approximately 167 kW while climbing maximum gradient of 8% slope at a speed of 45km/h.

For the selection of motor maximum torque, it should also meet the vehicle's starting torque requirements and maximum slope. In addition, the suitable gear ratio should be determined according to the requirements. The peak level of motor torque, T_{m_peak} , is approximated by equation (3.3).

$$T_{m_{peak}} = \frac{1}{\eta}.\frac{m_v g(c_r\, cos(\theta) + sin(\theta)) * r_w}{i} \quad (3.3)$$

As the gear ratio becomes higher, the motor torque decreases more for inclining the gradient, but the excessive gear ratio will reduce the vehicle's speed. Therefore, many different factors influence for the matching of motor torque.

3.2.3 Gear ratio

The function of this system is to make sure that there is an adequate wheel torque to keep the bus moving at the chosen top speed and maximum road grade and to minimize the power consumption. Suitable gear ratios are selected for this electric bus design.

The gear ratio design for the capability of climbing slope is considered to be crucial when elevating or downgrading driveways. In this scenario, the powertrain's overall gear ratio is determined by dividing the rolling resistance on a slope with a predetermined grade of 8% slope with the maximum torque of the motor as shown in equation (3.4). Aerodynamic drag resistance is neglected in this case.

$$i_1 = \frac{r_w(m_v g c_r\, cos(\theta) + m_v g sin(\theta))}{T_{m_{peak}}\eta} \quad (3.4)$$

Another ratio design is evaluated depending on the vehicle top speed. The maximum rotating speed of the selected motor and the capacity of the motor torque to achieve its top speed are taken account of this gear ratio calculation. The gear ratio is described as the ratio of maximum motor speed (N_m) and vehicle top speed (v_{max}) as in equation (3.5)

$$i_2 = \frac{3.6\pi N_m r_w}{30 v_{max}} \quad (3.5)$$

3.2.1 Battery

The role of the battery is very important because it is the only device providing vehicles power. To meet the requirements of vehicle power performance, batterypack for electric vehicles should have a greater power density. Total voltage, capacity,

energy, and battery numbers are considered for the choice of batterypack and to get these total variables, relevant characteristics of specific battery cells are integrated. The overall voltages of the batterypack and electric motor should be matched because the nominal voltage determine the size of the batterypack while considering for the power consumption of the additional accessories. To increase the operating voltage of the bus, there is a series relationship between each battery cell. The nominal voltage value of the batterypack (V_b) is considered to be 500V.

Capacity and power of the batterypack are the two fundamental requirements for the matching design of the batterypack. The endurance distance of the bus increases as the battery's overall capacity rises, but as the battery quality improves, so do the cost and power consumption per unit distance.

The capacity of the battery is determined by calculating the electric power consumption of the bus with the desired nominal voltage as shown in equation 3.6. The power of the batterypack relates to the power of the electric motor, this relationship is expressed in equation 3.7. In this equation 3.8, P_b is used as the demanded power at average speed of 35 km/h travelling the distance (s) 200km. The average energy consumption of the batterypack is taken in consideration at an average speed of 35 km/h for 200km with no gradient and 3% gradient of roadways. The designated electrical power consumption will be limited into these two considerations.

$$C_b = \frac{1000E_b}{V_b} \tag{3.6}$$

$$P_b = \frac{P_m}{\eta} \tag{3.7}$$

$$E_b = \frac{P_b s}{\eta v_w} \tag{3.8}$$

To meet the voltage and energy requirements of the batterypack, battery cells must be arranged in both series and parallel strings. Strings ranked in parallel can enhance energy capacity whereas strings ranked in series can rise the voltage. The

number of battery cells connected in series is calculated by dividing the nominal voltage of the whole batterypack (V_b) to the voltage of each cell (V_c) as shown in equation 3.9. Also, the number of cells linked in parallel is determined as the ratio of batterypack total capacity (C_b) and capacity of each battery cell (C_c).

$$N_{series} = \frac{V_b}{V_c}$$
$$N_{parallel} = \frac{C_b}{C_c} \quad (3.9)$$

3.3 Specifications of selected components

3.3.1 Electric motor

Dana TM4 electric motor is selected for this electric bus powertrain systems. Medium and heavy-duty electric and hybrid vehicles can be optimized for traction and auxiliary solutions from Dana TM4. It has very high drivetrain efficiency that helps to reduce the needs for the capacity of the batterypack. TM4 permanent magnet electric motors offer very high voltage range to get the great standards for electric vehicle's efficiency, reliability, and performance. The selected motor is TM4 SUMO MD series. This series is reluctance-assisted permanent magnet motor type that provides high torque and power density within low speed. The specifications of the selected TM4 SUMO motor are listed in Table 3.2. The characteristic curve and efficiency curve of that motor are displayed in Figure 3.2 and 3.3.

Table 3.2: Specifications of TM4 SUMO electric motor

Specifications	Values
Motor type	MD HV1800-3P
Peak Power (kW)	170
Continuous Power (kW)	100
Operating speed (rpm)	0-3250
Continuous torque (Nm)	680
Peak torque (Nm)	1775

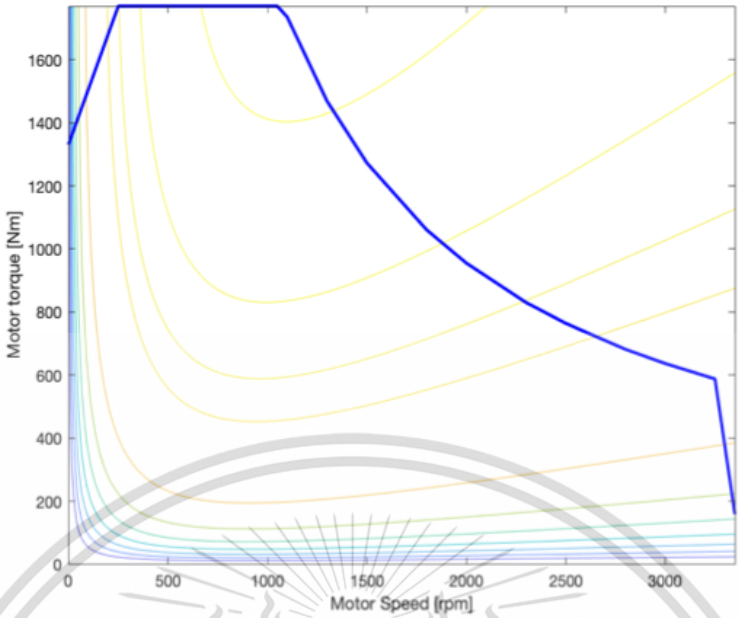

Figure 3.3 Electric motor torque and speed characteristics curve

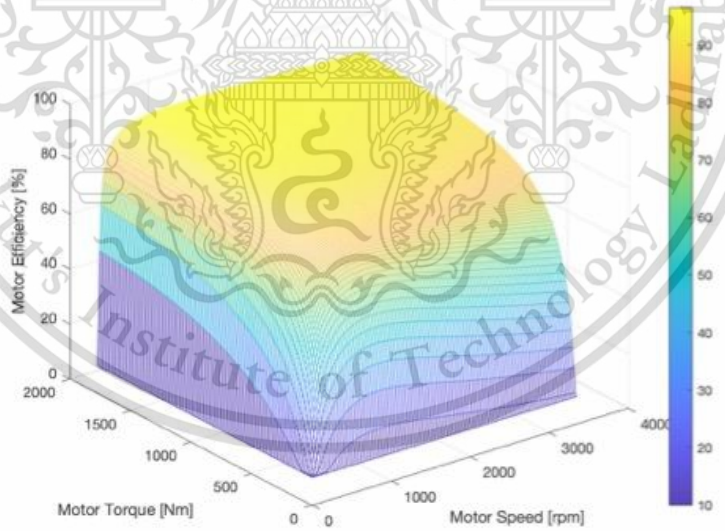

Figure 3.2 Electric motor efficiency map according to motor torque and speed characteristics

3.3.2 Battery

Electric bus's batterypack sizing design is mainly dependent on the parameter requirements of driving distance (s= 200km). Along with the designated route, the selected electric bus will be driven around 50 km per route. The total voltage of the batterypack is estimated to be 500V. The average energy of the batterypack without gradient is around 115 kWh. Then, the maximum energy of the batterypack with gradient is estimated to be around 300 kWh. So, the maximum capacity of the batterypack can be evaluated around 500 Ah by using equation (3.6). Table 3.3 shows the specification of Panasonic battery cells and based on these parameters and calculated estimations, batterypack consisting of battery cells, in which 19 cells connected in series in 7 modules and 152 cells connected in parallel. Table 3.4 illustrates the specifications of these batterypack. A series connection of batteries yields a 56kWh (113Ah, 500V) Panasonic batterypack.

Table 3.3 Specifications of Panasonic battery cell

Specifications	Values
Nominal voltage	3.7 V
Capacity (standard)	3.3 Ah
Maximum voltage	4.2 V
Discharge cut-off voltage	3.0 V
Max discharge current	3.3 A
Continuous discharge current	1.65 A
Weight	45.5 g

Table 3.4 Specifications of Panasonic batterypack

Specifications	Values
Nominal voltage	500V
Capacity (standard)	163 Ah (Discharge:0.2CmA)
Number of series	19
Number of parallel	152
Number of modules	7
Total number of battery cells	20,216

CHAPTER 4

ELECTRIC BUS POWERTRAIN MODEL DEVELOPMENT

4.1 Powertrain modeling process

The computation of the bus's energy and power needs for typical driving situations in accordance with the bus's dimensions, specifications and performance criteria is the first step in developing the electric bus's powertrain model. A power flow study is used to evaluate the size and capacity of bus components in accordance with the powertrain design criteria and requirements. The uppermost level of powertrain model has been created using theoretical basis. Briefly, the electric bus, composed of a discrete number of sub models/ block, called (1) driving cycle profile, (2) route profile, (3) driver model, (4) vehicle model, (5) gearbox, (6) electric motor, and (7) battery, are modeled in MATLAB/Simulink platform. The electric bus powertrain subsystem is a Simulink- implemented mathematical model of an electric bus subsystem. Figure 4.1 illustrates the overall simulation model of powertrain system. The development of each sub-models for each component will be discussed in the following sections.

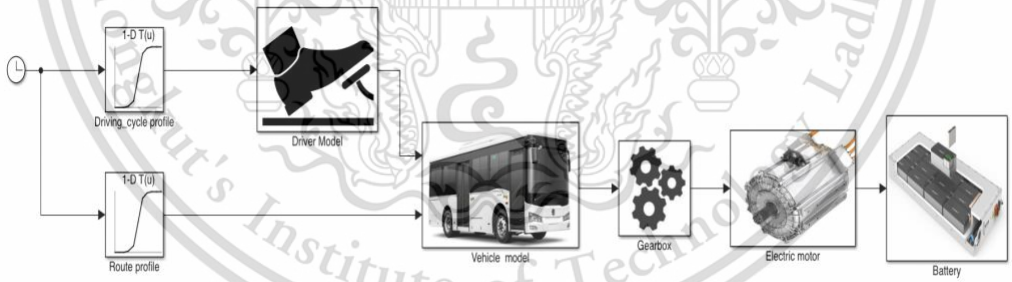

Figure 4.1 The overall simulation model of powertrain system

4.2 Route characterization development

One of the bus lines that is currently running on Thailand road is designated to develop the route characterization for this research. The road altitude condition is mainly considered for this study. The geometry data were obtained time, position and relative altitude measured from sensor logger application that logs reading from common motion related sensors on smartphones as shown in figure 4.2.

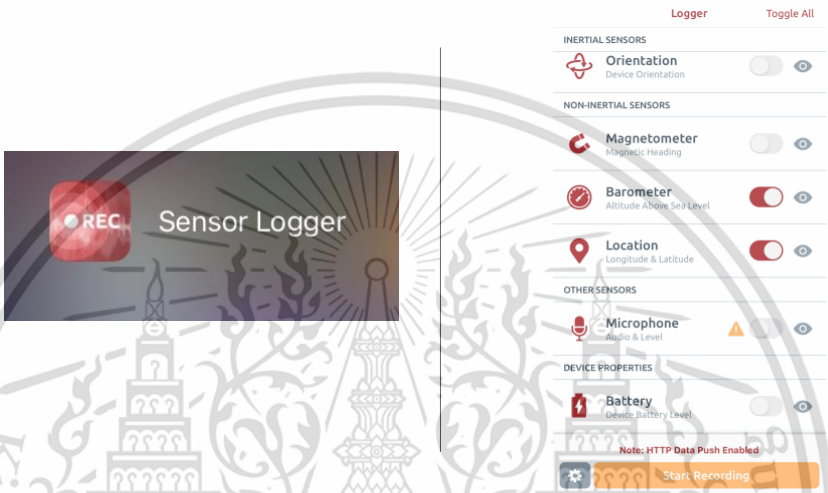

Figure 4.2 Sensor logger application

Bus line number 142 that departs from Samaedam bus depot and ends in Samut Prakan crocodile farm is selected as a representative route. The route scenario (red line) can be seen in figure 4.3. The distance for one route is around 50 km, so for back and forth, it is about 100 km total distance. As an additional information, it has 65 stops and the total trip duration for one route is approximately 87 minutes. Along Samaedam bus depot to Samut Prakan crocodile farm, this driving test study is focused on RAMA IX bridge crossing the Chao Pharya River connecting Thonburi and Bangkok, which has the highest elevation for that route. Figure 4.4 shows the geographical location of the RAMA IX bridge and its characterized route. Data collection using GPS and barometer has been performed for the determination of exact location and elevation for the designated route.

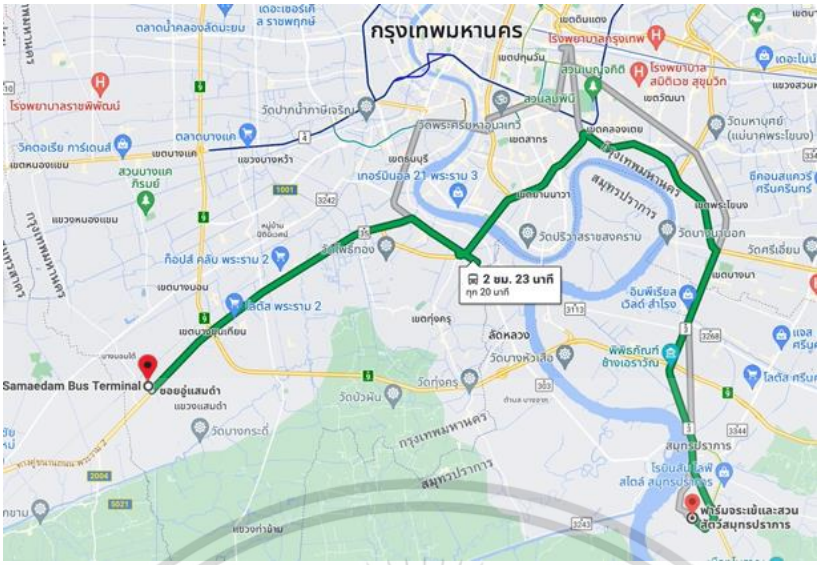

Figure 4.3 The route scenario of bus line 142

(Samutprakan crocodile farm – Samaedam bus depot)

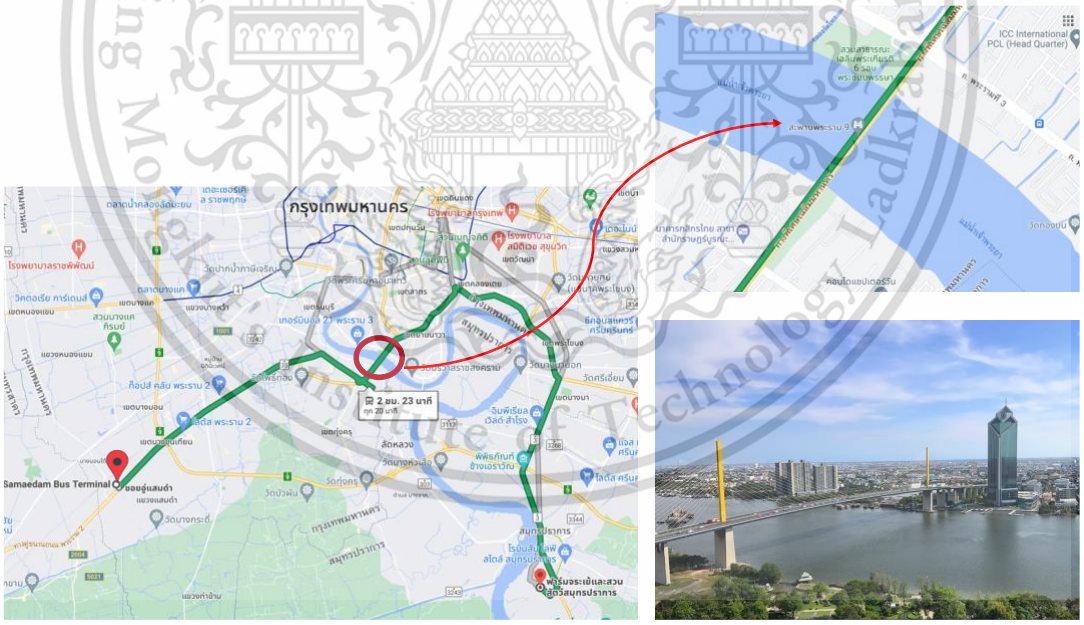

Figure 4.4 The geographical location of RAMA IX bridge

4.3 Driving cycle profile development

Driving cycles are represented as speed time series that depict driving behaviors[57]. The designated route can be driven in numerous scenarios, standing on different factors such as traffic jam, driving style and speed variations [58]. The main target for applying different scenarios is to evaluate the discrepancy un electric power output and power consumption for analyzing which factors has the most significant impact on bus performance. Figure 4.5 demonstrates the driving cycle profile model in the MATLAB/Simulink platform. Using the current simulation time, the block produces the desired vehicle speed that inputs the collected driving cycle data. In this case, four sets of scenarios have been assessed for the determination of the electric power consumption of the electric bus.

Figure 4.5 Driving cycle profile model in MATLAB/ Simulink environment

4.3.1 Driving profile based on constant speed

This constant speed scenario is an unreal scenario, looking over different cruising speed, where running speed is assumed as constant. This scenario is just set up for the comparison of the analysis of the results. These cruising speeds were varied from 5 to 100 km/h with a 5 km/h increments only for the case of having elevation level with same travelled distance.

4.3.2 Driving profile based on speed reduction

This driving profile is categorized into two types depending on speed range [59].The theorical explanation of speed reduction is described on route behavior, upward slope, or downward slope depending on the preceding literature reviews of vehicle's speed along grade sections [60]. While travelling the downhill without brake fading, buses often raise their speed to the highest limit, then hold that speed till the bottom of the slope. On ascent slope, the speed from the starting point gradually drops to a minimal and constant value and maintains at the speed until it reaches at the top of the slope. As a result, two regions may be separated for speed profiles: speed change region (accelerating or decelerating) and constant speed region (zero-acceleration or zero- deceleration). These two areas are clearly shown in Figure 4.6. L_{Up} in the figure stands for the length of the decelerating region on upward slope and L_D is the length for accelerating region on downward slope. In this study, L_{Up} and L_D may be changed concerning with the driving behavior of the drivers.

On ascending the slope, the speed gradually declines from the initial point until the end, since the traction force is greater than resistance forces, the remaining forces encourage movement. This situation happens in the decelerating region as shown in Figure 4.6. As the bus continues to climb the slope, acceleration decreases until the tractive force equals the resistive forces, at which point it zeros out. As a result, the bus is unable to accelerate, and it travels at a steady speed till the end of the slope.

The bus runs at a constant pace under this circumstance. This case has been investigated for the various speed changes with the same decelerating region length (L_{up}) [60]. The bus will travel at a speed of 90 km/h on both flat level and the initial point of the slope. The gradual speed reduction rate will be varied. It means that the bus will leave the decelerating region at the same length with the different speeds. The speed variation of 30 km/h, 45 km/h and 60 km/h will be explored for this speed variation case. Speed variation profiles can be seen in Figure 4.7.

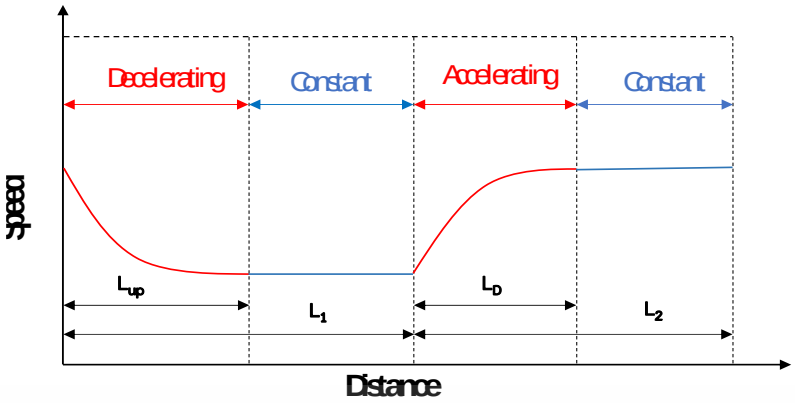

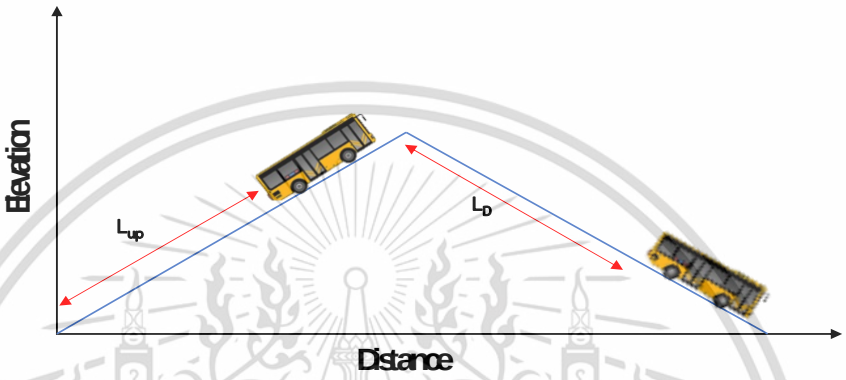

Figure 4.7 Speed reduction driving profile on the slope

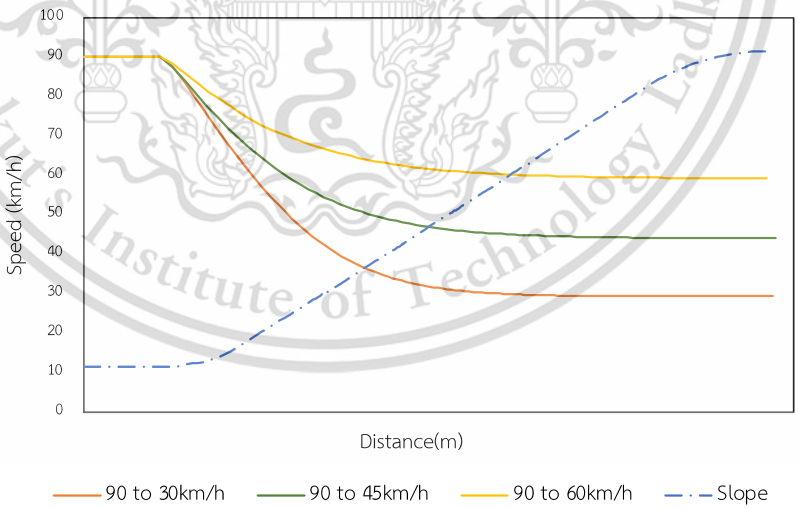

Figure 4.6 Three different speed variation profiles over distance

4.3.3 Driving profile based on standard driving cycle

There are several different standard driving cycles [61] such as extra urban driving cycle (EUDC), ECE 15, new European driving cycle (NEDC), EPA highway fuel economy test (HWFET), the world harmonized light vehicles test procedures (WLTC) and others. Depending on the kind of driving cycles profile mentioned above, these cycles include several accelerations and braking events over a specific period of time.

This study will be addressed only on NEDC and WLTC driving cycles. The main characteristics of these two driving cycles are tabulated in Table 4.1. The NEDC is a combined driving cycle of an urban part called ECE- 15 and an extra urban part, EUDC [62]. The experts declared thar it does not represent real world driving cycles because of soft accelerations and containing a lot of constant cruising speeds and idle conditions as shown in figure 4.8.

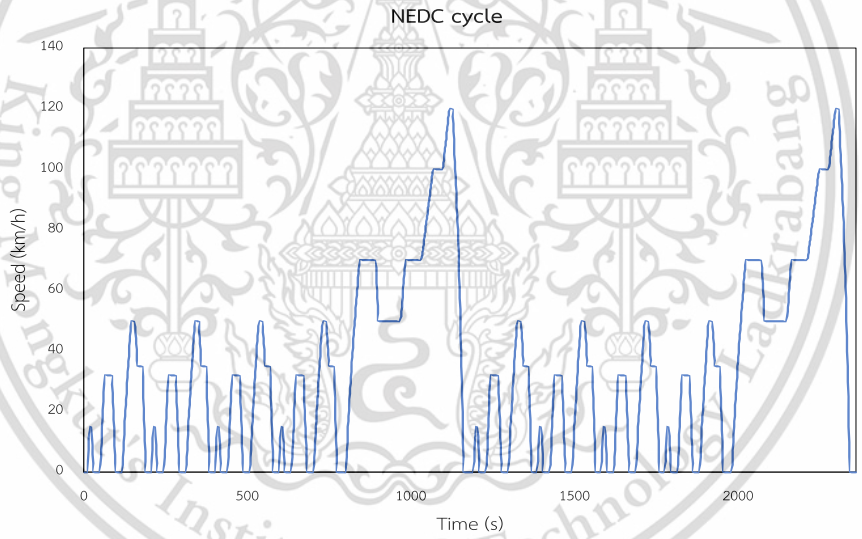

Figure 4.8 NEDC driving cycle profile

Experts from Europe, Japan and India created the WLTC to take the role of the NEDC [63]. This cycle allows for the evaluation of both electric range and fuel economy of the vehicles. This test procedure is divided into 3 classes, depending on a power to mass ratio of tested vehicle, namely Class 1 for urban driving, Class 2 for combined driving, including both low-speed and high-speed sections, and Class 3 for extra-urban

driving. These 3 classes are defined as given in the following Table 4.1. WLTC class 3 driving cycle is shown in figure 4.9. The maximum speed of these cycles will be limited at 90 km/h even though NEDC has 120 km/h maximum speed and WLTC has 132 km/h since Thailand government has ruled the speed limit regulations for buses not to be over 90 km/h on roadways.

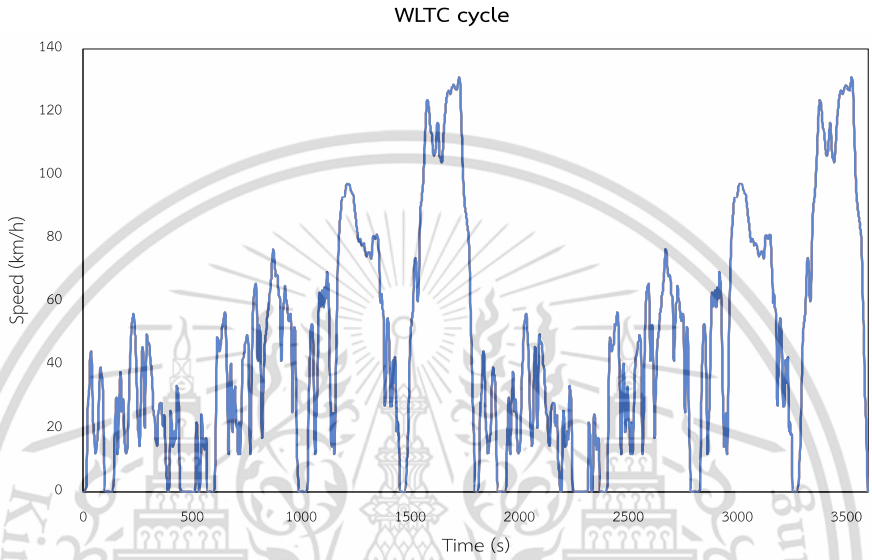

Figure 4.9 WLTC driving cycle profile

Table 4.1 Data of NEDC and WLTC standard driving cycle

	NEDC			WLTC		
	ECE-15	NEDC	EUDC	Class 1	Class 2	Class 3
Duration (s)	195	1220	400	1022	1477	1800
Stops (no:)	3	13	1	5	6	6
Distance (m)	995	11,016	6,995	8,091	14,644	23,266
Top Speed (km/h)	50	120	120	64.4	85.2	131.3
Average Speed (km/h)	18.4	33.4	62.4	28.5	35.7	46.5

4.3.4 Driving profile based on real data collection

This driving profile is real- world driving cycle, is developed using on- road data that is really captured while driving. This dynamic cycle is created as a consequence of the more aggressive driving that is encountered in real traffic driving situations. With the aid of a GPS logger VBox mounted on the bus, speed and geometry are measured. GPS antenna is also mounted on the bus as shown in figure 4.10. The position, speed, acceleration, and heading are recorded by the GPS logger and stored on a SD card. Up to eight satellites provided data to the device, ensuring data collecting during the data collection process [64]. To create a clean database for modeling the speed profiles, data pre-processing is done for GPS logger data. The position and speed data are initially coupled, and dropouts, where the satellite signal is lost and speed or location data are zero, are then erased. After pre-processing, filtering is processed for debugging the speed and position data. Raw speed data profile for each 1 second is generated after debugging. The data must then be compressed using smoothing in order to eliminate some variations and provide a smoothed speed profile. Figure 4.11 describes the generated speed profile of collected data.

Figure 4.10 Experimental setup of GPS logger Vbox on the bus

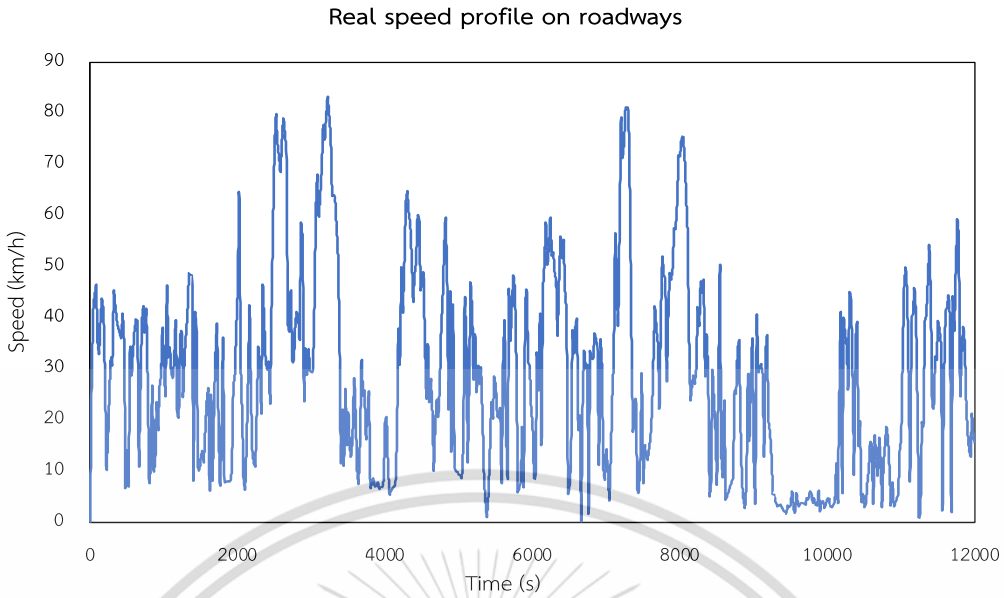

Figure 4.11 Real speed profile for Bus line 142 roadways

4.4 Driver model

The driver model in MATLAB/Simulink is represented in figure 4.12. The driver model determines the bus's desired speed and manages the brakes, electric motor inputs and loads accordingly. The driver block receives input of desired driving cycle for the bus to adopt. This block will include a PI controller to continually match the actual vehicle's speed with the desired one and to reduce the discrepancy between the desired and actual speed. The reference speed is matched by the PI controller to

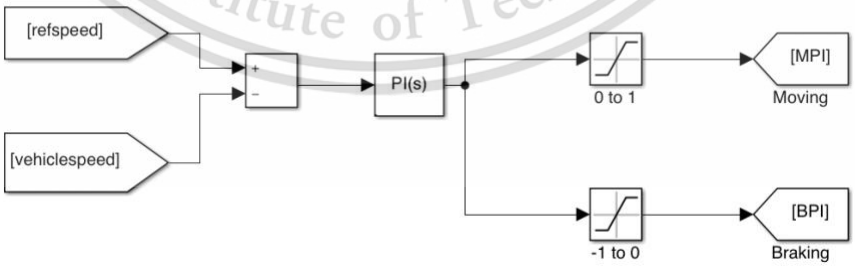

Figure 4.12 Block diagram of driver model in MATLAB/ Simulink

the output vehicle speed of the model. The output range of the PI controller is determined to be -1 and 1. The range of 0 to 1 control the condition of the vehicle moving, and -1 to 0 range indicate braking.

4.5 Vehicle model

The vehicle model is used for representing the behavioral characterization of the bus to calculate the demanded values from the wheels and to evaluate its power consumption. The tractive force required by the wheels to propel the bus F_{tr} is evaluated based on the resistive forces acting on it according to equation 2.1, as represented in section 2.2. In this model, all of the resistance forces are taken into account because grade resistance cannot be taken as zero owing to the consideration of gradients for upgrading and downgrading.

Power consumption is computed using Newton's equation of motion with the longitudinal vehicle dynamics as a function of speed on multiple driving cycles. Taking into the calculated tractive force F_{tr} , power (P) can be computed as

$$P = F_{tr} \times v \tag{4.1}$$

By integrating the power over time, energy of the bus (E_{Joule})can be calculated as

$$E_{Joule} = \int P \, dt \tag{4.2}$$

Then by dividing the calculated value of the energy (E_{kWh}) to the total length of the route (s_{total}), it can get average power consumption of the bus as presented in equation (4.3). The vehicle dynamic simulation model for the bus is as shown in figure 4.13.

$$\frac{kWh}{km} = \frac{E_{kWh}}{s_{total}} \tag{4.3}$$

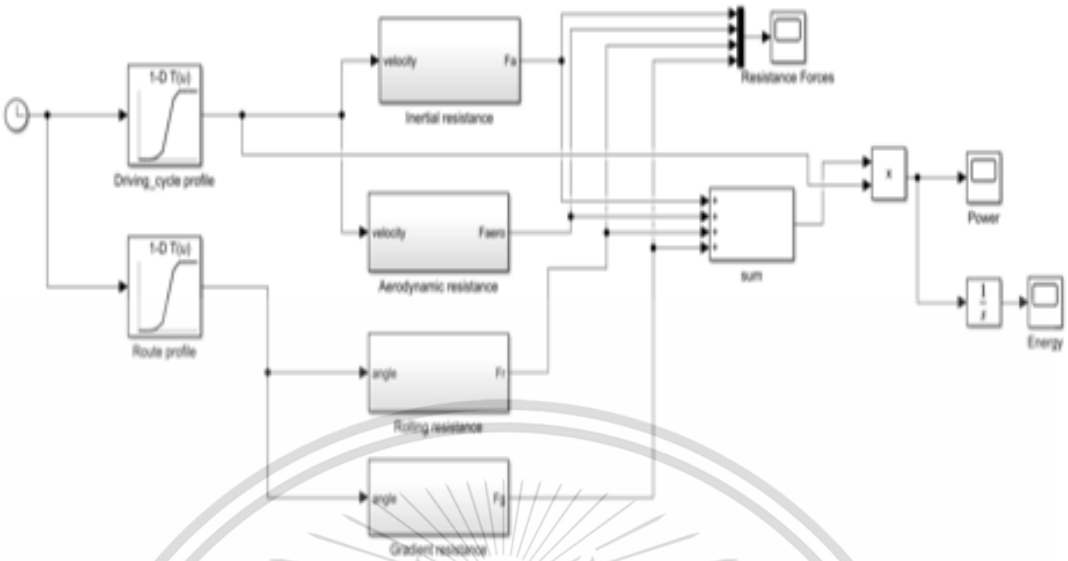

Figure 4.13 Block diagram of vehicle dynamic system in MATLAB/ Simulink

4.6 Braking Model

When the bus goes idling or slowing down or downgrading, acceleration of the vehicle goes to negative and braking system is designed to be activated. The negative output of the PI controller is the main input of the vehicle, and it controls the desired braking force that comes from the driver's brake pedal. Part of the braking force is limited to be regenerative braking force. That force is provided the kinetic energy of

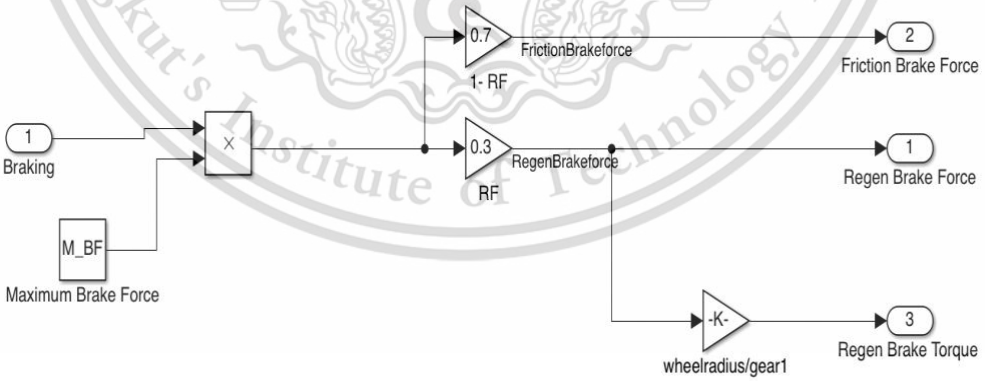

Figure 4.14 Block diagram of brake system in MATLAB/ Simulink

the vehicle to be recovered by braking the electric motor in the generator mode and by charging the battery. Figure 4.14 represents the simulation model of the braking system.

4.7 Gearbox Model

Figure 4.15 displays how the gear ratio works on MATLAB/ Simulink. Also, the rotational speed of the wheel that is provided from the motor via gear ratio is computed the output of the vehicle speed using the following equation.

$$\omega_m = v_w \times \frac{i}{r_{wheel}} \tag{4.4}$$

Where v_v is the bus speed, ω_m is the rotational speed of the motor in rad/s and r_w is the radius of the bus wheel.

Figure 4.15 Block diagram for gearbox model in MATLAB/Simulink

4.8 Electric Motor Model

Figure 4.16 shows the main input and output of the electric motor model. The wheel velocity is converted into the rotational speed of the electric motor using gear box. Using that motor rotational speed as an input, the output torque is obtained from the limitation of the maximum torque and power of the reference motor. The reference motor mentioned in section (3.3.1) is used to simulate in the model. The simulation block design of this positive output torque is shown in figure 4.17 . As the motor works as a generator when the bus decelerates, this simulation is considered about the regenerative braking system. The simulated regenerative braking force is converted into torque using selected gear ratio, and it will act as the negative output

torque of the motor. Then, these two positive and negative torques will combine to get the total output of the motor torque as shown in figure 4.18 . Using motor output torque T_m and the rotational speed, its output power P_m is computed using equation 4.5.

$$P_m = T_m \times \omega_m \tag{4.5}$$

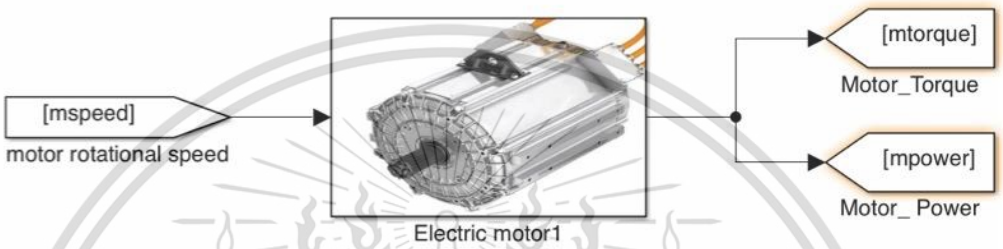

Figure 4.16 Input and output of the electric motor model

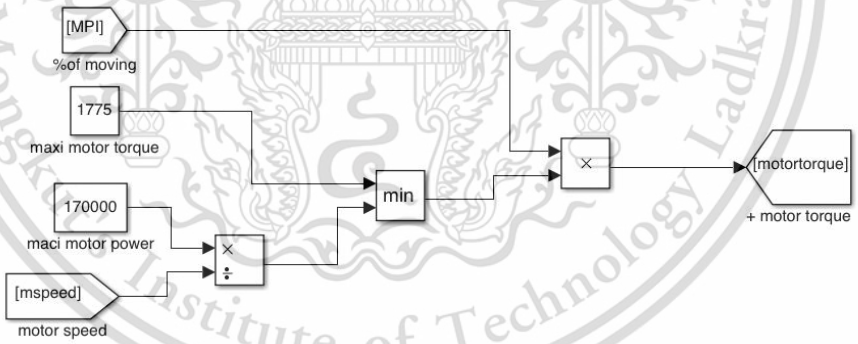

Figure 4.17 Block diagram for calculating positive motor torque in MATLAB/Simulink

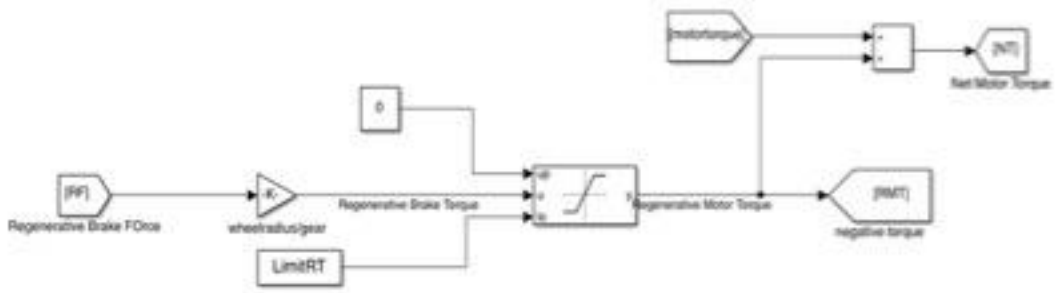

Figure 4.18 Block motor output torque in MATLAB/Simulink

4.9 Battery Model

The inputs and outputs of the battery model are demonstrated as figure 4.19. The power output from the motor is the desired input. That power informs how much power needed for the batterypack to supply to bus. The energy management system controller receives information from the SOC about the current, or the quantity of energy stored in the batterypack, and uses this information to choose the driving mode that is appropriate for the current driving circumstances.

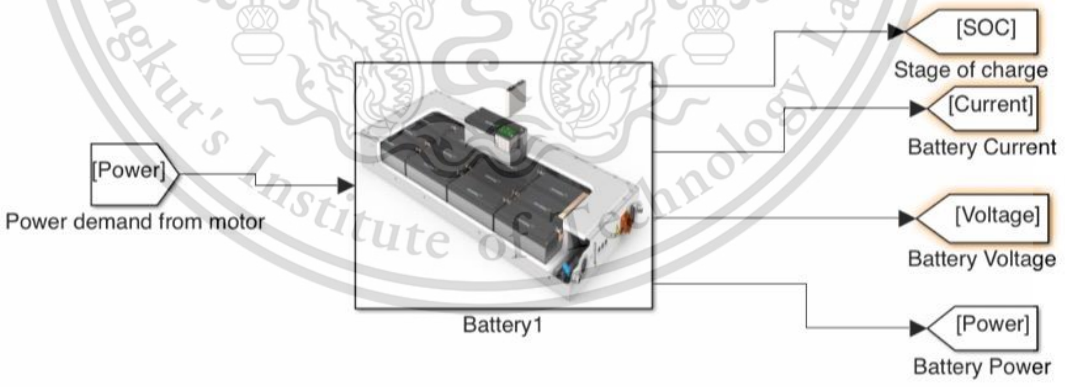

Figure 4.19 Input and output of the battery model

The battery model is composed of five functional subsystems: (1) open circuit voltage (OCV) and internal resistance (R_{int}) of the battery calculation, (2) input power limitation, (3) SOC calculation, (4) output current of the batterypack (I_{out}) calculation and (5) output voltage of the batterypack (V_{out}) calculation. Figure 4.20 shows the overall simulated battery model of the electric bus.

The block design for calculating OCV and R_{int} in MATLAB/Simulink system is shown in figure 4.21. The method to calculate OCV and R_{int} for a prior SOC and power demand is shown in the functional block of OCV and R_{int} calculation. The charging and discharging internal resistances, R_{ch} and R_{dis}, and open circuit voltage, OCV, for a particular kind of battery, are the functions of SOC as presented in equation 4.6 and 4.7. Look- up tables based on experimental data presented in figure 4.21 are utilized in this function block to compute OCV, R_{ch} and R_{dis} by first order interpolation. Depending on whether the battery is charged or discharged i.e power demand goes to positive or negative, the internal resistance is selected between R_{ch} and R_{dis}.By multiplying the number of batteries that are connected in series, the OCV and R_{int} can be obtained.

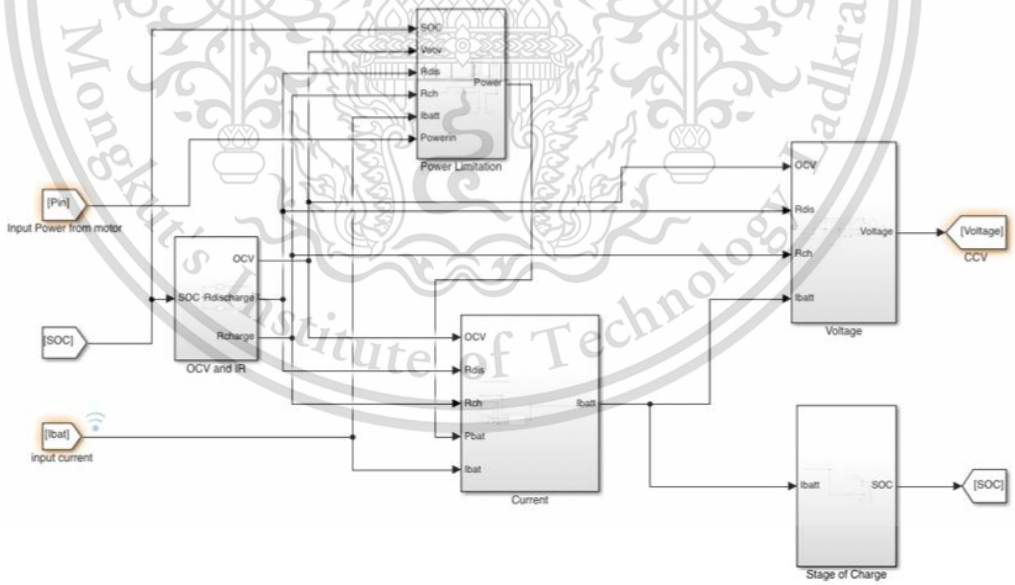

Figure 4.20 Overall simulation of the battery model

$$OCV = f_1(SOC) \tag{4.6}$$

$$R_{int} = \begin{cases} R_{ch} = f_2(SOC)\ charging \\ R_{dis} = f_3(SOC)\ discharging \end{cases} \tag{4.7}$$

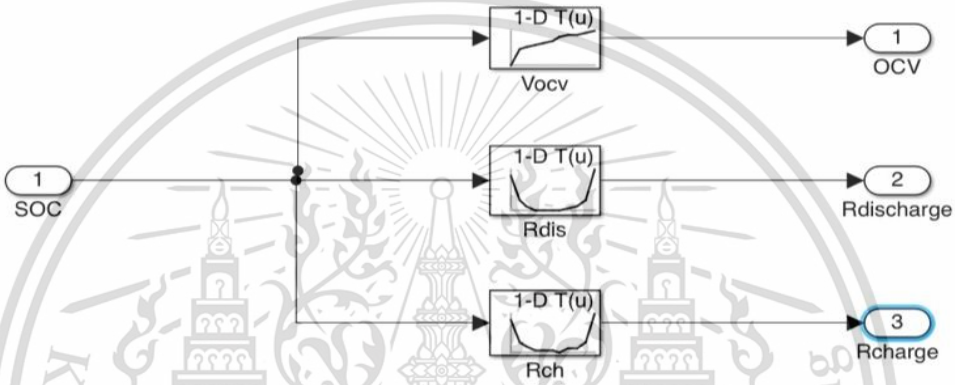

Figure 4.21 Block diagram for calculating OCV and Rint in MATLAB/Simulink

Figure 4.22 illustrates the block diagram of SOC calculation in MATLAB/Simulink. The battery's remaining capacity is referred to as SOC , measured in percentage points (0 percent equals empty and 100 percent equals full). When describing a battery's present status in operation, SOC is typically utilized. In addition to preventing overcharging and over discharging, the calculation of SOC may be used to assist determination of the thresholds for each battery operating mode, such as charging or discharging. Equation 4.8 is used to determine SOC, which is the ratio of the capacity that is currently accessible to the maximum capacity. The efficiency η in equation 4.9 is determined based on the battery's charge / discharge condition.

$$SOC = SOC_{int} - \int \frac{\eta I_{out}}{Q}\, dt \tag{4.8}$$

$$\eta = \begin{cases} \eta_{ch} = \dfrac{OCV}{OCV - I_{out}R_{ch}}, charging \\ n_{dis} = \dfrac{OCV - I_{out}R_{dis}}{OCV}, discharging \end{cases} \quad (4.9)$$

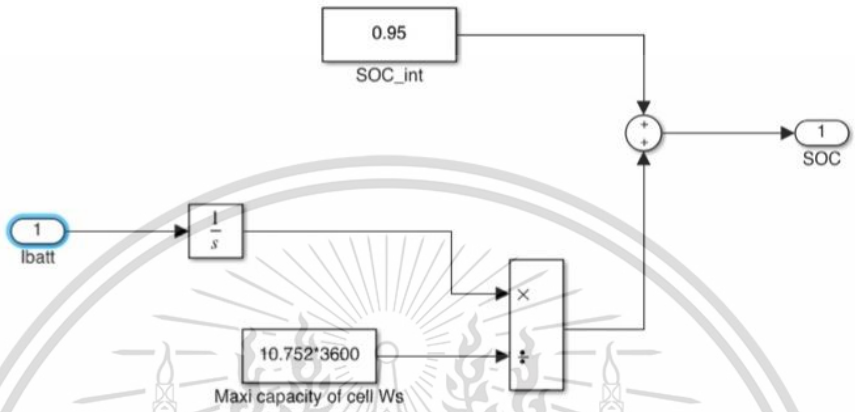

Figure 4.22 Block diagram of SOC calculation in MATLAB/Simulink

The OCV and power demand can be used to compute the I_{out} that the batterypack produces. The calculation of the output voltage is shown in figure 4.23. The voltage equation for the batterypack may be expressed as a result of Kirchhoff's law as

$$V_{out} = \begin{cases} OCV - R_{int} \times I_{out} \\ OCV + R_{int} \times |I_{out}| \end{cases} \quad (4.10)$$

The following equation is used to determine the batterypack's corresponding output power.

$$P_{out} = V_{out} \times I_{out} \quad (4.11)$$

The I_{out} of the battery can be calculated by solving equation 4.12 as

$$I_{out} = \frac{(OCV - \sqrt{OCV^2 - 4R_{int}P_{out}})}{2R_{int}} \quad (4.12)$$

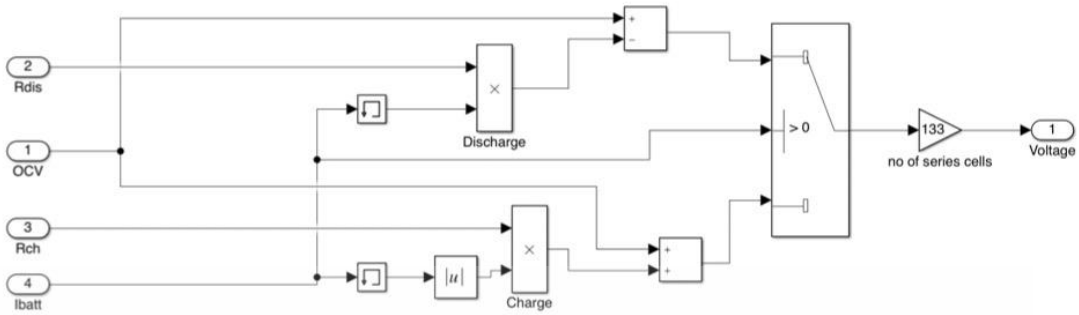

Figure 4.23 Block diagram for output voltage calculation in MATLAB/ Simulink

CHAPTER 5
RESULTS AND PERFORMANCE ANALYSIS

5.1 Analysis of bus performance based on different driving styles

5.1.1 Model Scenarios Development

Numerous scenarios are developed for setting the designated RAMA IX route, depending on specified variables including traffic congestion, driving behaviors and speed variations. According to the collected data along the route, that bridge has the entire horizontal distance ,2.75 km and its elevation of 54 m in relation to the starting point of the bus. The major goal of applying different scenarios is to access the discrepancy between power consumption and demanded power in order to examine diverse driving behaviors while crossing the RAMA IX bridge. In this instance, three scenarios for upgrading and downgrading case have been examined to evaluate the power consumption of electric bus. Figure 5.1 shows the elevation and slope profile of RAMA IX bridge.

5.1.2 Constant speed

For speed ranges of 5 to 90 km/h, a simulation model is utilized . Each step speeds up by 5 km/h for the elevation with the same distance. Figure 5.2 shows the amount of maximum demanded power which is varied with speed for upgrading and Figure 5.3 is for downgrading. Also, the amount of consumed power per distance for each speed variation is tabulated in table 5.1. According to resulted data, the value of demanded power rises with increasing speed in upgrading and in downgrading case, power goes to more negative while speed values go up. It means that as the bus travels quicker, increasing amount of power are consumed in a short period while reaching the upward slope. In downward slope, this negative power went back to the battery as recuperation.

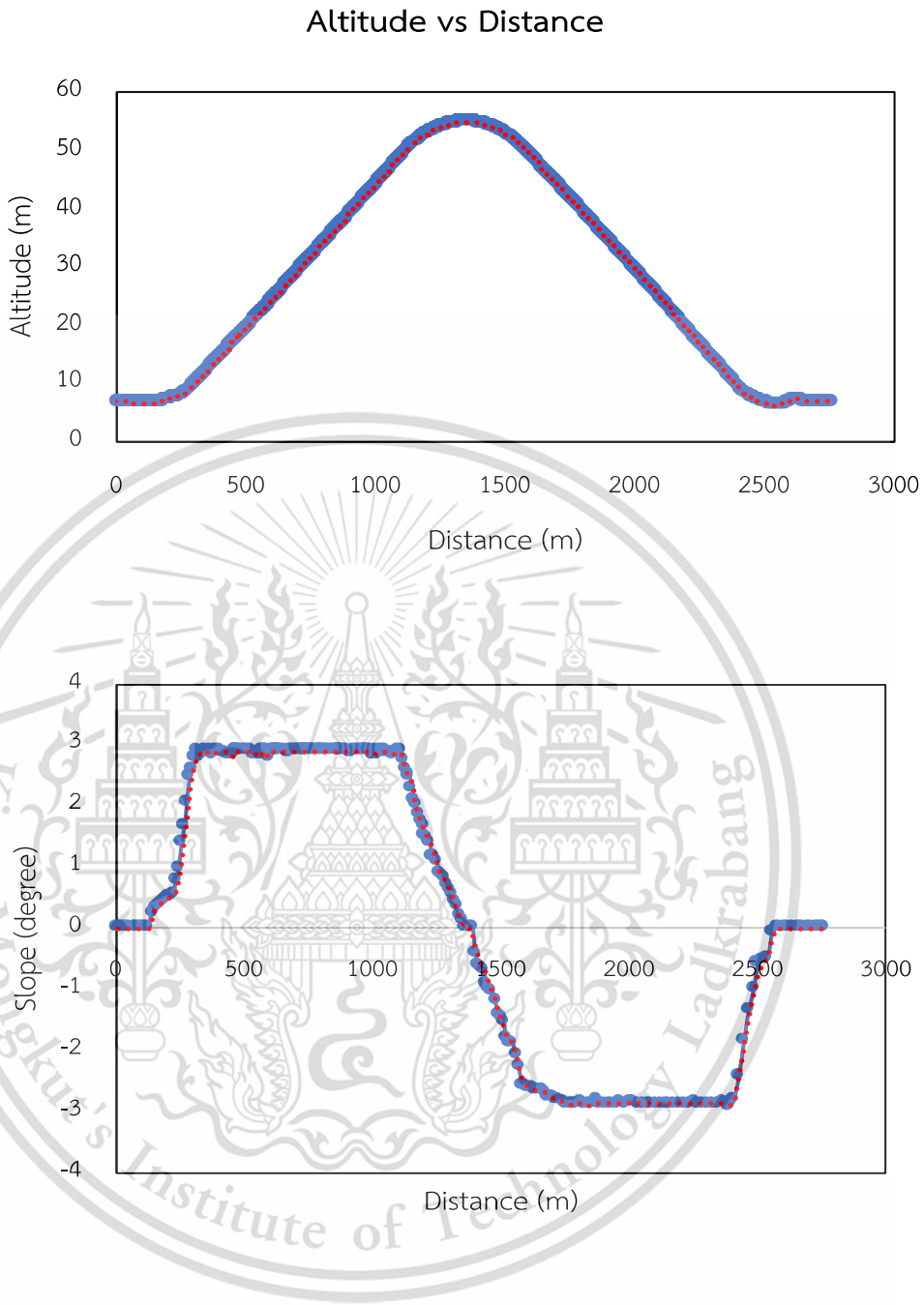

Figure 5.1 Altitude and slope profile of RAMA IX bridge

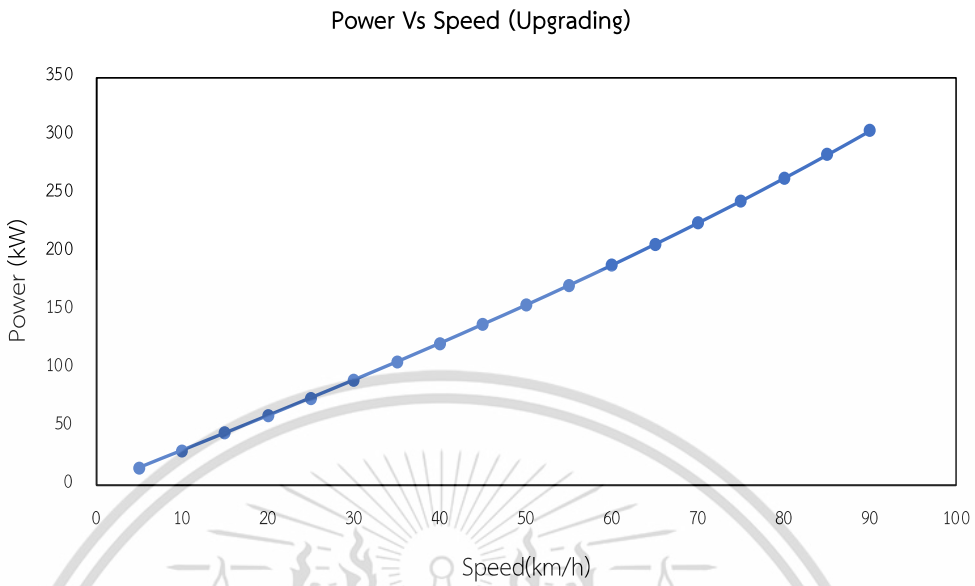

Figure 5.2 Demanded power on different cruising speed (upgrading)

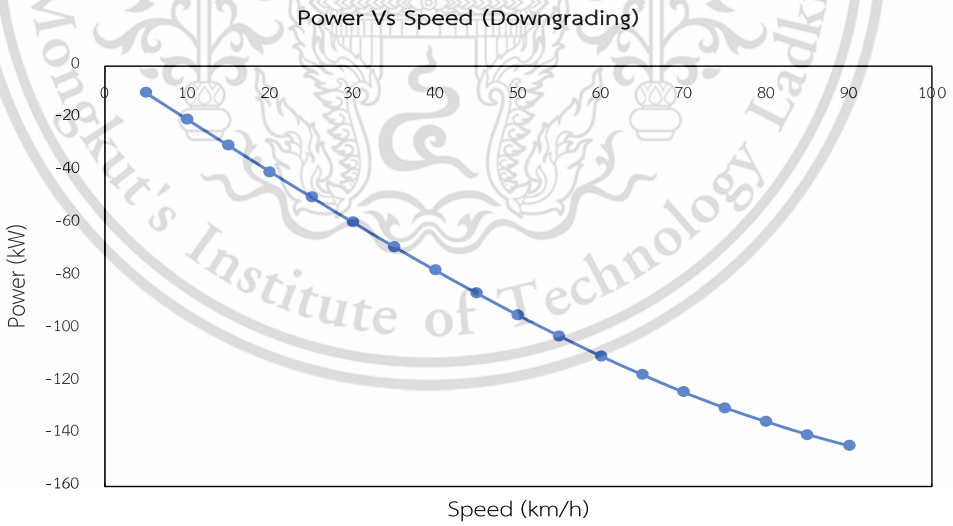

Figure 5.3 Demanded power on different cruising speed (downgrading)

Table 5.1 Power consumption over different cruising speed

Speed (km/h)	kWh/ km	Speed (km/h)	kWh/km
5	2.24	55	2.41
25	2.28	70	2.51
40	2.33	90	2.65

5.1.3 Speed reduction

Three driving profiles with different speed variations are constructed with the same length of decelerating zone (L_{up}). In this scenario, L_{up} is set as 700 m for the length of speed reduction region. The power demand and its consumption have been evaluated for each speed variations of 90 to 30 km/h, 90 to 45 km/h and 90 to 60 km/h. Figure 5.4 represents the three speed variation profiles, and it can be seen how the speed reduction works along the destinated road slope. In figure 5.5, the demanded power outputs per unit distance for each speed variation are indicated. According to the simulated outputs, it can be seen that the power demand runs at constant when there is no slope. However, as soon as it starts to climb the slope, the speed goes down from the constant value and power demand begins to reduce until the end of the decelerating region. After that decelerating region, it is designed to continue running at constant speed, so the power value goes up again along the rest of the slope. Also, speed range difference has a great influence on the power demand. The deceleration rate in 90 to 30 km/h is slower than that the other two because of its high speed variation. Therefore, the slower deceleration rate results in less consumption of power because the power demand goes to more negative. Moreover, although the power consumption per unit distance travelled is not proportional with high speed, the decelerating time is shorter while running at high speed, and power consumption has been increased. For that reason, power in 90 to 60 km/h is more consumed at 1.883 kWh per unit distance than the other.

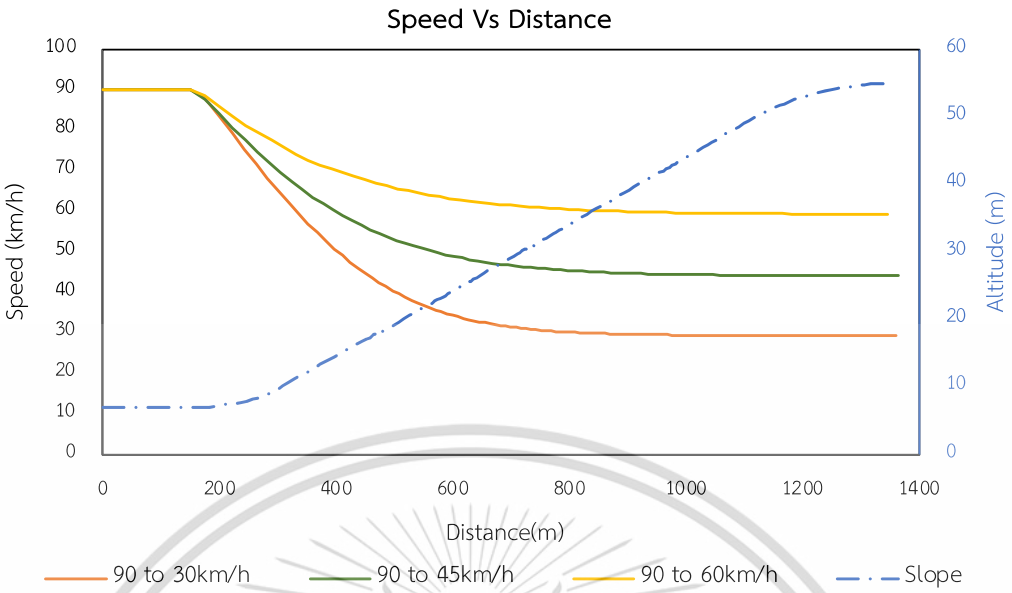

Figure 5.4 Speed profiles over distance on three types of speed variations

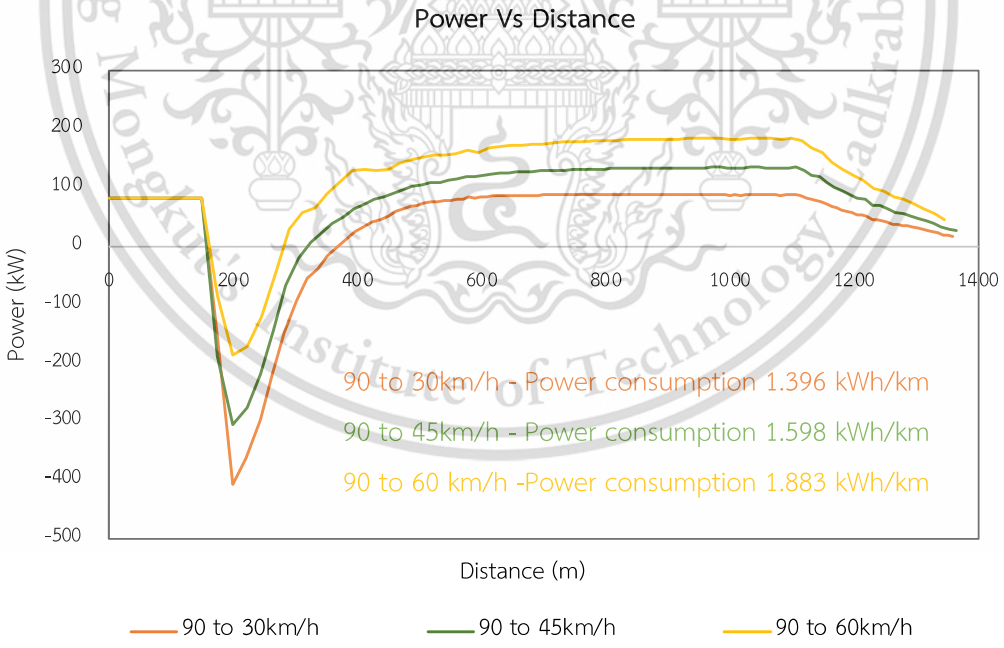

Figure 5.5 Power demand over distance for three speed variations

5.1.4 Go and stop

This scenario is developed to evaluate the bus performance on electric power and power consumption for dealing with traffic congestion on the uphill and downhill roadways. It recognizes various acceleration levels, engaging in several accelerating and decelerating procedures and frequent stops. Also, stopping distance and time change, depending on how congested the road is. For this simulation, actual speed data that was gathered on the bridge is used in which the bus is running with an average speed of 30km/h. The recorded speed profile for the whole slope, upgrading and downgrading, is as shown in figure 5.6 Figure 5.7 describes the required power and its consumption for the speed input while running on that slope. As shown in the results, the power requirement running on uphill roadway is higher than running on normal roadway. Furthermore, the resulting power demand stays at negative on downhill. It means that the negative power can be used in power recuperation for activating regenerative braking and recharging the battery.

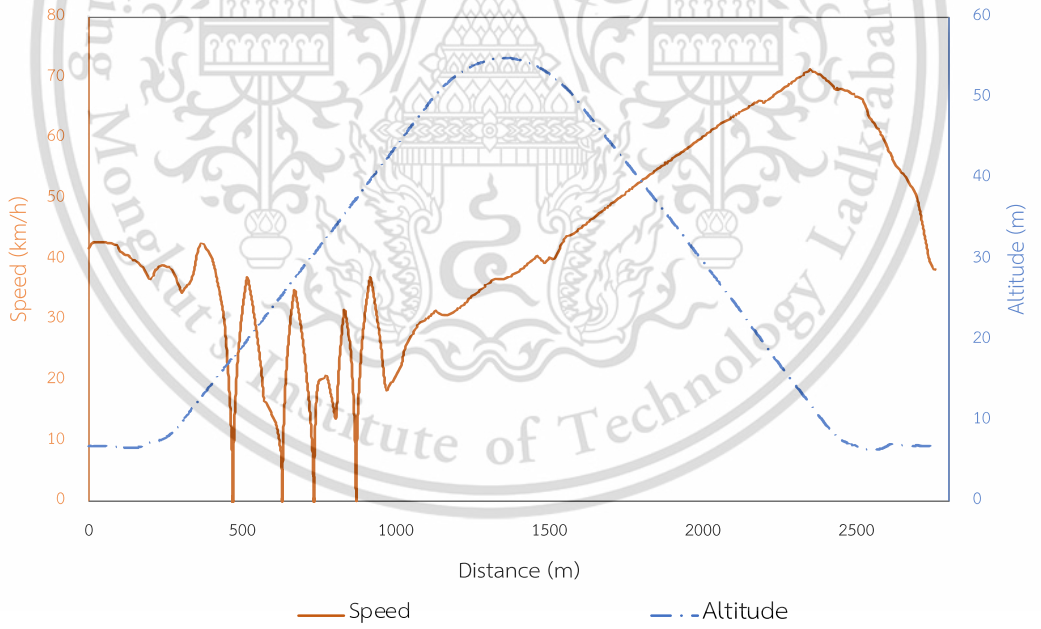

Figure 5.6 Actual speed profile over distance for RAMA IX slope

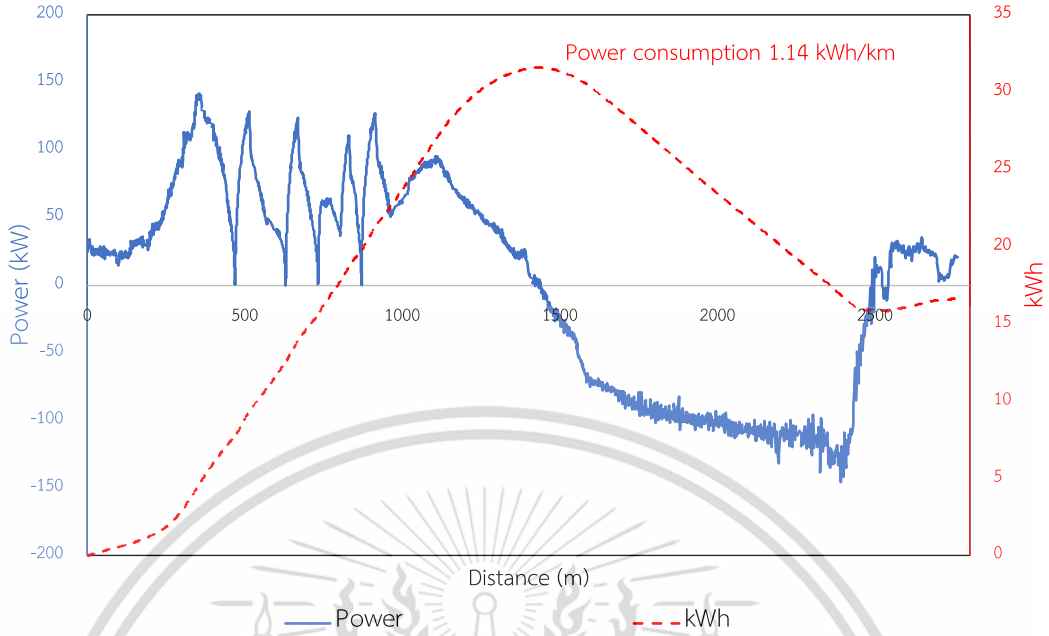

Figure 5.7 Power demand and its consumption over distance for Rama IX slope

5.2 Performance analysis for standard driving cycles

5.2.1 Vehicle performance

Two standard driving cycles, which are NEDC and WLTC class 3, are simulated by the simulation model mentioned in chapter 4. Figures 5.8 and 5.9 illustrate the bus's acceleration profiles as a function of speed of the NEDC and WLC driving cycles obtained by the simulation. For NEDC driving cycle, the bus begins by pausing for 11 seconds, then slowly picking up speed to 15km/h for 4 seconds, cruising at a constant pace for 8 seconds, braking to a complete stop in 5 seconds, pausing again for 21 seconds. The bus gradually speeds up over the following 49 seconds, reaching 32km/h in 12 seconds, cruises for 24 seconds and takes 11 seconds to come to a complete halt before pausing for another 21 seconds. At 117s , the bus gradually picks up speed to 50km/h in 26 seconds, cruises for 12 seconds, slows down to 35km/h in 8 seconds, cruises for a further 13 seconds, brakes to a complete stop in 12 seconds and finally

rests for 7 seconds. The cycle stops on 195 seconds, after which it repeats itself four times. Total 780 seconds pass by at an average speed of 18.35 km/h. After then, a more aggressive high- speed driving mode is activated. The top speed is restricted at 90 km/h. After a 20- second pause, the bus gradually increases its speed to 70 km/h in 41 seconds, cruises for 50 seconds, quickly slows to 50km/h in 8 seconds, and again accelerates to 70km/h in 13 seconds. At 201 seconds, the bus travels at 70 km/h for 50 seconds before gradually increasing its speed to 90 km/h and maintaining it for the rest of the cycle. That cycle has a 400 second total time and 62.6 km/h average speed. It has maximum acceleration of 1.04 m/s^2 and minimum acceleration at -1.39 $m/s^{2.}$

The WLTC class 3 driving cycle, which is more dynamic than standard driving cycle like NEDC, is representative of the majority of existing vehicles. It is more comprehensive and accurate to actual driving circumstances. The driving stages of the WLTC replicate various urban, suburban, rural and highways settings, with an equal distribution of urban and non- urban pathways. Each one has a unique top speed, up to 56.5 km/h in 589 second for urban, 76.6 km/h in 433 second for suburban ,and 90km/h in 455 second and 323 second for other two. So, the whole WLTC cycle travels at a maximum speed of 90km/h, with an average speed of 43.5 km/h for the duration of 1800 second. Compared to NEDC, it provides a wider travelling range and travels at higher speed, with shaper accelerations and decelerations, and with less idle time. The maximum acceleration runs at 1.75 m/s^2 and minimum at -1.5 m/s^2. In figures 5.10 and 5.11, the traction force obtained by the two driving cycles are compared favorably with each other. Comparing to the simulation results of power demand for these two cycles as shown in figures 5.12 and 5.13, it can be seen that demanded power and consumption in WLTC is much higher than that of NEDC because of higher acceleration and deceleration.

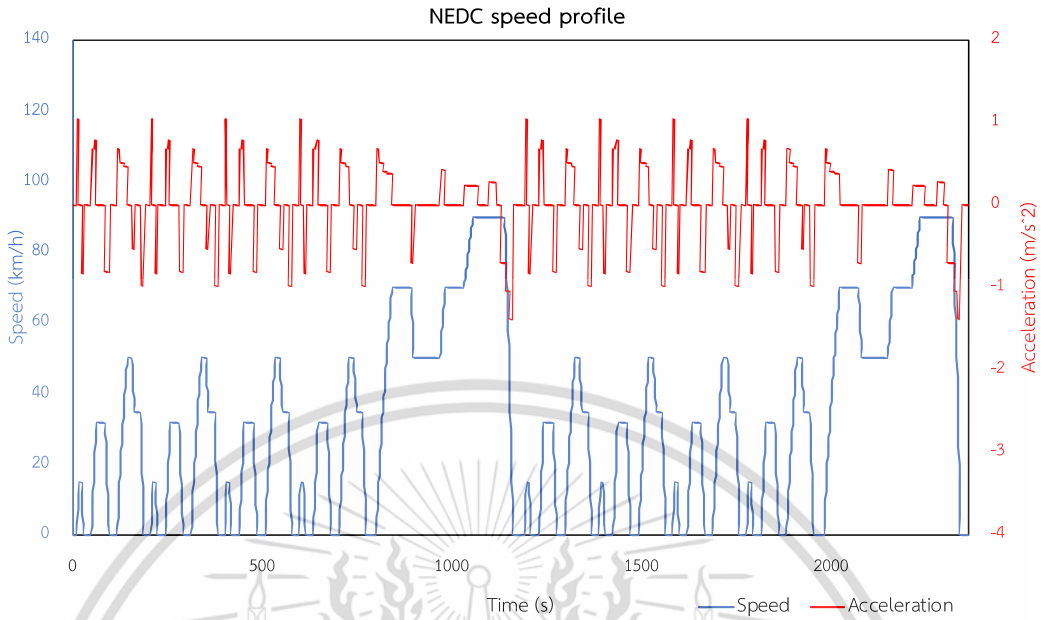

Figure 5.8 Speed and acceleration of NEDC driving cycle

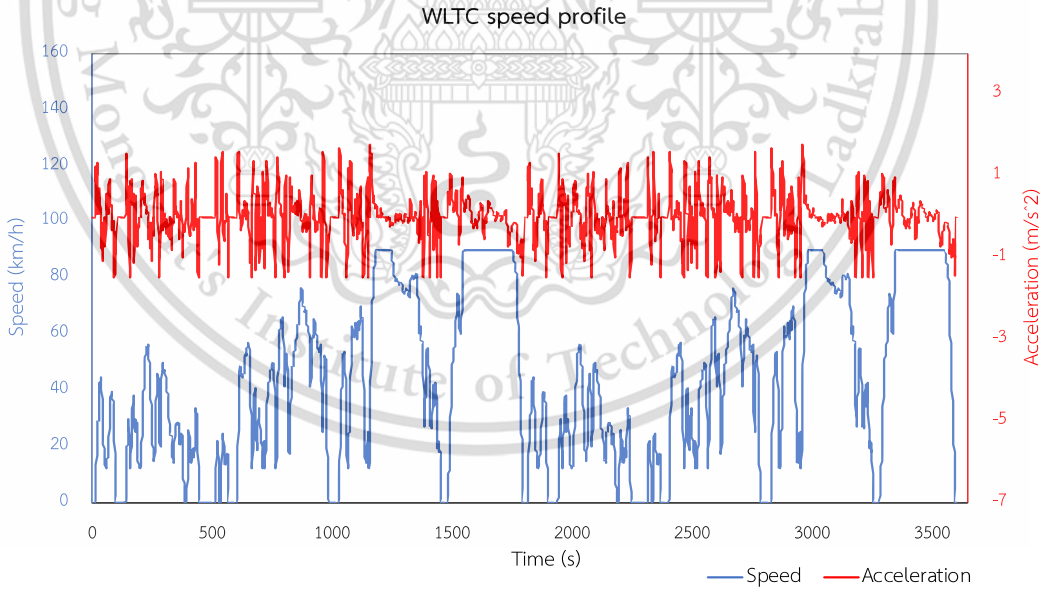

Figure 5.9 Speed and acceleration of WLTC driving cycle

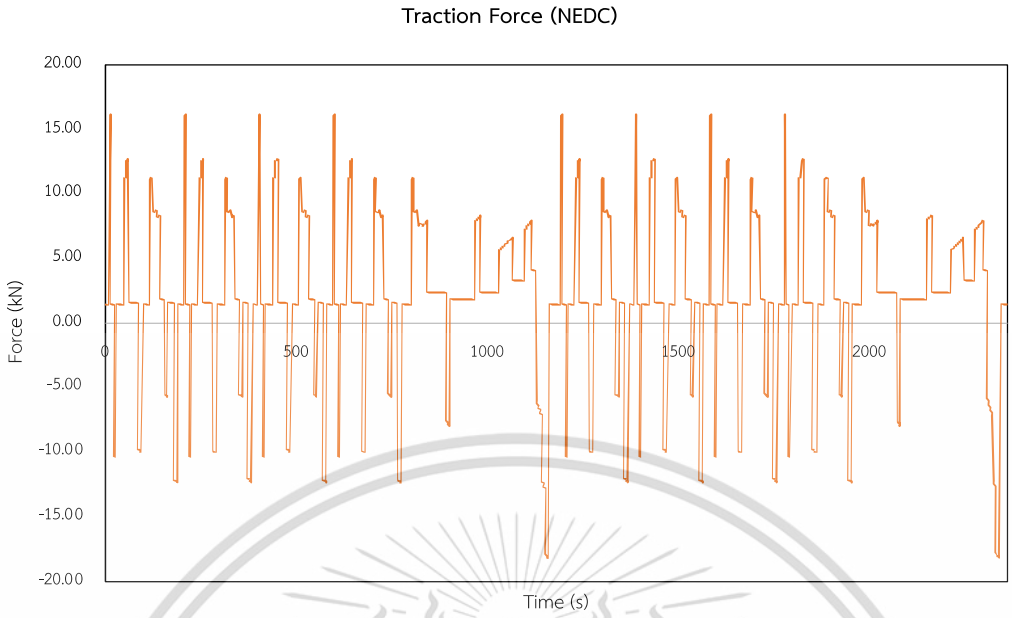

Figure 5.10 Traction force of NEDC driving cycle

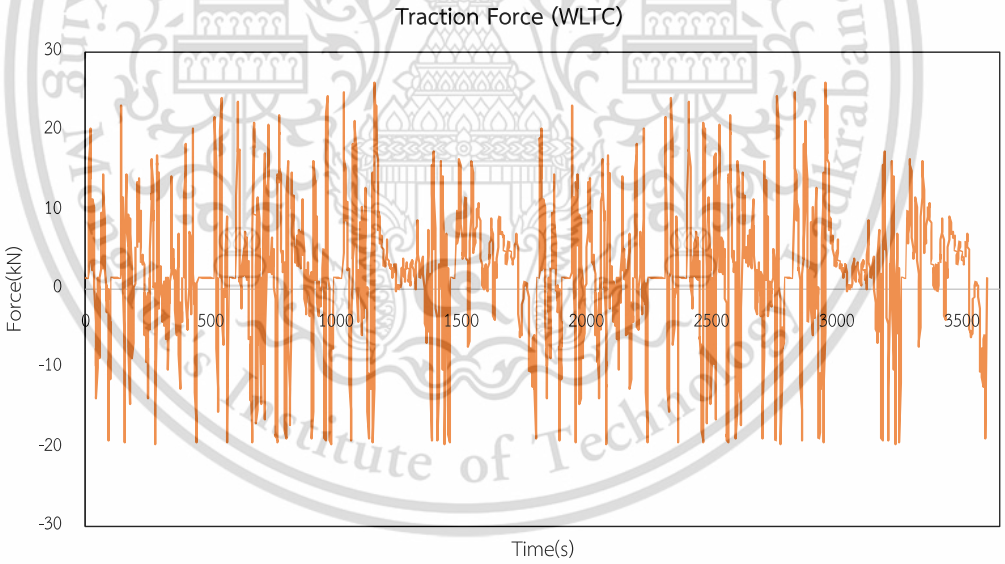

Figure 5.11 Traction force of WLTC driving cycle

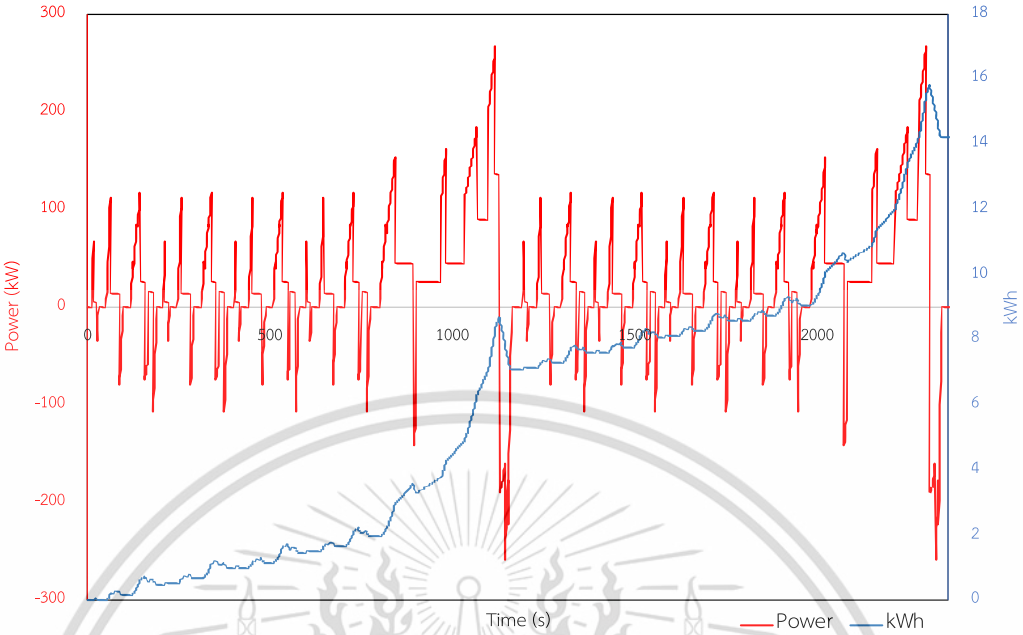

Figure 5.12 Demanded power and its consumption of NEDC cycle

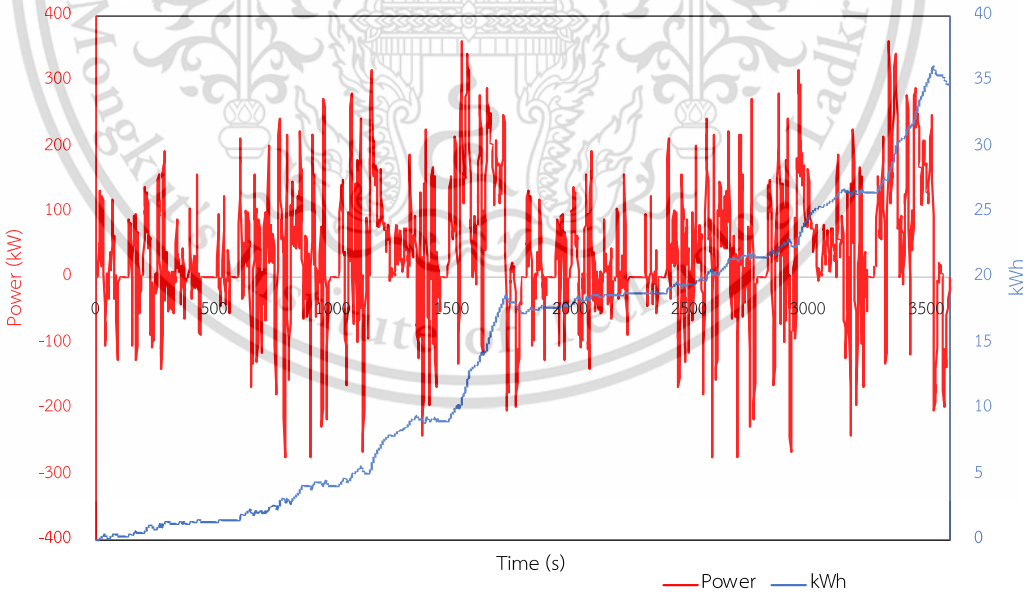

Figure 5.13 Demanded power and its consumption of WLTC cycle

5.2.2 Battery performance

Figure 5.14 – 5.17 display the results of the modeling of the whole batterypack's current, voltage, power, and consumption of the two cycles, NEDC and WLTC. The peak currents are displayed as the significant results of the high power demand for achieving rapid vehicle accelerations during the corresponding intervals. The negative values of the results on the graph reflect as the regenerative braking for the circumstances of the bus braking. According to the resulted battery voltage of the graphs, the voltage rises during regenerative braking and falls during high current discharge, which is power demand is at its highest. The negative value of the current means that the battery is being charged, hence the voltage increases, and positive value shows the discharging of the battery and the voltage decreases. Comparing to the power consumption results of the two driving cycles, WLTC consumes more than NEDC because of the rapid acceleration and deceleration. For the case of the battery SOC obtained by the two driving cycles, NEDC and WLTC, as shown in figure 5.17, SOC by NEDC drops off from 95% to 86% and WLTC is from 95% to 83% during the same

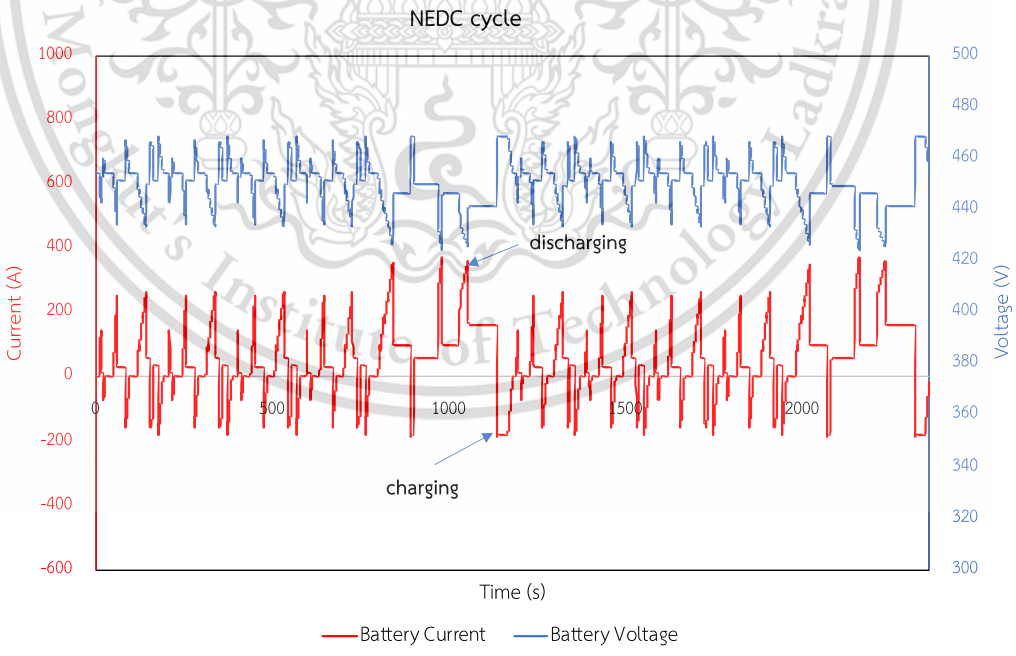

Figure 5.14 Battery current and voltage of NEDC cycle

time interval. In some points, the SOC goes up a little bit because the charging process occurs during regenerative braking.

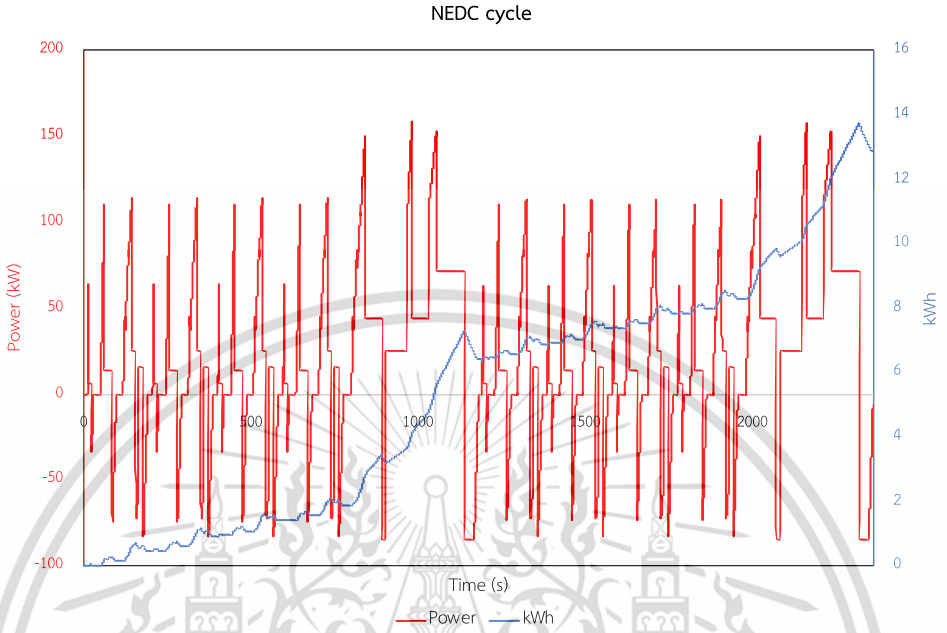

Figure 5.15 Battery power and its consumption of NEDC cycle

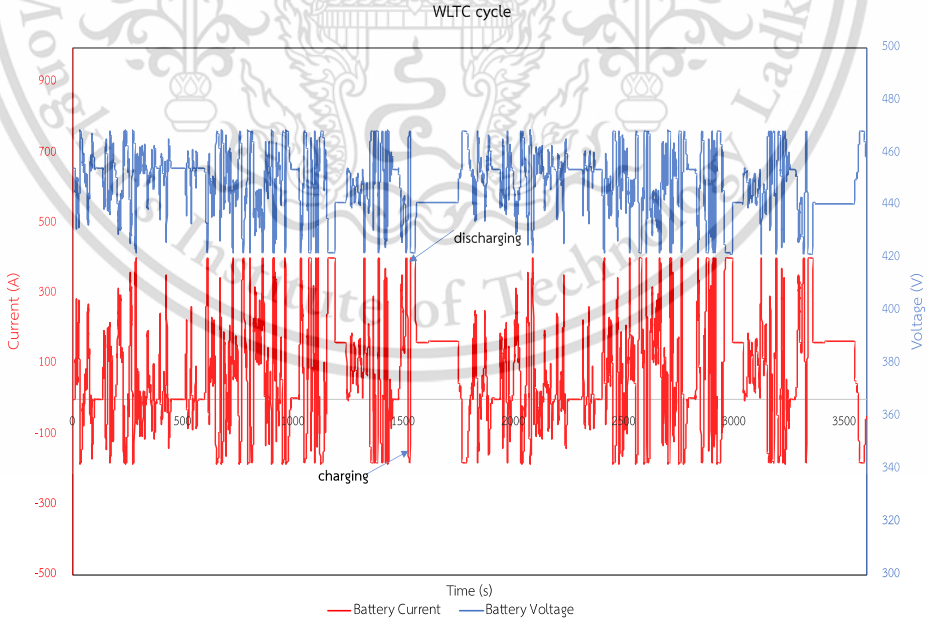

Figure 5.16 Battery current and voltage of WLTC cycle

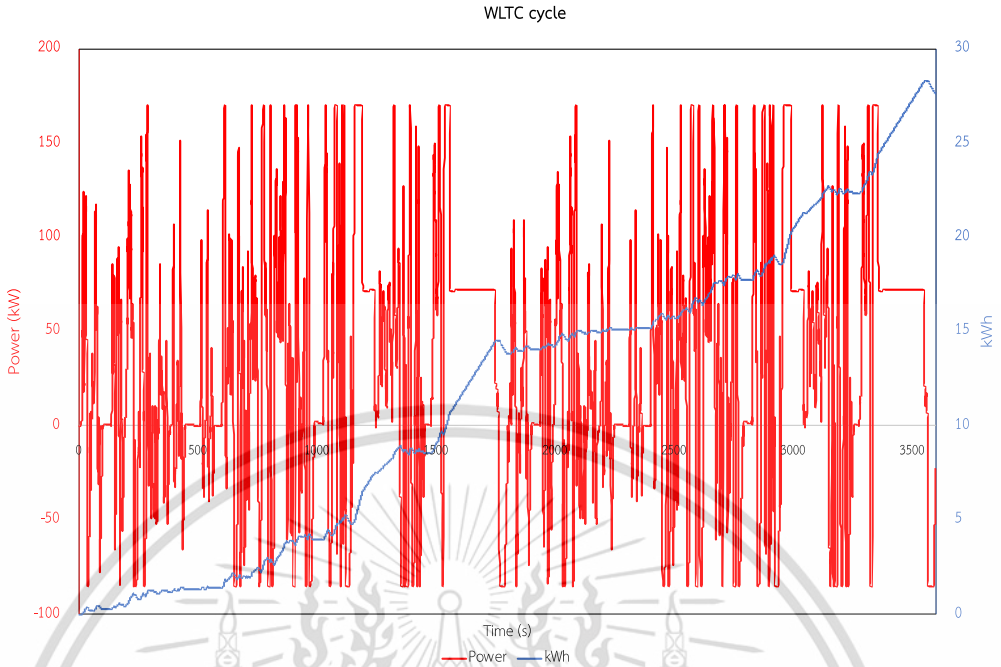

Figure 5.17 Battery power and its consumption of WLTC cycle

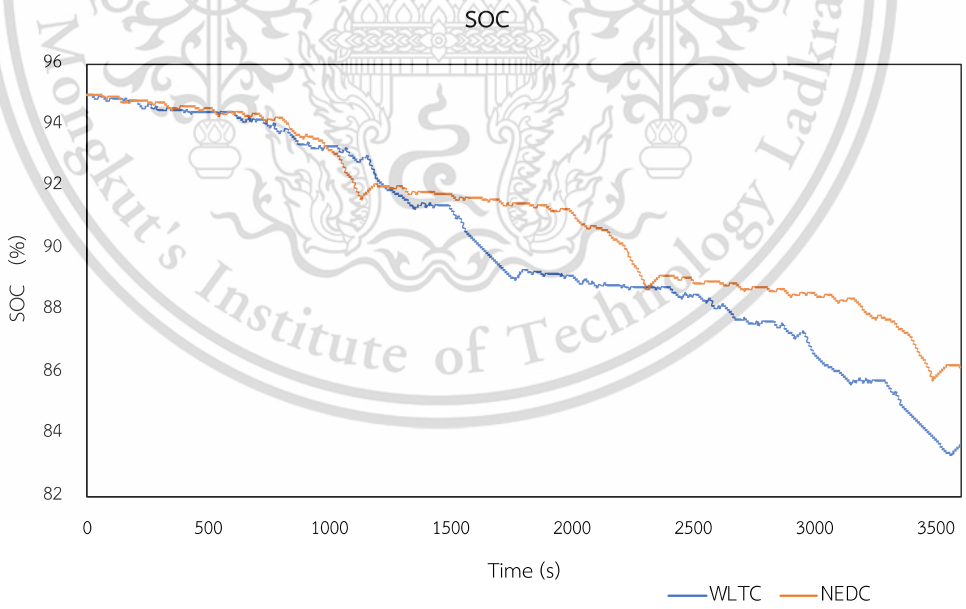

Figure 5.18 The battery SOC comparison of NEDC and WLTC cycles

5.2.3 Electric Motor Performance

This bus is designed to use only one the electric motor for propulsion. This single motor provides the torque needed to drive the bus. As a result, the electric motor which has the maximum power 170kW is decided to use in this simulation. As per selecting the suitable gear ratio mentioned in section 3.2.3, the gear ratio is designed to allow two criteria, the maximum motor torque and maximum velocity of the bus. For the first condition, the gear ratio is calculated to be around 2.5 and gear ratio for second condition is around 7. To meet these two conditions, the value of gear ratio is set as 5. The electric motor torque and power for the NEDC and WLTC driving cycles are represented in figures 5.19- 5.22. In accordance with the simulation results, the motor torque rises as the bus accelerates, and when it reaches the steady level, torque became less to get around the resistance and air drag. The negative value of torque mentions that the motor is working as a generator because of recuperation energy from braking. In figures 5.23 and 5.24, the operating points of the motor for three different gear ratios are illustrated. The simulation shows that motor operates along its maximum value area. It can be seen that when the gear ratio is low , the motor operates at lower speed and higher torque, and also it operates at higher speed and lower speed when the gear ratio becomes high. With low gear ratio 2.5, motor is working at high speed region, and it is at low speed region with high ratio 7.

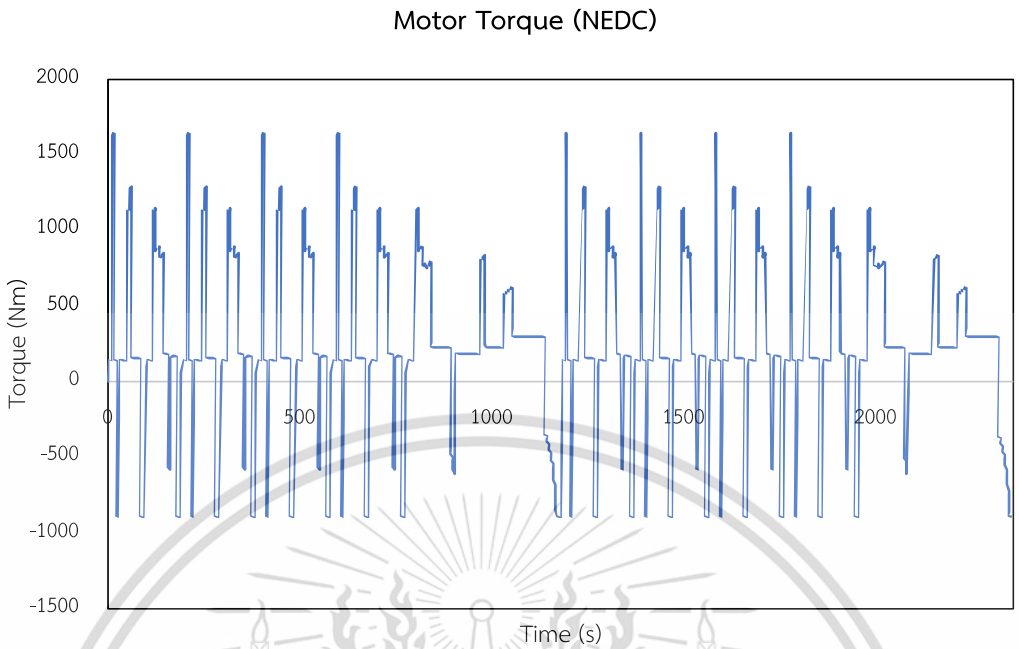

Figure 5.19 Electric motor torque of NEDC cycle (Gear ratio=5)

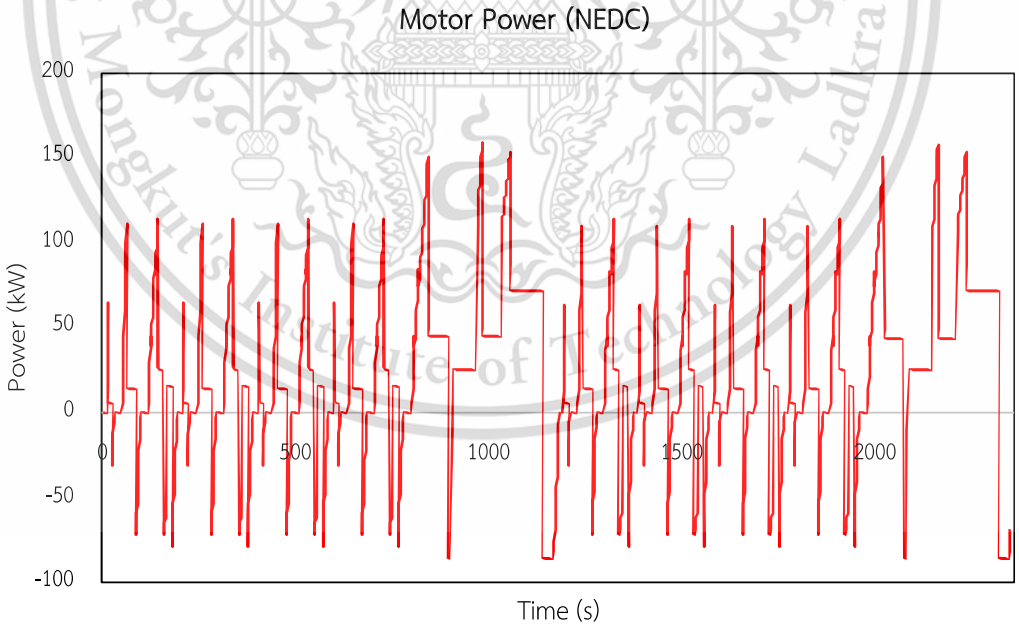

Figure 5.20 Electric motor power of NEDC cycle (Gear ratio=5)

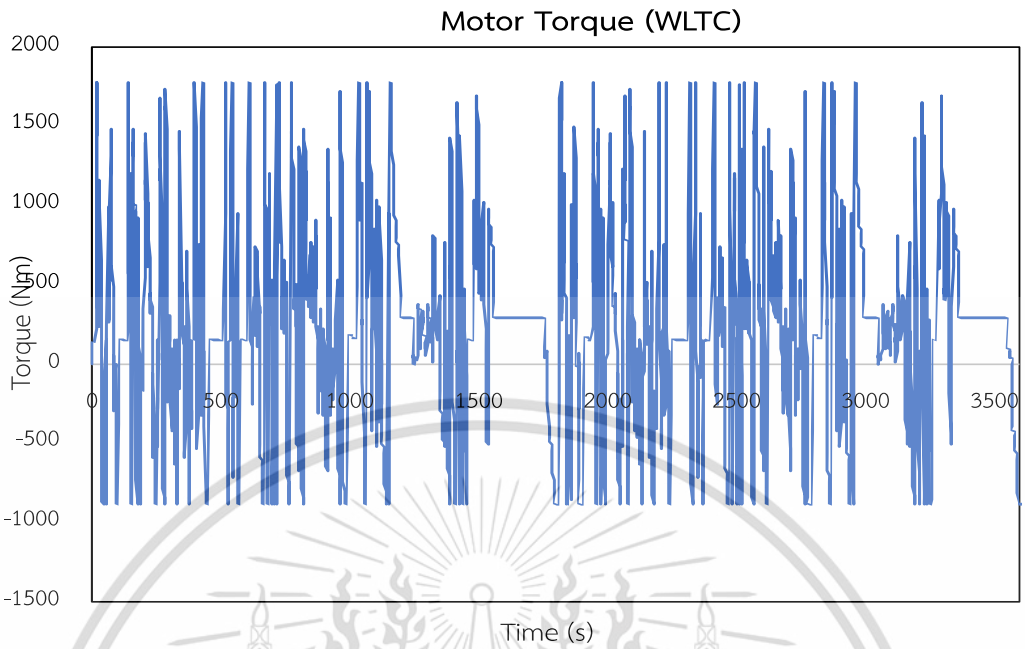

Figure 5.21 Electric motor torque of WLTC cycle (Gear ratio=5)

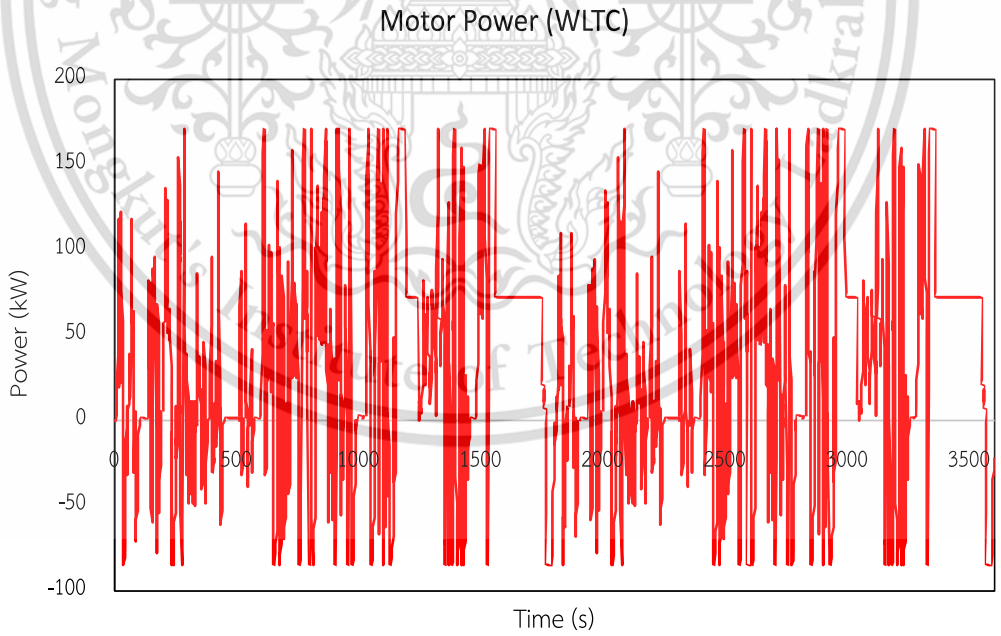

Figure 5.22 Electric motor power of WLTC cycle (Gear ratio=5)

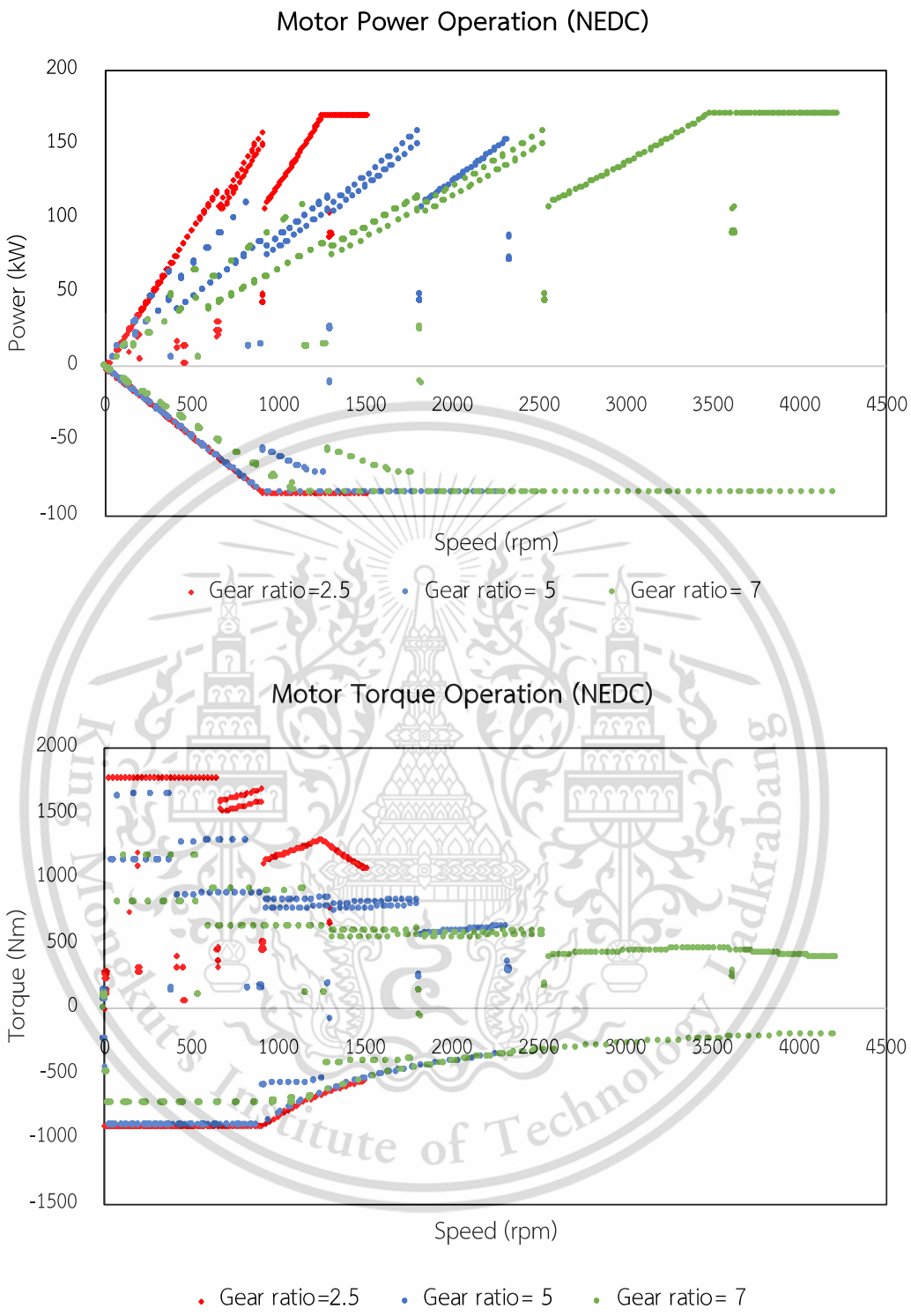

Figure 5.23 Motor operating points of NEDC cycle

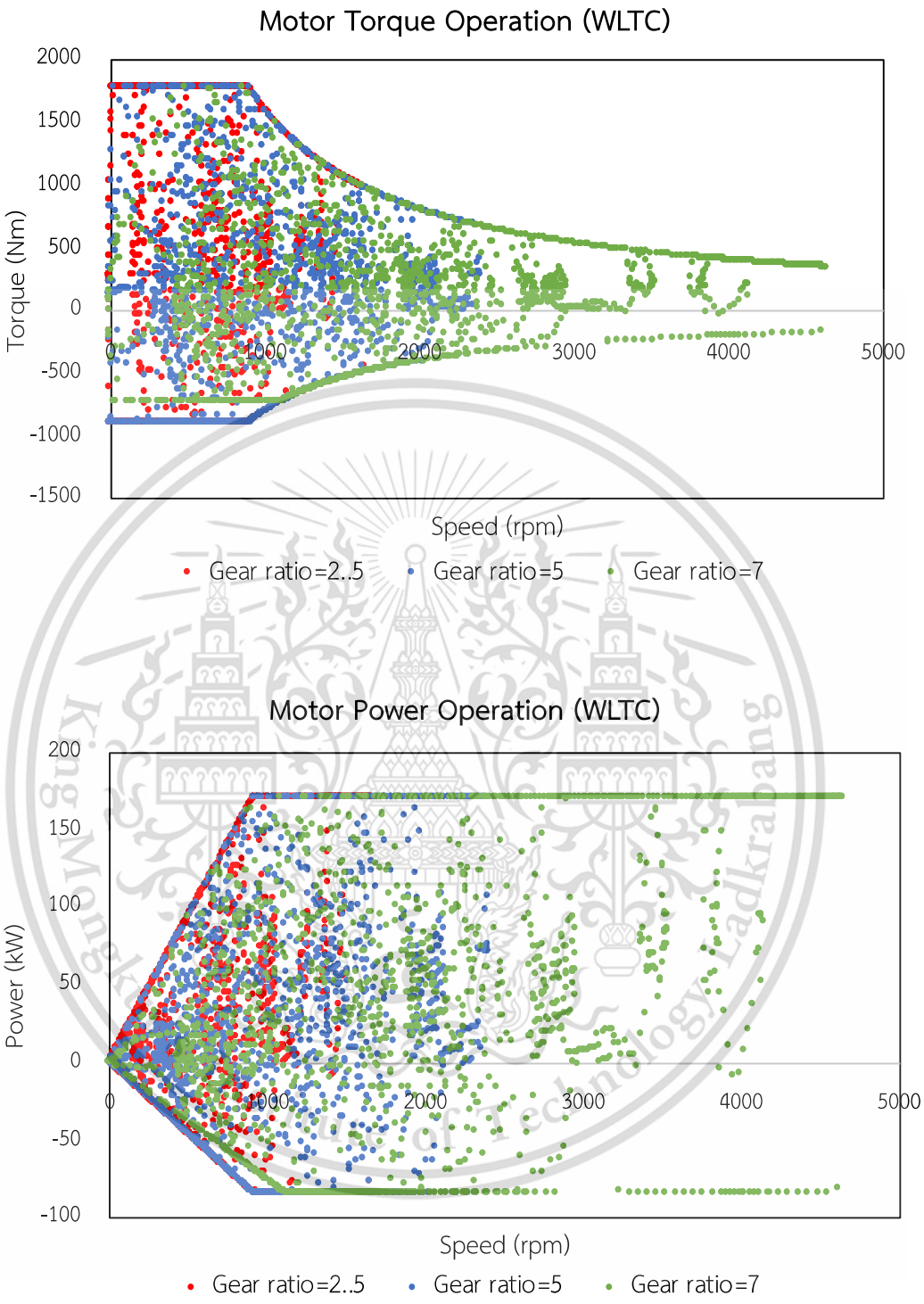

Figure 5.24 Motor operating points of WLTC cycle

5.3 Performance analysis for the case study of bus line 142

5.3.1 Analysis of real data collection for the driving test

As mentioned in section 4.2 about the development of route characterization, the road condition of bus line 142 is designed to test for this study. The route scenario is already mentioned in section 4.2. The distance for one round is approximate 100km, with RAMA IX bridge which has the highest altitude of 54 m, relative to the starting point of the bus. Figure 5.25 describes the recorded altitude and slope profile over the horizontal distance for the whole route of one complete round. The collected data of speed profile, driving from Samaedam bus depot to Samutprakan crocodile farm and back, is expressed in figure 5.26. The bus is running with the average speed of 28.45 km/h and maximum speed of 83.4 km/h. Summary of the simulated results for the bus performance is given in table 5.2. Simulated rated power demand from the bus for going is around 16kW and maximum at 140kW. For coming back, it is required around 165kW as its maximum demanded power. Simulated average power consumption per kilometer from Samaedam bus depot to Samutprakan crocodile farm is 0.502 kWh/km and 0.482kWh/km from Samutprakan crocodile farm to Samaedam. The result of power demand for the whole round is as shown in Figure 5.27. The result shows that power is demanded the most when the bus is climbing on the bridge because the bus requires to provide more traction force to climb the bridge while considering of gradient resistance.

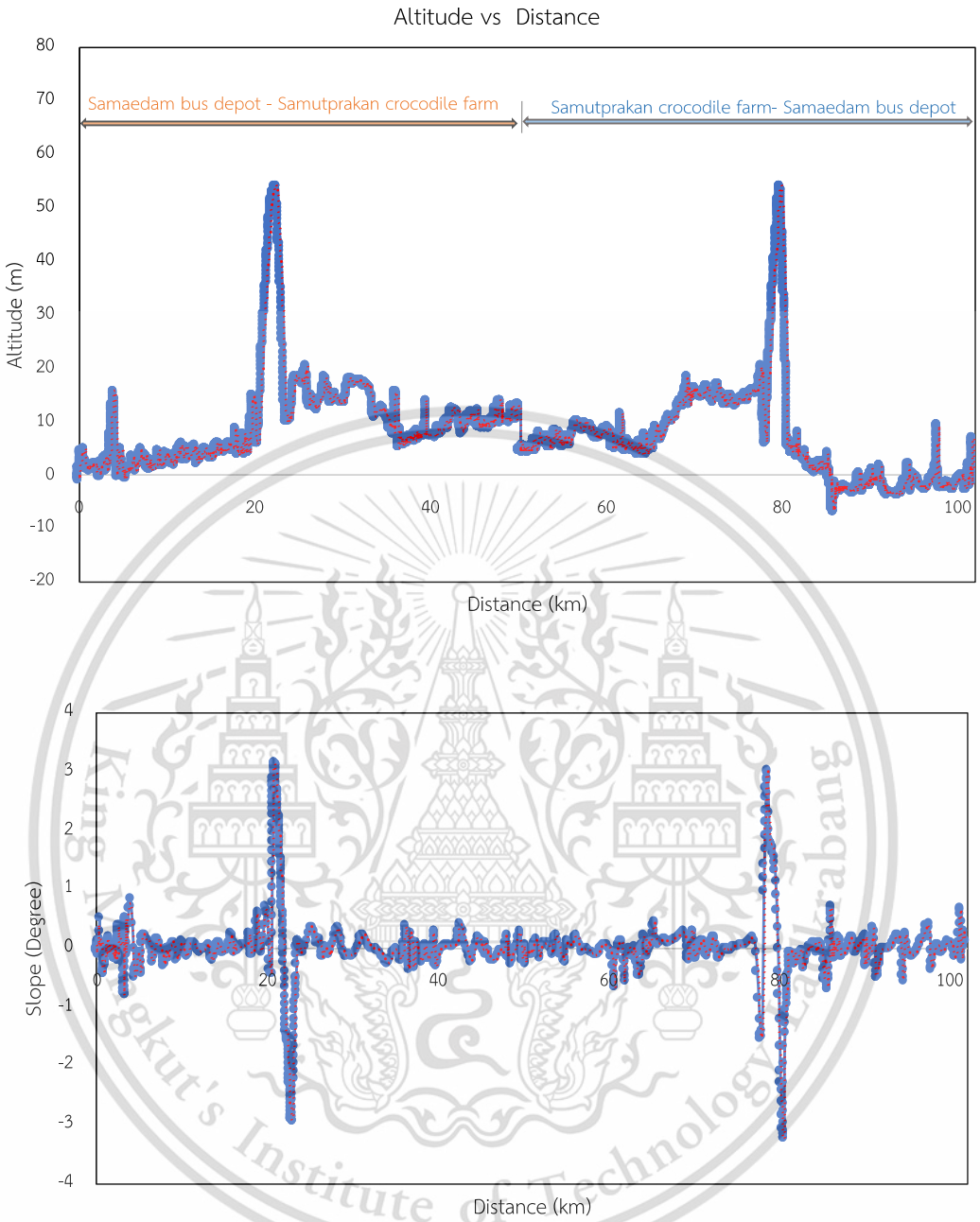

Figure 5.25 Altitude and slope profile for the route of bus line 142

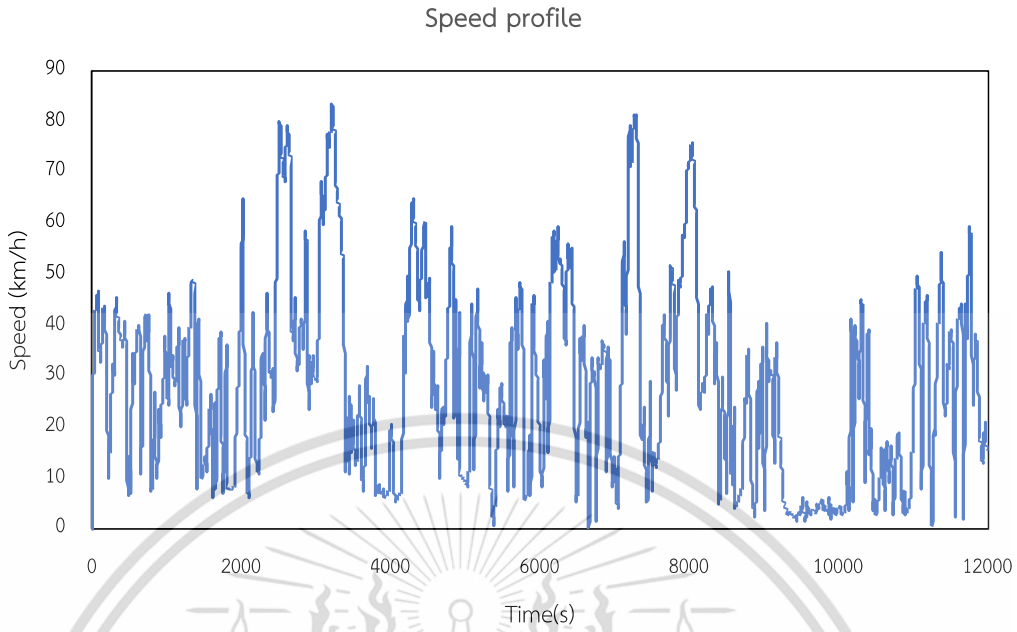

Figure 5.26 Real speed profile of bus line 142

Table 5.2 Summary of bus performance for real driving test

Attribute	Samaedam bus depot to crocodile farm	Crocodile farm to Samaedam bus depot
Time(s)	5340	6680
Average speed(km/h)	32.10	25.5
Maximum speed(km/h)	83.36	81.33
Rated power demand(kW)	16.21	12.41
Maximum power demand(kW)	139.70	164.89
Net energy consumption (kWh)	23.90	22.82
Power consumption per km (kWh/km)	0.502	0.482

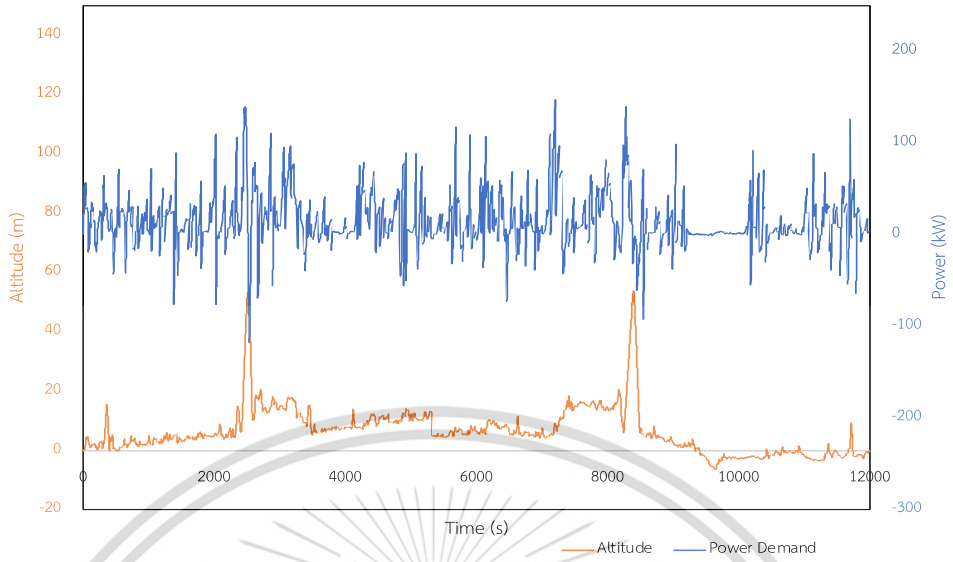

Figure 5.27 Simulated power demand of real driving cycle

5.3.2 Battery and motor performance analysis for real driving test

For the sake of battery performance, the simulated battery voltage stays in control of desired maximum operation voltage of electric bus design, 500V as shown in figure 5.28. It can be seen that output voltage will vary regarding the power request of electric bus. The maximum battery current drawn by the bus is approximately 340A. The behavior of battery current is also represented in figure 5.28. The maximum battery power output is approximately 190kW in simulation as illustrated in figure 5.29. Power consumption is around 0.635 kWh/km while heating and air-conditioning is not taken into consideration and regenerative braking is fully applied.

In the case of the performance analysis of electric motor with the selected value of gear ratio,5, the speed of motor operates 0- 2200 rpm with the nominal speed of 750rpm. Figures 5.30 and 5.31 present the torque and power of the electric motor over the real test driving cycle. The maximum torque and peak power of approximately 1300Nm and 170kW, respectively. Since climbing the high- slope bridge takes a lot of traction, the bus draws these maximum torque and power. Figure 2.32 shows the motor operation points of the selected electric motor for the real test driving. It operates within the limited range of motor speed, torque, and power.

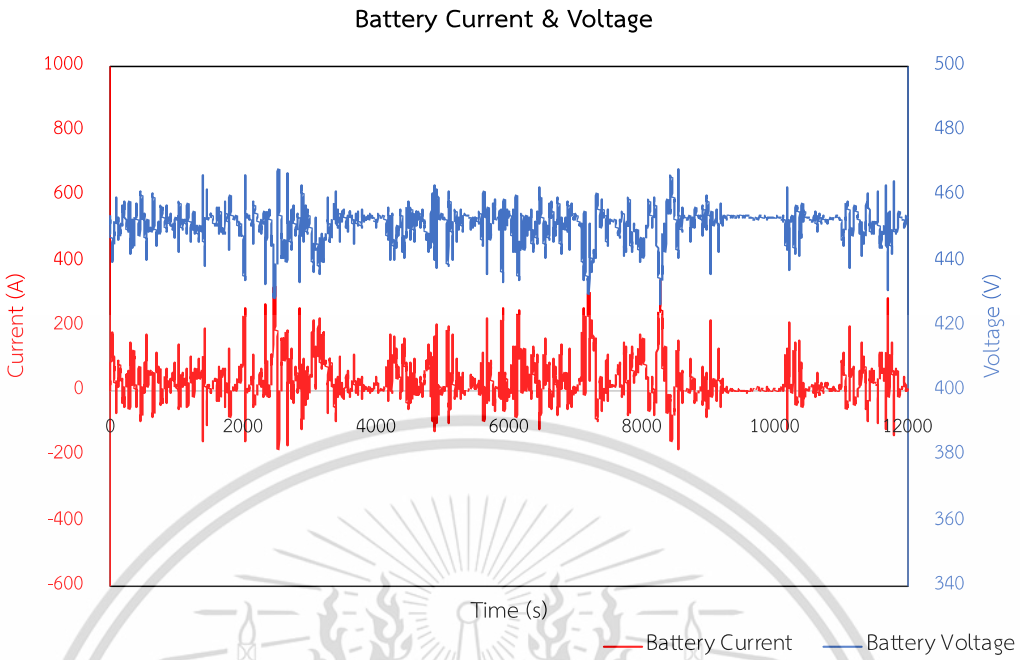

Figure 5.28 Battery current and voltage of real driving cycle

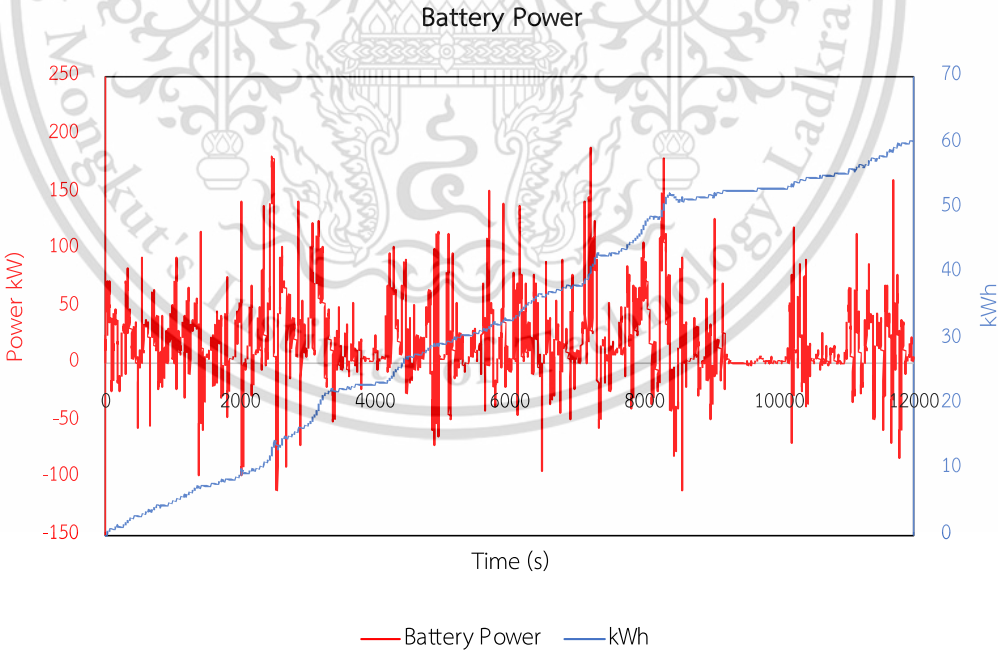

Figure 5.29 Battery power of real driving cycle

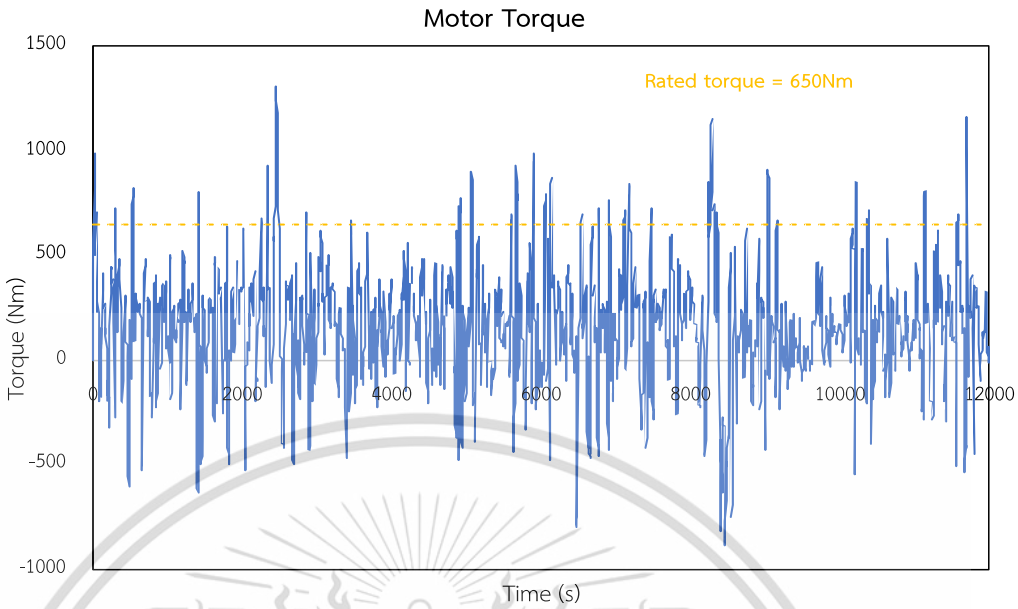

Figure 5.30 Motor torque for real driving cycle

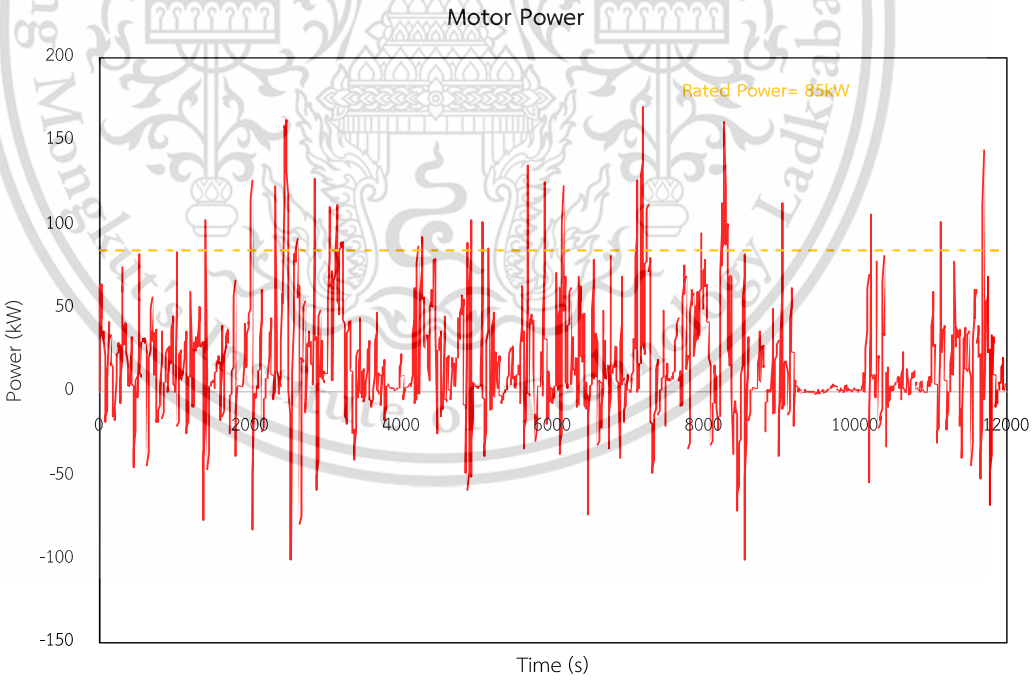

Figure 5.31 Motor power for real driving cycle

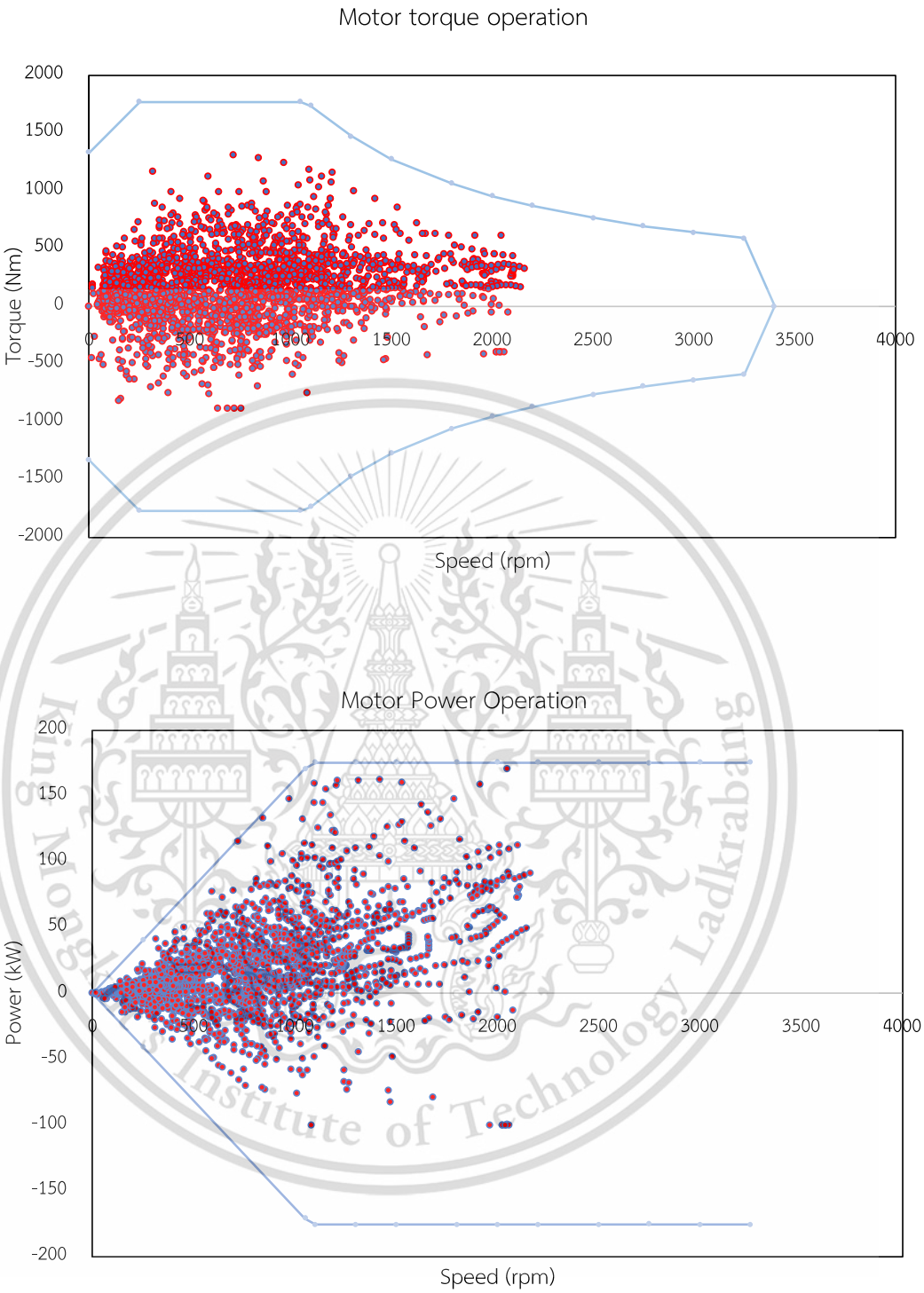

Figure 5.32 Motor operating points for real driving cycle

5.4 Analysis of the effect of regenerative braking on battery performance

To analyze the impact of regenerative braking on power consumption, three different variables are defined for the braking system. The first level is “no recharging”, zero percent of regenerative braking, which corresponds to the no regenerative braking. The second one limits recharging for the batterypack and only recovers some percentage of the brake force. The last one represents full regenerative braking, 100 percent.

The batterypack provides not only for positive (for propulsion) but also for negative (for recharging- power recovery through braking) power values. So, negative power went back to recharge the battery and for the present analysis, the amount of recharging power are determined according to the abovementioned three variables. In figure 5.33, it represents how each limitation of regenerative braking affect the battery output power. The variable of regenerative braking shows varying correlations with power consumption, as compared in figure 5.34. Apparently, regenerative braking reduces the power consumption of the bus according to its various limitations. When it is looked into the SOC, SOC levels have increased as long as the battery is charged due to the regenerative braking. Comparison of different SOC levels for each stage of regenerative braking is shown in figure 5.35.

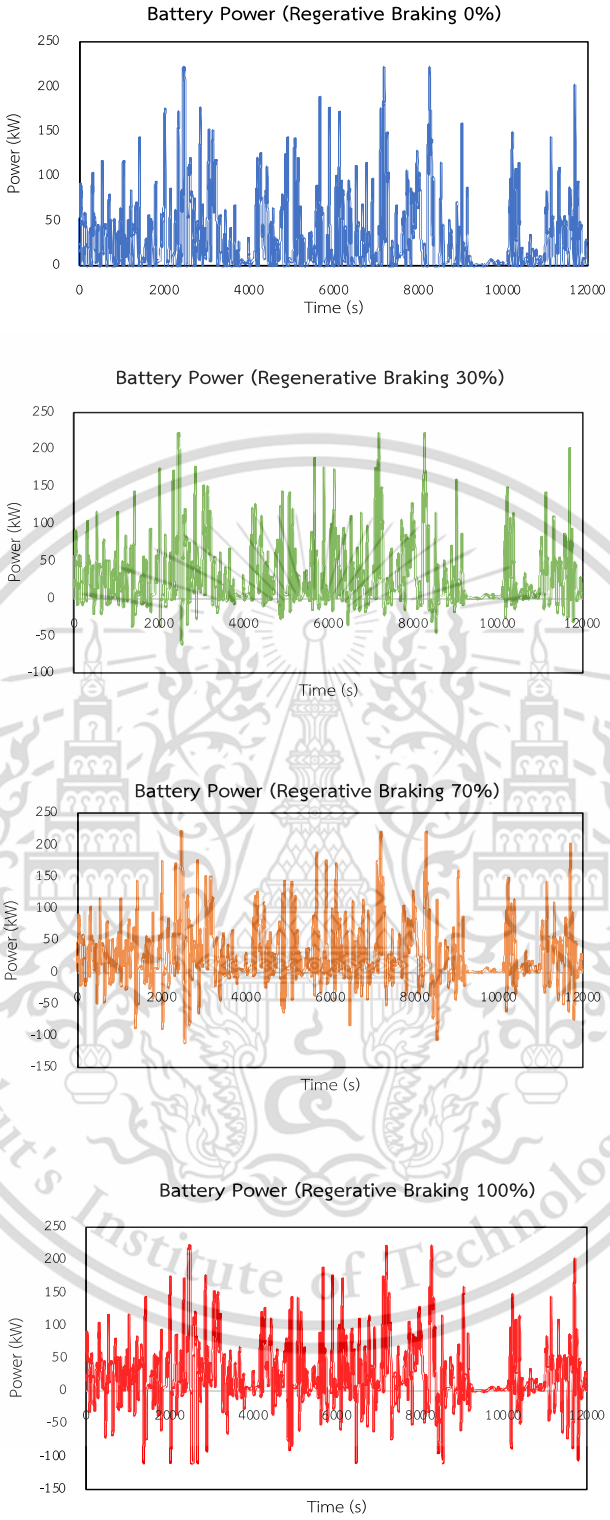

Figure 5.33 Battery power output with four levels of regenerative braking

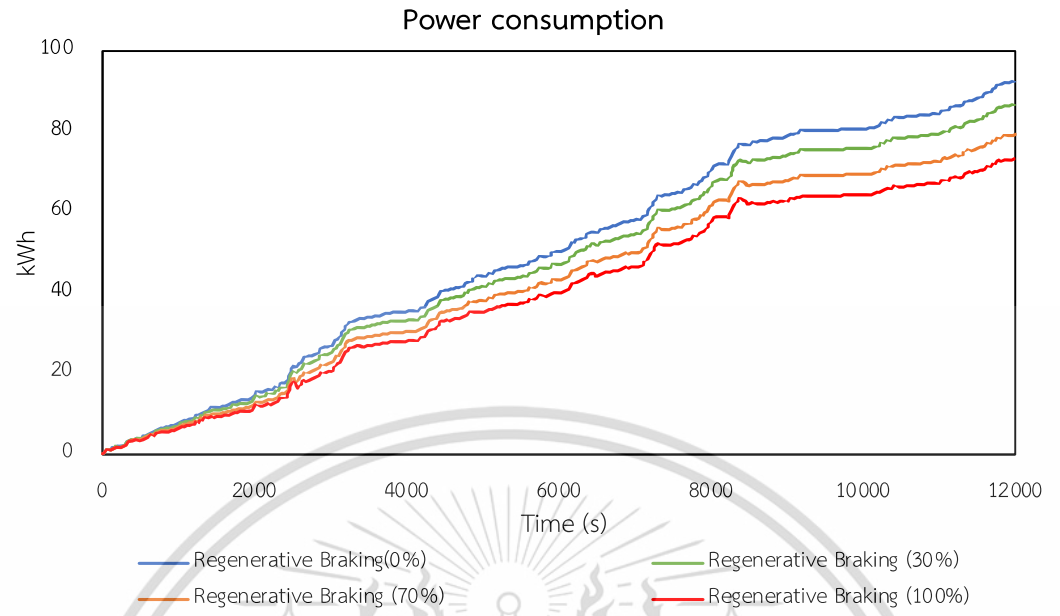

Figure 5.34 Comparison of power consumption for four levels of regenerative braking

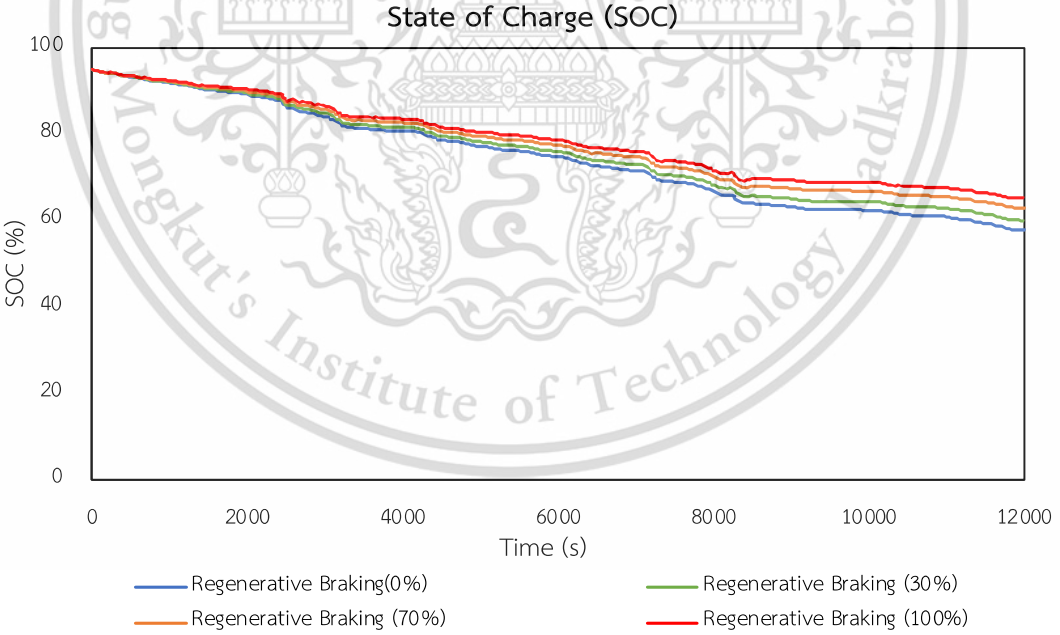

Figure 5.35 Comparison of SOC for four levels of regenerative braking

5.5 Analysis of effect of different parameters on performance of the bus

5.5.1 Gear ratio

The effect of gear ratio on the performance of the vehicle is analyzed. According to the above mentioned in section 3.2.3, the gear ratio is made to accommodate the maximum moto torque and the bus's maximum speed. The gear ratio for the first situation is estimated to be approximately 2.5, while the gear ratio for the second condition is estimated to be 7. As shown in figure 5.36, with the gear ratio of 2.5:1, average power consumption per distance goes to 0.74 kWh/km, and the motor torque is 1775 Nm with the maximum operational motor speed, 1127 rpm. Whereas with the gear ratio of 7:1, motor runs at the motor torque of 1650Nm with the maximum speed of 3200 rpm and average power consumption per distance is 0.77kWh/km. In accordance with the simulated results with higher gear ratio, the motor runs at low torque in high operational speed range, enabling the bus to go for higher accelerations, however, the motor has a surge in torque when climbing up the bridge because it runs at low speed along the bridge. And also, the power in higher gear ratio is more consumed than the lower one. With the lower gear ratio, the motor runs only at low speed, so it needs higher torque to provide the wheel. Figure 5. 37 demonstrates how the motor operates with these two gear ratios.

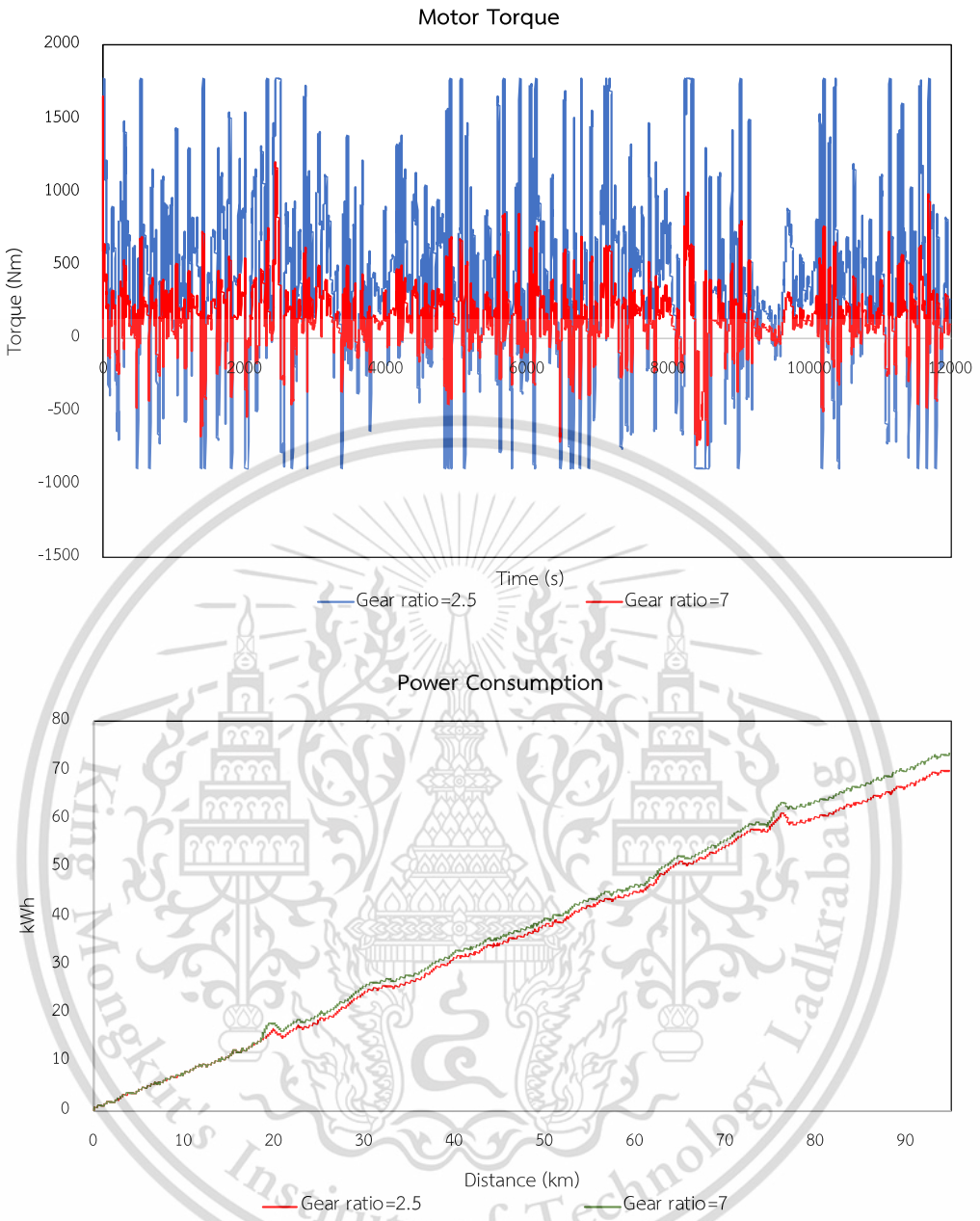

Figure 5.36 Comparison of motor torque and power consumption for two different gear ratios

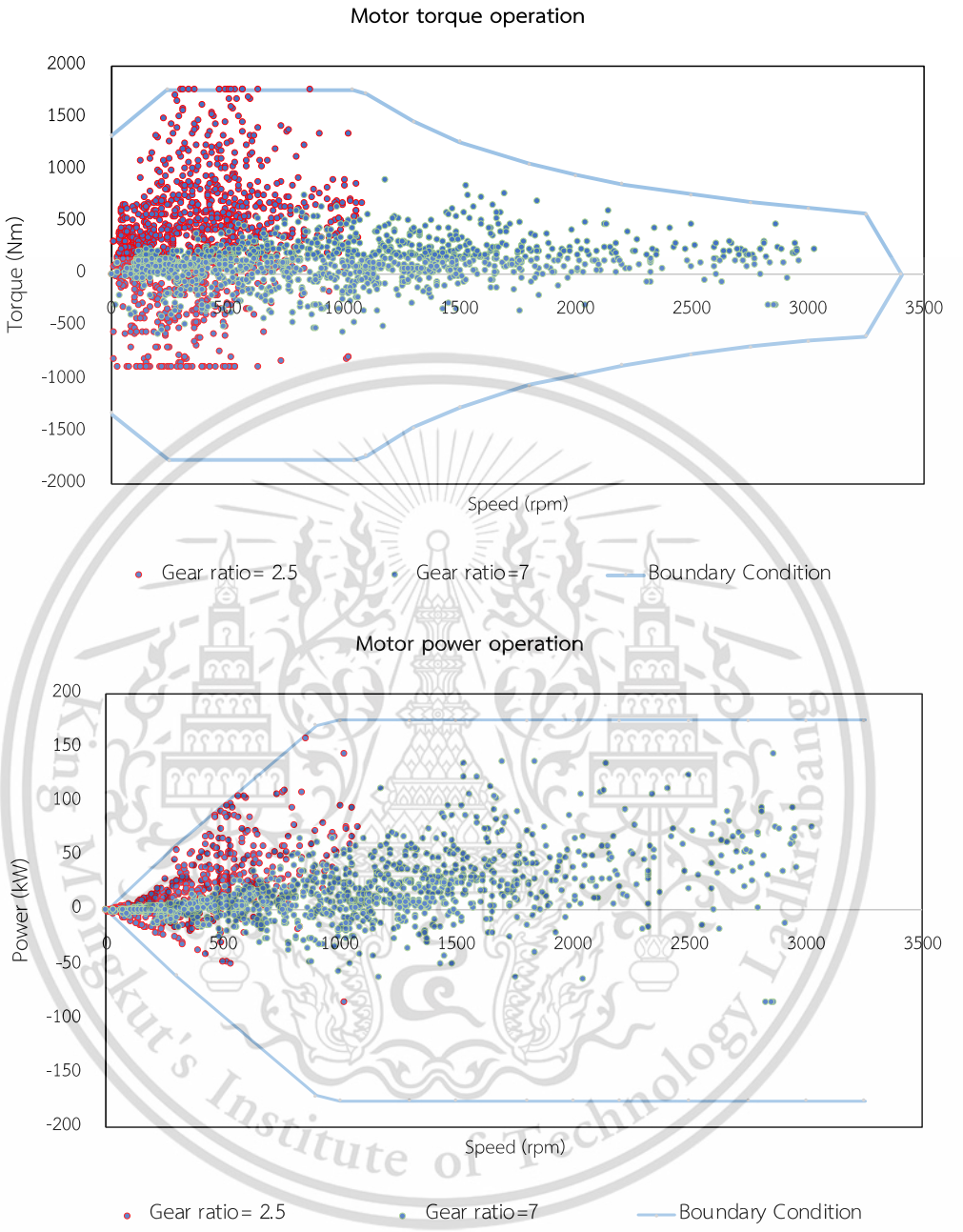

Figure 5.37 Motor operating points for two different gear ratios

5.5.2 Electric motor

Analysis of the impact of the motor's maximum power and motor torque on the performance of the bus is looked into this section. For this observation, two electric motors with different motor torque and power are compared for the motor performance. As a motor 1, reluctance- assisted permanent magnet motor with peak torque of 1775 Nm and peak power of 170kW within speed range of 0- 3250rpm is selected. And asynchronous traction motors that produce maximum power of 2 x 125kW and maximum torque 2 x 485 Nm from relatively high speeds of 11,000 rpm is chosen as the motor 2. The gear ratio can be changed to 22:1 in motor 2 since that operational speed range is wide. Figure 5. 38 shows the operating points of these two motors for our recorded driving cycle. It can be seen from figure that all of these operating points are not over than the maximum limits of their own motor. As the motor 1 works in lower operational speed range than motor 2, the torque of motor 1 operates in higher range. For the investigation of the efficiency of the two motors, they are represented in figure 5.39. As the simulated results, motor 1 keeps the maximum efficiency of 94% and motor 2 has 91% of maximum efficiency. As the results, it is noticeable that motor design and its selection has a strong relationship with the operational speed range. So, the manufactures can make a choice from this information for resizing the motor to be larger or smaller according to the requirements of their product design and needs. Also, both motors can satisfy the design requirements of this study, especially, the case for the RAMA IX slope.

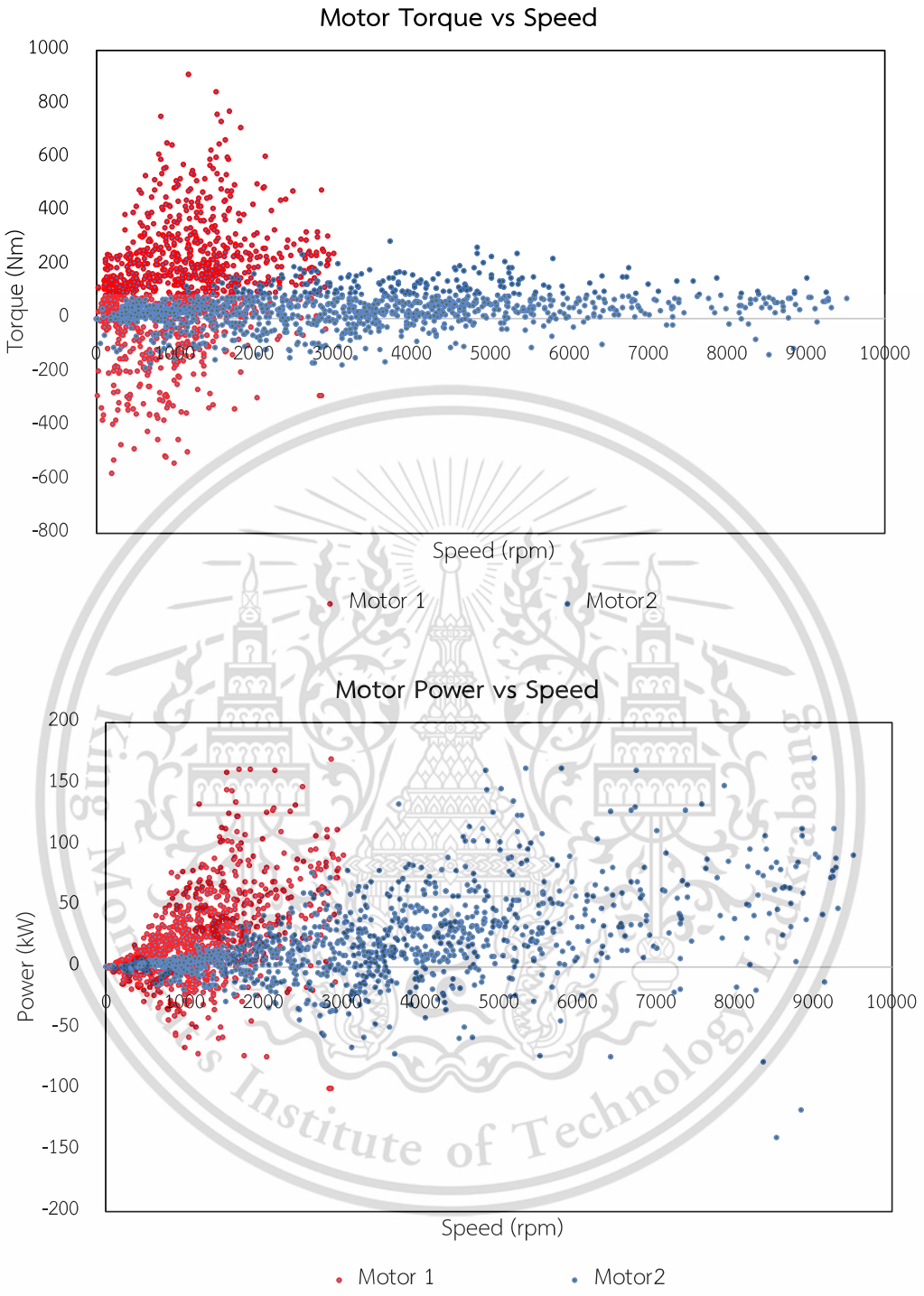

Figure 5.38 Motor operating points for two different motors

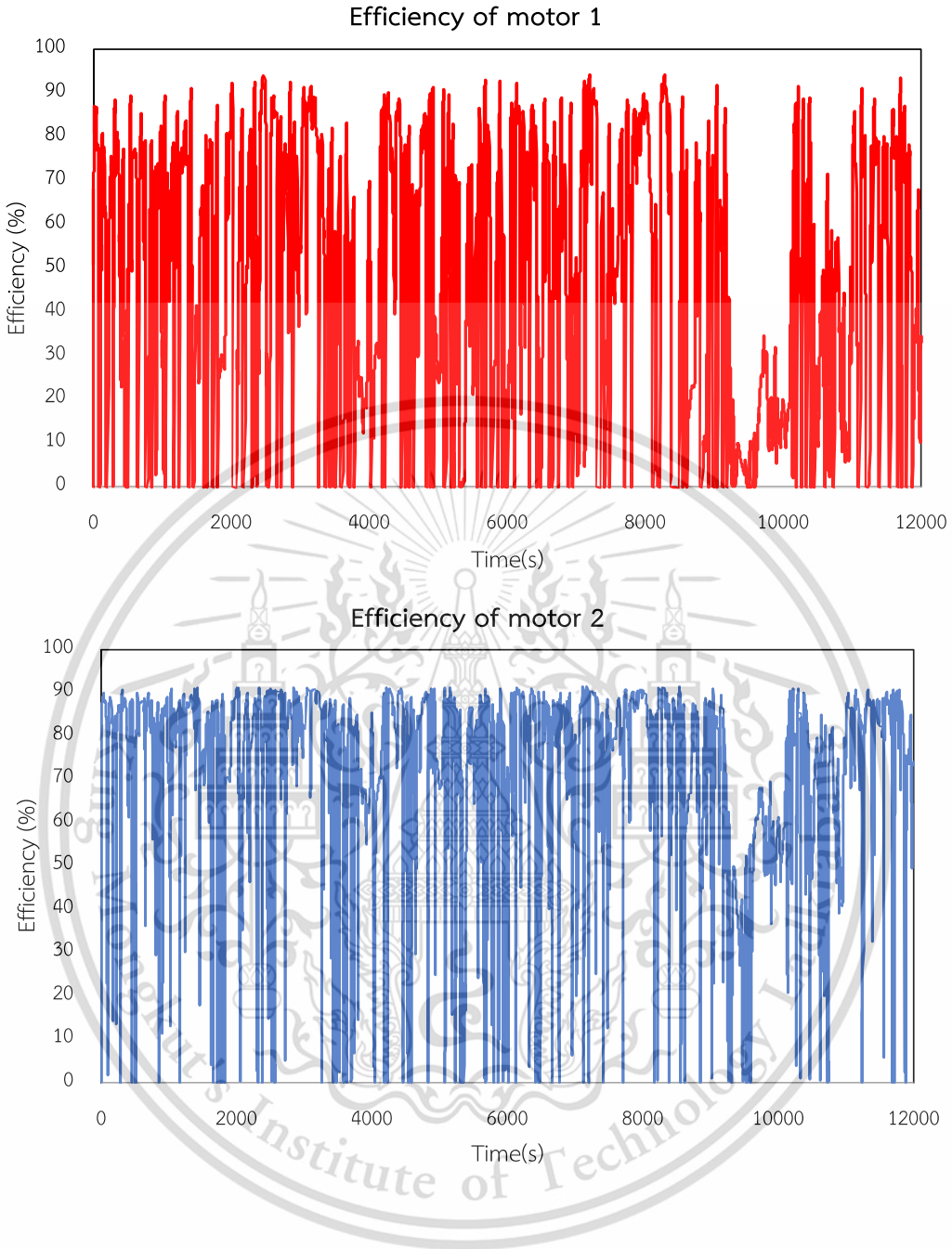

Figure 5.39 Efficiency for two different motors

5.5.3 Battery

This section focuses on the analysis of the performance characteristics of the batterypack of the electric bus when using different types of battery. Without changing the equipped 175kW permanent magnet electric motor and a fixed gear ratio, the two different types of Lithium ion batteries are compared the different results between them. In this study, lithium- iron phosphate (LFP) battery and lithium- nickel-manganese- cobalt-oxide (NMC) battery are selected as the energy sources. As the LFP battery, A123/ANR 26650M1Lithium ion battery with the capacity of 2300 mAh and 3.3 V is chosen and Panasonic NCR 18650PR with the nominal voltage of 3.6 V and 2700mAh is selected as NMC battery.

The LFP battery cells are connected in 152 cells in series and 260 cells in parallel. In the case of Panasonic battery cells battery consisting of battery cells, in which 138 cells connected in series and 222 cells connected in parallel. Table 5.2 contains the detailed information these two battery kinds.

Table 5.2 Details of two types of batterypack used

Specifications	Lithium- iron phosphate (LFP)	Lithium- nickel-manganese-cobalt- oxide(NMC)
Nominal Voltage (V)	3.3	3.6
Capacity (mAh)	2300	2700
No of series	152	138
No of parallel	260	222
Weight (g)/ cell	72	48
Weight (kg) (Whole pack)	2,845	1,471

In this simulation test, it is focused on how each battery responds to the desired speed profile of the model and how each battery discharge electric current without considering about the regenerative braking. The results without the regenerative braking are shown in figure 5.40 and 5.41. According to the results, both batteries

could deliver enough electric power for the bus to run the whole route. Also, the range of electric voltage of NMC runs between 455 and 484 V, for LFP battery will be around 476- 487V. NMC battery might discharge electric bus a little bit higher than the LFP when the bus demands high electric power Nevertheless, the electric voltage drawn by LFP battery is higher than that of NMC. In addition, when the behavior of SOC is looked into, the percentage of SOC in LFP after running the whole route is lower than that of NMC as shown in figure 5.41.

The electric power consumption of these two batterypack are also studied in this study. The results are tabulated in table 5.3. The simulation is performed in accordance with the regenerative braking criteria. Meanwhile, the electric power consumption of each type of batterypack for three levels of regenerative braking, 0%, 30% and 100%, are recorded . The results in table 5.3 shows the average consumption of the electric bus when powered by LFP battery and NMC battery for each percentage of regenerative braking. It is obvious that LFP battery has higher energy consumption than NMC battery. The fact is that the total weight for the whole batterypack in LFP is higher than that of NMC as presented in table 5.2. It requires more power to accelerate and maintain speed, as a result, power consumption becomes increased while carrying a heavier battery.

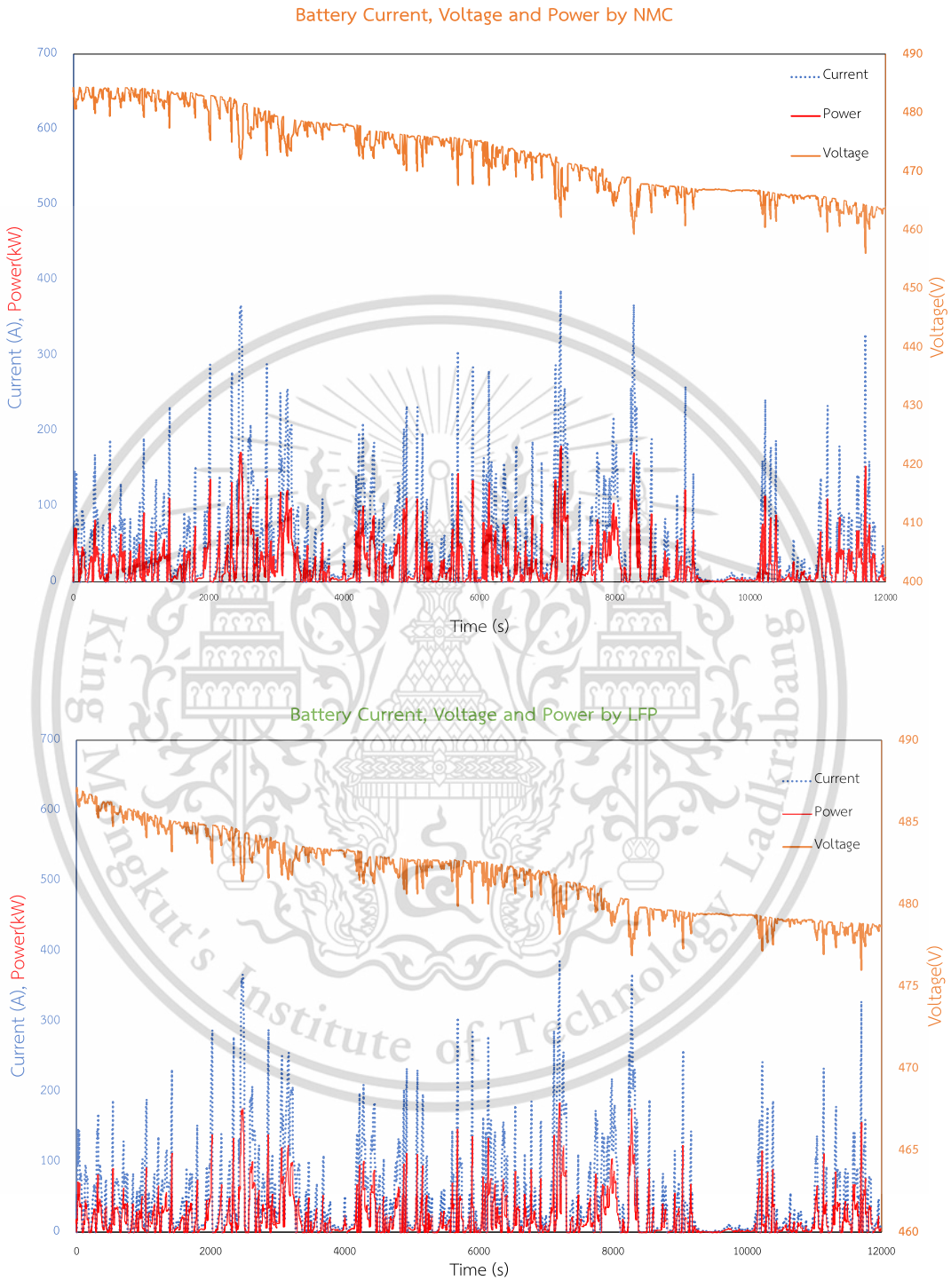

Figure 5.40 Battery current, voltage, and power of LFP and NMC battery

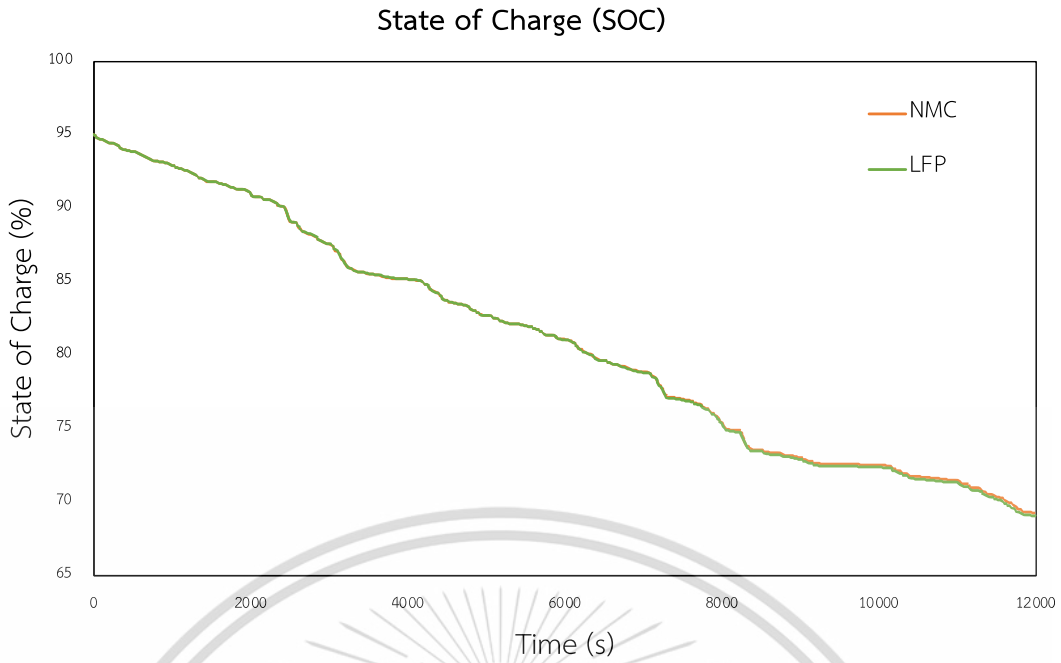

Figure 5.41 Comparison of SOC for two types of battery, LFP and NMC

Table 5.3 Results for electric power consumption by LFP and NMC

	LFP		NMC	
Levels of regenerative braking	Electrical energy (kWh)	Electric power consumption (kWh/km)	Electrical energy (kWh)	Electric power consumption (kWh/km)
0%	74.100	0.781	73.421	0.774
30%	69.784	0.736	69.113	0.728
100%	59.745	0.629	59.127	0.623

CHAPTER 6

CONCLUSION

This thesis has coped with the performance analysis of the electric bus's powertrain system on different kinds of factors and multiple design variables, considering for the slope the roadways. The required components for the powertrain of the selected electric bus are designed to meet with the requirements of the propulsion system. The suitable electric motor and batterypack are selected by calculation to use in the simulation model. The road test along the Samaedam bus depot and Samutprakan crocodile farm is performed using the bus line 142. From that road test, the raw data of geographic data of the roadways and speed profile of the bus are obtained. The speed profile represents the different conditions of the road test, including traffic jams, bus stops and other conditions. These processed data are used in the simulation test of the powertrain system under different scenarios.

The simulated test results under various designs of driving cycles, gear ratios, electric motors ,batterypack and percentages of regenerative braking are compared and displayed. According to the driving behaviors on RAMA IX bridge, the behaviors of power and its consumption are influenced by the rate of acceleration and deceleration. The power demand and its consumption are at its peak on the bride with the real driving cycle. When electricity power consumption is looked into the design variables of gear ratio and electric motor, power consumption varies according to the motor efficiency depending on the operational motor speed range. This fact applies not only for the different gear ratios and electric motor types. For the case of the different types of battery, LFP and NMC, LFP battery has higher power consumption than NMC because of the effect of its heavier weight. The analysis of the consumption for regenerative braking is concluded according to the uphill and downhill. In uphill, the bus requires high power consumption depending on the multiple factors. For downhill, the bus does not require much power, otherwise, it can get the power from the motor to recharge the battery, and also all power stays at negative, so, it results the reduction of power consumption.

As for the future works, the development of simulation model for this powertrain while considering for the additional loads of the electric bus, example, air conditions and other electrical accessories. This simulation model will help the electric bus's manufacturers to reveal the data of power management under different roadways.

REFERENCES

[1] “https://www.epa.gov/transportation-air-pollution-and-climate-change/history-reducing-air-pollution-transportation”.

[2] “https://vinfastauto.com/vn_en/benefits-and-barriers-to-full-implementation-of-electric-buses.”

[3] “https://www.transportation.gov/utc/transportation-air-pollution-and-public-health—are-we-doing-right-thing-and-doing-it-right.”

[4] A. Koch, O. Teichert, S. Kalt, A. Ongel, and M. Lienkamp, “Powertrain Optimization for Electric Buses under Optimal Energy-Efficient Driving,” *Energies (Basel)*, vol. 13, no. 23, p. 6451, Dec. 2020, doi: 10.3390/en13236451.

[5] O. A. Hjelkrem, K. Y. Lervåg, S. Babri, C. Lu, and C.-J. Södersten, “A battery electric bus energy consumption model for strategic purposes: Validation of a proposed model structure with data from bus fleets in China and Norway,” *Transp Res D Transp Environ*, vol. 94, p. 102804, May 2021, doi: 10.1016/j.trd.2021.102804.

[6] “https://corporate.enelx.com/en/stories/2022/02/advantages-of-electric-buses.”

[7] T. Boonraksa, P. Boonraksa, G. Sakulphaisan, and B. Marungsri, “Strategic Planning of Charging Stations for Electric Public Transportation Bus Systems: a Case Study,” *International Review of Electrical Engineering (IREE)*, vol. 15, no. 6, p. 512, Dec. 2020, doi: 10.15866/iree.v15i6.18764.

[8] *Bangkok Mass Transit Authority (BMTA). BMTA rehabilitation plan 2018. Bangkok; 2018.*

[9] *Bangkok Mass Transit Authority (BMTA). The suitability of the fuel system for buses of the Bangkok Mass Transit Authority. Bangkok; 2014.*

[10] “https://thainews.prd.go.th/en/news/detail/TCATG220722113833079.”

[11] “Department of Land Transport, BMTA rehabilation plan 2020, ministry of transport EV plan(2022-2037).”

[12] “EGAT receives model electric bus developed by Thais to support green public transport.”

[13] “https://www.thansettakij.com/technology/527105.”

[14] J. Larminie and J. Lowry, *Electric Vehicle Technology Explained*. Chichester, UK: John Wiley & Sons, Ltd, 2003. doi: 10.1002/0470090707.

[15] A. O. Kıyaklı and H. Solmaz, “Modeling of an Electric Vehicle with MATLAB/Simulink,” *International Journal of Automotive Science And Technology*, pp. 9–15, Jan. 2019, doi: 10.30939/ijastech..475477.

[16] C. Sunanda, “Modeling and Performance Analysis of an Electric Vehicle with MATLAB/Simulink,” *International Research Journal of Engineering and Technology*, p. 1098, 2008, [Online]. Available: www.irjet.net

[17] A. Karki, S. Phuyal, D. Tuladhar, S. Basnet, and B. Shrestha, “Status of Pure Electric Vehicle Power Train Technology and Future Prospects,” *Applied System Innovation*, vol. 3, no. 3, p. 35, Aug. 2020, doi: 10.3390/asi3030035.

[18] Z. Yang, F. Shang, I. P. Brown, and M. Krishnamurthy, “Comparative Study of Interior Permanent Magnet, Induction, and Switched Reluctance Motor Drives for EV and HEV Applications,” *IEEE Transactions on Transportation Electrification*, vol. 1, no. 3, pp. 245–254, Oct. 2015, doi: 10.1109/TTE.2015.2470092.

[19] W. Cai, X. Wu, M. Zhou, Y. Liang, and Y. Wang, “Review and Development of Electric Motor Systems and Electric Powertrains for New Energy Vehicles,” *Automotive Innovation*, vol. 4, no. 1, pp. 3–22, Feb. 2021, doi: 10.1007/s42154-021-00139-z.

[20] Z. Yang, F. Shang, I. P. Brown, and M. Krishnamurthy, "Comparative Study of Interior Permanent Magnet, Induction, and Switched Reluctance Motor Drives for EV and HEV Applications," *IEEE Transactions on Transportation Electrification*, vol. 1, no. 3, pp. 245–254, Oct. 2015, doi: 10.1109/TTE.2015.2470092.

[21] T. Finken and K. Hameyer, "Design of Electric Motors for Hybrid-and Electric-Vehicle Applications."

[22] M. Ehsani, Yimin Gao, and S. Gay, "Characterization of electric motor drives for traction applications," in *IECON'03. 29th Annual Conference of the IEEE Industrial Electronics Society (IEEE Cat. No.03CH37468)*, pp. 891–896. doi: 10.1109/IECON.2003.1280101.

[23] Y. Gao, H. Maghbelli, M. Ehsani, G. Frazier, J. Kajs, and S. Bayne, "Investigation of Proper Motor Drive Characteristics for Military Vehicle Propulsion," Jun. 2003. doi: 10.4271/2003-01-2296.

[24] M. Ehsani, Y. Gao, S. E. Gay, and A. Emadi, "Modern Electric, Hybrid Electric, and Fuel Cell Vehicles: Fundamentals, Theory, and Design."

[25] "Plug-in electric vehicles Changing perceptions, hedging bets Accenture end-consumer survey on the electrification of private transport 2."

[26] Sandeep. Dhameja, *Electric vehicle battery systems*. Newnes, 2001.

[27] "Handbook Of Batteries 3rd Edition-2".

[28] B. Kampman, "Impacts of electric vehicles-Assessment of electric vehicle and battery technology, Delft." [Online]. Available: https://www.researchgate.net/publication/292744715

[29] S. S. Bhurse and A. A. Bhole, "A Review of Regenerative Braking in Electric Vehicles," in *2018 Internat2018 International Conference on Computation of Power, Energy, Information and Communication (ICCPEIC)ional conference on*

computation of power, energy, Information and Communication (ICCPEIC), Mar. 2018, pp. 363–367. doi: 10.1109/ICCPEIC.2018.8525157.

[30] Xiaohong Nian, Fei Peng, and Hang Zhang, "Regenerative Braking System of Electric Vehicle Driven by Brushless DC Motor," *IEEE Transactions on Industrial Electronics*, vol. 61, no. 10, pp. 5798–5808, Oct. 2014, doi: 10.1109/TIE.2014.2300059.

[31] G. Xu, W. Li, K. Xu, and Z. Song, "An Intelligent Regenerative Braking Strategy for Electric Vehicles," *Energies (Basel)*, vol. 4, no. 9, pp. 1461–1477, Sep. 2011, doi: 10.3390/en4091461.

[32] L. Li, X. Li, X. Wang, J. Song, K. He, and C. Li, "Analysis of downshift's improvement to energy efficiency of an electric vehicle during regenerative braking," *Appl Energy*, vol. 176, pp. 125–137, Aug. 2016, doi: 10.1016/j.apenergy.2016.05.042.

[33] K. Liu, T. Yamamoto, and T. Morikawa, "Impact of road gradient on energy consumption of electric vehicles," *Transp Res D Transp Environ*, vol. 54, pp. 74–81, Jul. 2017, doi: 10.1016/j.trd.2017.05.005.

[34] C. Lorf, R. F. Martínez-Botas, D. A. Howey, L. Lytton, and B. Cussons, "Comparative analysis of the energy consumption and CO2 emissions of 40 electric, plug-in hybrid electric, hybrid electric and internal combustion engine vehicles," *Transp Res D Transp Environ*, vol. 23, pp. 12–19, Aug. 2013, doi: 10.1016/j.trd.2013.03.004.

[35] G. de Filippo, V. Marano, and R. Sioshansi, "Simulation of an electric transportation system at The Ohio State University," *Appl Energy*, vol. 113, pp. 1686–1691, Jan. 2014, doi: 10.1016/j.apenergy.2013.09.011.

[36] M. Gallet, T. Massier, and T. Hamacher, "Estimation of the energy demand of electric buses based on real-world data for large-scale public transport

networks," *Appl Energy*, vol. 230, pp. 344–356, Nov. 2018, doi: 10.1016/j.apenergy.2018.08.086.

[37] Z. Qi, J. Yang, R. Jia, and F. Wang, "Investigating Real-World Energy Consumption of Electric Vehicles: A Case Study of Shanghai," *Procedia Comput Sci*, vol. 131, pp. 367–376, 2018, doi: 10.1016/j.procs.2018.04.176.

[38] N. Hinov, P. Punov, B. Gilev, and G. Vacheva, "Model-Based Estimation of Transmission Gear Ratio for Driving Energy Consumption of an EV," *Electronics (Basel)*, vol. 10, no. 13, p. 1530, Jun. 2021, doi: 10.3390/electronics10131530.

[39] T. Markel *et al.*, "ADVISOR: a systems analysis tool for advanced vehicle modeling," *J Power Sources*, vol. 110, no. 2, pp. 255–266, Aug. 2002, doi: 10.1016/S0378-7753(02)00189-1.

[40] J. Wang and H. A. Rakha, "Convex Fuel Consumption Model for Diesel and Hybrid Buses," *Transportation Research Record: Journal of the Transportation Research Board*, vol. 2647, no. 1, pp. 50–60, Jan. 2017, doi: 10.3141/2647-07.

[41] *Essential MATLAB for Engineers and Scientists*. Elsevier, 2017. doi: 10.1016/C2015-0-02182-7.

[42] P. Cicero-Fernândez, J. R. Long, and A. M. Winer, "Effects of Grades and Other Loads on On-Road Emissions of Hydrocarbons and Carbon Monoxide," *J Air Waste Manage Assoc*, vol. 47, no. 8, pp. 898–904, Aug. 1997, doi: 10.1080/10473289.1997.10464455.

[43] K. Zhang and H. C. Frey, "Road Grade Estimation for On-Road Vehicle Emissions Modeling Using Light Detection and Ranging Data," *J Air Waste Manage Assoc*, vol. 56, no. 6, pp. 777–788, Jun. 2006, doi: 10.1080/10473289.2006.10464500.

[44] K. Zhang and H. C. Frey, "Road Grade Estimation for On-Road Vehicle Emissions Modeling Using Light Detection and Ranging Data," *J Air Waste Manage Assoc*, vol. 56, no. 6, pp. 777–788, Jun. 2006, doi: 10.1080/10473289.2006.10464500.

[45] L. Raykin, M. J. Roorda, and H. L. MacLean, “Impacts of driving patterns on tank-to-wheel energy use of plug-in hybrid electric vehicles,” *Transp Res D Transp Environ*, vol. 17, no. 3, pp. 243–250, May 2012, doi: 10.1016/j.trd.2011.12.002.

[46] W. Vaz, A. K. R. Nandi, R. G. Landers, and U. O. Koylu, “Electric vehicle range prediction for constant speed trip using multi-objective optimization,” *J Power Sources*, vol. 275, pp. 435–446, Feb. 2015, doi: 10.1016/j.jpowsour.2014.11.043.

[47] W. Vaz, A. K. R. Nandi, R. G. Landers, and U. O. Koylu, “Electric vehicle range prediction for constant speed trip using multi-objective optimization,” *J Power Sources*, vol. 275, pp. 435–446, Feb. 2015, doi: 10.1016/j.jpowsour.2014.11.043.

[48] K. Liu, J. Wang, T. Yamamoto, and T. Morikawa, “Exploring the interactive effects of ambient temperature and vehicle auxiliary loads on electric vehicle energy consumption,” *Appl Energy*, vol. 227, pp. 324–331, Oct. 2018, doi: 10.1016/j.apenergy.2017.08.074.

[49] S. C. Burgess and J. M. J. Choi, “A parametric study of the energy demands of car transportation: a case study of two competing commuter routes in the UK,” *Transp Res D Transp Environ*, vol. 8, no. 1, pp. 21–36, Jan. 2003, doi: 10.1016/S1361-9209(02)00016-0.

[50] N. Javani, I. Dincer, and G. F. Naterer, “Thermodynamic analysis of waste heat recovery for cooling systems in hybrid and electric vehicles,” *Energy*, vol. 46, no. 1, pp. 109–116, Oct. 2012, doi: 10.1016/j.energy.2012.02.027.

[51] K. R. Kambly and T. H. Bradley, “Estimating the HVAC energy consumption of plug-in electric vehicles,” *J Power Sources*, vol. 259, pp. 117–124, Aug. 2014, doi: 10.1016/j.jpowsour.2014.02.033.

[52] R. Zhang and E. Yao, “Electric vehicles’ energy consumption estimation with real driving condition data,” *Transp Res D Transp Environ*, vol. 41, pp. 177–187, Dec. 2015, doi: 10.1016/j.trd.2015.10.010.

[53] M. Juhala, “Improving vehicle rolling resistance and aerodynamics,” in *Alternative Fuels and Advanced Vehicle Technologies for Improved Environmental Performance*, Elsevier, 2014, pp. 462–475. doi: 10.1533/9780857097422.2.462.

[54] D. Hasen, S. Elangovan, M. Sundararaj, and K. M. Parammasivam, “CFD Analysis of Aerodynamic Drag Reduction in Heavy Vehicles by Changing its Frontal Area: Techinical Note,” *International Journal of Vehicle Structures and Systems*, vol. 11, no. 5, Dec. 2019, doi: 10.4273/ijvss.11.5.10.

[55] H. Abdelaty and M. Mohamed, “Uncertainty in Electric Bus Energy Consumption: The Impacts of Grade and Driving Behaviour The Social Costs and Benefits of Electric Mobility in Canada View project A Systemic Assessment and Optimization of Hamilton Street Railway (HSR) Network View project.” [Online]. Available: https://www.researchgate.net/publication/344693197

[56] H. Abdelaty and M. Mohamed, “Uncertainty in Electric Bus Energy Consumption: The Impacts of Grade and Driving Behaviour The Social Costs and Benefits of Electric Mobility in Canada View project A Systemic Assessment and Optimization of Hamilton Street Railway (HSR) Network View project.” [Online]. Available: https://www.researchgate.net/publication/344693197

[57] J. Huertas, M. Giraldo, L. Quirama, and J. Díaz, “Driving Cycles Based on Fuel Consumption,” *Energies (Basel)*, vol. 11, no. 11, p. 3064, Nov. 2018, doi: 10.3390/en11113064.

[58] O. Travesset-Baro, M. Rosas-Casals, and E. Jover, “Transport energy consumption in mountainous roads. A comparative case study for internal combustion engines and electric vehicles in Andorra,” *Transp Res D Transp Environ*, vol. 34, pp. 16–26, Jan. 2015, doi: 10.1016/j.trd.2014.09.006.

[59] D. Arellano, T. Echaveguren, and S. Vargas-Tejeda, “A model of truck speed profiles on short upward slopes,” *Proceedings of the ICE - Transport*, vol. 168, no. 5, pp. 475–483, Oct. 2015, doi: 10.1680/tran.13.00012.

[60] L. Y. Phyo, N. Depaiwa, M. Yamakita, B. Kerdsup, and M. Masomtob, “Impact of Driving Behavior on Power Consumption of Electric Bus: A Case Study on Rama IX Bridge,” in *2022 International Electrical Engineering Congress (iEECON)*, Mar. 2022, pp. 1–4. doi: 10.1109/iEECON53204.2022.9741622.

[61] T. J. BARLOW, S. LATHAM, I. S. MCCRAE, and P. G. BOULTER, “a reference book of driving cycles for use in the measurement of road vehicle emissions,” no. 0968–4093, 2009.

[62] D. Chindamo and M. Gadola, “What is the Most Representative Standard Driving Cycle to Estimate Diesel Emissions of a Light Commercial Vehicle?,” *IFAC-PapersOnLine*, vol. 51, no. 5, pp. 73–78, 2018, doi: 10.1016/j.ifacol.2018.06.213.

[63] “https://www.car-engineer.com/the-different-driving-cycles/.”

[64] “VBOX Sport Guide,” 2014.

APPENDIX A

CONFERENCE PARTICIPATION AND CERTIFICATE

*i*EECON2022

Rajamangala University of Technology Isan, Khon Kaen Campus and Chiang Mai University, Thailand

This certificate is awarded to

Lwin Yamon Phyo, Nattawoot Depaiwa, Burin Kerdsup, Manop Masomtob and Masaki Yamakita

for paper entitled:

Impact of Driving Behavior on Power Consumption of Electric Bus: A Case Study on Rama IX Bridge

presented at
2022 10th International Electrical Engineering Congress (iEECON2022)
9 - 11 March 2022, Khon Kaen, Thailand

Assoc. Prof. Dr. Athikom Roeksabutr President Electrical Engineering Academic Association (Thailand)	Assoc. Prof. Dr. Kidsanapong Puntsri General Chair	Assoc. Prof. Dr. Sermsak Uatrongjit Technical Program Committee

Paper ID: P01964

APPENDIX B

PUBLICATION

Impact of Driving Behavior on Power Consumption of Electric Bus: A Case Study on Rama IX Bridge

Lwin Yamon Phyo
Department of Mechanical Engineering, School of Engineering
King Mongut's Institute of Technology Ladkrabang
Bangkok, 10520, Thailand
63601192@kmitl.ac.th

Nattawoot Depaiwa
Department of Mechanical Engineering, School of Engineering
King *Mongut's Institute of Technology Ladkrabang*
Bangkok, 10520, Thailand
nattawoot.de@kmitl.ac.th

Masaki Yamakita
School of Engineering, Department of Systems and Control Engineering
Tokyo Tech Institute of Technology
Tokyo, 152-8552, Japan
yamakita @ctrl.titech.ac.jp

Burin Kerdsup
National Electronic and Computer Technology Center (NECTEC)
National Science and Technology Development Agency
Pathum Thani, 12120, Thailand
burin.kerdsup@nectec.or.th

Manop Masomtob
National Energy and Technology Center(ENTEC)
National Science and Technology Development Agency
Pathum Thai, 12120, Thailand
manop.mas@entec.or.th

***Abstract*— Recently, the influence of the bus transportation system in Thailand has become the most critical impact on our surroundings. Government of Thailand has initiated the projects to replace internal combustion engine buses with net zero-emission. However, there are the problems of power consumption in battery electric buses, especially on climbing resistance which is a major impact on the power demand and recuperation. This paper aims to investigate the impact of driving behavior on power consumption of electric buses. Many scenarios have been created to study such behavior. Also, driving across Rama IX bridge which is the critical scenario on the performance of electric buses in Thailand has been evaluated.**

***Keywords*—Power demand, Power consumption, Driving behavior, Road grade.**

I. Introduction

Bus is one of the most significant public transport systems in many cities that is essential for the daily life of most citizens. At present, it can be seen that diesel and compressed natural gas (CNG) have been dominated in Thailand bus transportation system. In order to reduce air pollution, the government of Thailand has recently proposed a strategy to gradually replace conventional buses with hybrid or battery electric buses [1]. All relevant policies and rules have been announced to Thai local car manufacturers for annual increase in production quantity. Most of the bus operators in Thailand are also trying to go with electric bus for the renewal of bus transportation system. Electric buses are driven by an electric motor having a batterypack as energy storage. Therefore, a larger batterypack is required to operate for the whole bus route. Another consideration is that buses are not always travelled on the flat road, they are also run on bridges, inclined, or declined the lane. As a result, the required power of mounting the incline will not be the same as that of running on flat road. Thai electric bus manufacturers are now facing with difficulties in controlling the increased demand for power and reducing its power consumption while operating on sloping areas.

There are many major factors which influence on the performance of the electric buses such as length of the driving cycle [2], weather and temperature [3], driving style [4], wind exposure, traffic conditions [5] and the use of air conditioning or heater [6]. Moreover, a speed limit of the bus, several bus stops per distance [7-9], bus parameters such as total weight of the bus including other components of the bus [10] are the dominant factors on its power consumption. For the consideration of road topology, the consumed energy of battery electric buses with and without road gradient is calculated for each driving cycle, including the driving behavior of the drivers in accelerating and decelerating-normal driving style and aggressive driving style. It has been approved that higher road gradient leading to consume more energy is directly affected by the driving performance, especially in aggressive style [11].

In case of accounting the impact of road gradients, it has been found that the energy consumption of the electric vehicle can be minimized in downward grading [12]. The reason is that drivers hit the brake pedal more frequently during downgrading than upgrading which might lead to an increase in energy consumption. A regenerative braking system that has used to generate the energy back to the batterypack has been essentially built for both plug-in hybrid and battery electric vehicles to reduce the energy consumption of the entire bus. Lower- level electric energy consumption and emissions can be induced due to electric regenerative braking system, but it must be noticed that there are still some limitations to model recuperated energy [13].

This paper mainly focuses on evaluating the simulated results of the demanding power and its consumption based on the major influencing factors, such as driving behavior and traffic congestion when the electric bus crosses on the RAMA IX bridge. It also intends to assess how the characteristics of electric buses affect power demand when regenerative braking has been applied during the downgrading performance.

In general, the paper is outlined regarding to the upcoming sections. Section II points out the theoretical formulation of the model and explains about various scenarios for the model simulation. The simulation results of each scenario are presented in section III, where it also

978-1-6654-0206-4/22/$31.00 ©2022 IEEE

evaluates and discuses about these results. In section IV, some conclusion remarks are finalized.

II. Methodology

A MATLAB/ Simulink model has been developed for simulating power consumption of the bus based on the characteristic routes of RAMA IX bridge. The used route in the model is RAMA IX bridge across Chao Pharya River connecting Thonburi and Bangkok. The measured data of altitude and slope profile over distance for Rama IX bridge, which has been recorded using GPS VBOX tool, is presented in Fig.1.

To specify the initial conditions of the model, the input from the driving situations and speed profile of the bus is added as the components of the model. The specific parameters of the studied electric bus are mentioned in Table 1. This section presents the vehicle dynamic model considering the grade, and different scenarios which relate to the power consumption of electric buses.

A. Vehicle Dynamic Modeling

Vehicle Specific Power (VSP) equation is used for representing the behavioral characterization of the bus and evaluating the power consumption. The tractive force required by the wheels to propel the bus F_{tr} is evaluated based on the resistive forces acting on it. Resistive force, called force opposing the bus motion, is defined as the total of rolling resistance F_{rr}, aerodynamic resistance F_{aero}, hill climbing resistance F_{grade}, and inertial resistance F_a as shown in (1). In this model, hill climbing resistance is not zero owing to the consideration of gradients for upgrading and downgrading.

$$F_{tr}=F_{rr}+F_{aero}+F_{grade}+F_a \quad (1)$$

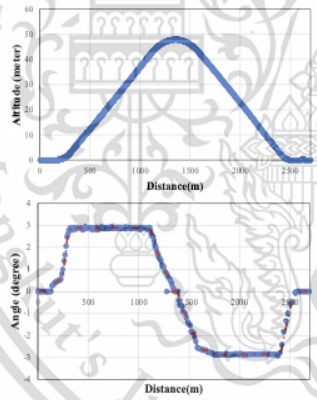

Fig. 1. Altitude and slope profile of Rama IX bridge

TABLE I: SPECIFICATIONS OF ELECTRIC BUS

Parameters	Abbreviations	Values
Mass of the bus	m_v	18,500 kg
Frontal Area	A_v	8.1 m^2
Density of air	ρ	1.23 kg/m^3
Coefficient of drag force	C_d	0.5
Coefficient of rolling resistance	C_r	0.01
Wheel Diameter	D_w	1.064 m

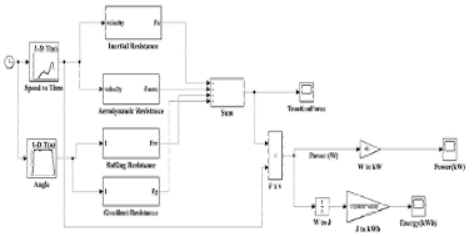

Fig. 2. Electric bus model with Simulink

Taking into the calculated tractive force F_{tr} and the bus velocity v_{wheel} , power at the wheels of the bus P_{wheel} can be computed in (2).

$$P_{wheel}=F_{tr}*v_{wheel} \quad (2)$$

By integrating the power P_{wheel} over time, energy of the bus $E_{wheel,J}$ can be calculated in (3)

$$E_{wheel,J}=\int P_{wheel}*dt \quad (3)$$

Then, the average power consumption of electric buses can be calculated by dividing energy (E_{kWh}) by the total route length. Vehicle dynamic simulation model for the bus is presented in Fig.2.

B. Model Scenarios Development

The designated route can be set in numerous scenarios, standing on different factors such as traffic jam, driving style and variable speed. The main target for applying different scenarios is to evaluate the discrepancy in power demand and its consumption to analyze the various driving behaviors. In this case, three scenarios have been assessed for determining the power consumption of the electric bus.

Scenario 1: Constant Speed: Power demand and consumption have been studied over different cruising speeds.

Scenario 2: Speed Reduction: It can be categorized into two types of speed range for a uniform gradient level. While descending the bus without fading the brake, it normally accelerates to its maximum speed, and maintains the speed until it reaches the bottom of the slope. Moreover, the speed at the beginning of the uphill slope progressively drops to a minimal constant speed, which it maintains until arriving the peak of the slope. Two regions are separated for speed profiles- accelerating or decelerating region and constant region where acceleration or deceleration becomes zero. These two regions are clearly shown in Fig.3. L_{Up} stands for the length of the decelerating region on upward slope and L_D is the length of the accelerating region for downward slope.

This case has been explored for variable speeds with the same length of the decelerating region (L_{Up}). The bus starts ascending the slope at high speed and, after passing the bottom of the slope, speed gradually decreases throughout the distance travelled and it begins to slow down. This speed shift occurs in the deceleration region, and it maintains a constant speed throughout the rest of the route. The evaluation has conducted by varying the speed range.

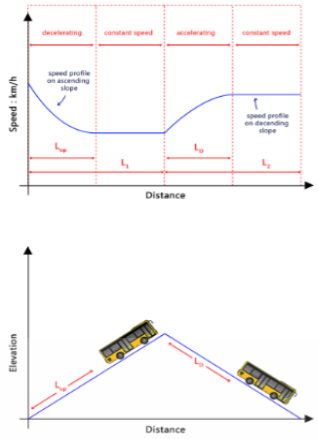

Fig. 3. Bus speed profiles on the slope

Scenario 3: Go and Stop: It deals with traffic congestion on the roadway uphill and downhill grades. This scenario involves many acceleration and deceleration processes recognizing multiple acceleration levels. Actual speed data collected on Rama IX bridge has been used in this scenario. Thus, acceleration or deceleration levels vary according to the driver's behavior. Additionally, to recover the power of the electric bus on decelerating or downgrading, the regenerative braking has been minded for this scenario.

III. RESULTS AND DISCUSSION

The comparison results for each three scenarios that are calculated using the MATLAB/Simulink model are described in the following sections.

Scenario 1: The simulated model was used for the values of speed between 5 and 90 km/h. Each step is increased by 5 km/h for the uniform elevation level with the same distance. Fig. 4 shows the amount of power consumption which is varied with speed. More and more power are consumed in a shorter time while covering the same distance traveled as the bus goes faster. According to Table 2, due to the effect of wind resistance, the value of the demanded power rises with increasing speed.

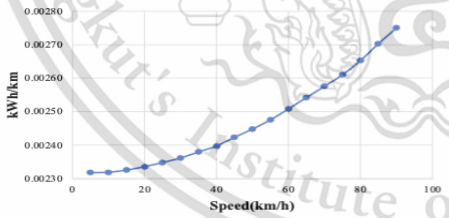

Fig. 4. Power consumption over various cruising speeds

TABLE II: POWER DEMAND ON DIFFERENT SPEEDS

Speed (km/h)	Power (kW)	Speed (km/h)	Power (kW)
5	15.23	65	212.60
20	61.33	80	270.95
40	125.23	90	312.99

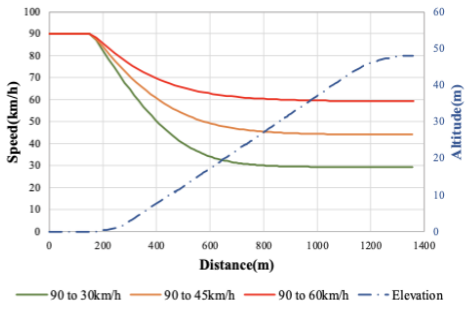

Fig. 5. Speed profiles over distance on three types of speed variations

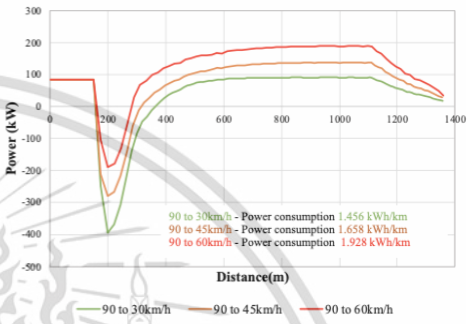

Fig. 6 . Power demand over distance for three speed variations

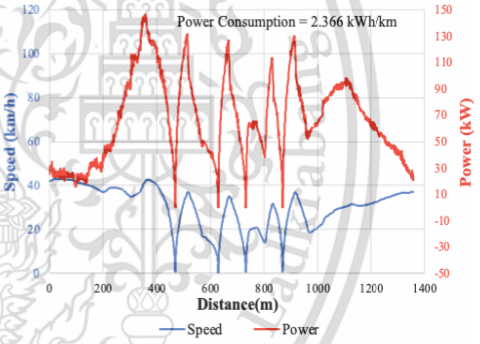

Fig. 7. Speed profile and power demand on upgrading

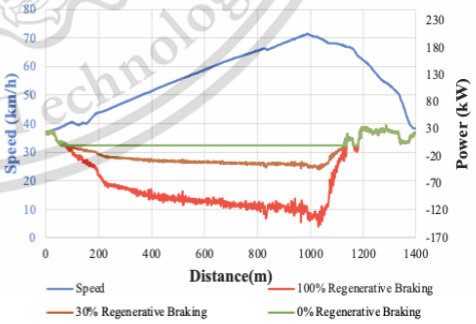

Fig. 8. Speed profile and power demand on downgrading

Scenario 2: For this scenario, three driving cycles with different driving styles are built for variable speeds with the same length of decelerating zone (L_{Up}). The power demand of the electric bus and its consumption have been explored by setting the speed variations of 90 to 30 km/h, 90 to 45 km/h and 90 to 60 km/h. Fig. 5 indicates the three speed variation profiles and Fig.6 describes the result of power demand per unit distance for each speed variation. In accordance with the results, it can be seen that power demand is negative and recuperates as long as the speed range difference becomes larger. Because of the high speed variation in 90 to 30 km/h, the deceleration rate is faster than the other two speed variations, 90 to 45 km/h and 90 to 60 km/h. The power recovery during deceleration is much higher than the power demand in 90 to 30 km/h. Apart from that, when the speed variation decreases, the power demand trend is positive. Therefore, the power demand is much greater than power recuperation in 90 to 60 km/h. Besides, the power consumption per unit distance travelled does not proportionally increase even when running at high speeds. However, while running at a high speed, the deceleration time is shorter, and the power consumption has been increased. For that reason, the power is consumed 1.928 kWh/km in 90 to 60 km/h more than the others.

Scenario 3: The behavior of electric bus is evaluated under the go-and-stop conditions for dealing with traffic congestion on uphill and downhill roadway. The data used in this scenario is real speed data recorded on the RAMA IX bridge in every second. In real traffic conditions, the speed profiles are fluctuated by many reasons such as frequent stops, accelerations, decelerations and driving behavior of the drivers. The recorded speed profiles are as shown in Fig. 7 and Fig. 8. Fig. 7 and Fig. 8 illustrate the speed profile of upgrading and downgrading respectively. Fig. 7 also describes the vehicle power demand when the bus goes for upgrading. The power value is positive when the bus requires thrust on accelerating. Otherwise, the value of the power decreases when the speed of the bus decelerates. Power consumption rate is recorded as 2.366 kWh/km with 1.36 km, average speed at 20 km/h and maximum speed at 42.94 km/h.

Since the electric bus goes for downhill, the resulting power demand stays at a negative gradient, which equates to power recuperation. The value of power recuperation with and without regenerative is shown in Fig. 8. When the acceleration pedal is not pressed, the regenerative braking feature automatically engages, allowing inertia of the bus to be converted into electrical energy and went back to the battery. In such case, the percentage of regenerative braking is set to a total amount of 0% and 30% of the power recuperation. It can be observed that no power is delivered back to the battery with 0% regenerative braking. Without regenerative braking, it's the same as regenerative braking at 100%, and all negative power is returned to the battery.

IV. CONCLUSION

Based on different driving behaviors, three scenarios have been investigated the impact of power consumption of the electric bus. According to these scenarios, the following results can be discovered from the simulations. The higher the speed of the bus is, the larger the power demand is. However, the power consumption relies not only on the speed, but also on accelerating and decelerating rates based on changing the travelling time. When the bus decelerates faster or goes downhill, the power demand moves to negative value which recuperates the energy back to the battery. It has been found that the consumed power is higher in traffic congestion conditions than the other cases. Moreover, the power consumption by varying the different lengths of the speed region (L_{Up}) has been evaluated as explained.

ACKNOWLEDGMENT

The author would like to thank the National Energy and Technology Center, National Science and Technology Development Agency for research funding.

REFERENCES

[1] "Pollution Control Department Booklet on Thailand State of Pollution 2018," Bangkok, 2019.

[2] W. Vaz, A. Nandi, R. Landers and U. Koylu, "Electric vehicle range prediction for constant speed trip using muti-objective optimization," Journal of Power Sources 275, pp. 435- 446, 2015.

[3] K. Liu, J. Wang, T. Yamamoto and T. Morikawa, "Exploring the interactive effects of ambient temperature and vehicle auxiliary loads on electric vehicle energy consumption," Applied Energy, vol. 227, pp. 324-331, 2018.

[4] MC.Coelho and M. Luzia, "Evaluating the energy performance of a SUV hybrid electric vehicle," Transport Research Part D: Transport and Environment, vol. 15, pp. 443-450, 2010.

[5] S. Burgess and J. Choi, "A parametric study of the energy demands of car transportation: a case study of two competing commuter routes in the UK," Transportation Research Part D: Transport and Environment, vol. 8, no. 1, pp. 21-36, 2003.

[6] K. Kambly and T. Bradley, "Estimating the HVAC energy consumption of plug-in electric vehicles," Journal of Power Sources, vol. 259, pp. 117-124, 2014.

[7] M. Gallet, T. Massier and T. Hamacher, "Estimation of the energy demand of electric buses based on real- world data for large-scale public transport networks," Applied Energy, vol. 230, pp. 344-356, 2018.

[8] K. Kivekas, J. Vepsalainen, K. Tammi and J. Anttila, "Influence of driving cycle uncertainty on electric bus energy consumption," in IEEE Vehicle Power and Propulsion Conference (VPPC), 2017.

[9] J.Vepsalainen, K. Kivekas, K. Otto, A. Lajunen and K. Tammi, "Development and validation of energy demand uncertainty model for electric city buses," Transportation Research Part D: Transport and Environment, vol. 63, pp. 347-361, 2018.

[10] R. Zhang and E. Yao, "Electric vehicles'enerfy consumption estimation with real driving condition data," Transportation Research Part D: Transport and Environment, vol. 41, pp. 177-187, 2015.

[11] H. Abdelaty and M. Mohamed, "Uncertainty in electric bus energy consumption: the impacts of grade and driving behaviour," in Proceedings of the 55th annual Canadian Transportation Research Forum, Montreal QC, 2020.

[12] K. Genikomsakis and G. Mitrentsis, "A computationally efficient simulation model for estimating energy consumption of electric vehicles in the context of route planning applications," Transport Research Part D: Transport and Environment, vol. 50, pp. 98- 118, 2017.

[13] C. Lorf, R. Martinez-Botas, L. Lytton and B. Cussons, "Comparative analysis of the energy consumption and CO2 emissions of 40 electric, plug-in hybrid electric, hybrid electric and internal combustion engine vehicles," Transportation Research Part D: Transport and Environment, vol. 23, pp. 12-19, 2013.

CURICULUM VITAE

NAME	Ms. Lwin Yamon Phyo
DATE OF BIRTH	30 July, 1997

EDUCATION RECORD

BACHELOR'S DEGREE	Bachelor of Engineering (Mechatronics) Yangon Technological University, Myanmar, 2020
MASTER'S DEGREE	Master of Engineering (Automotive and Advanced Transportation Engineering) King Mongkut's University of Technology, Ladkrabang, 2023
SCHOLARSHIP	TAIST-Tokyo Tech scholarship Master's Degree in Automotive and Advanced Transportation Engineering 2020-2023 Founded by National Science and Technology Development Agency (NSTDA, Thailand), Tokyo Institute of Technology (Tokyo-Tech, Japan) and King Mongkut's University of Technology Ladkrabang (KMITL, Thailand)
EMPOLYMENT RECORD	Service Advisor Toyota Taw Win, 2019-2020

PUBLICATION

International Conference Proceeding	Phyo, L. Y., Depaiwa, N., Yamakita, M., Kerdsup, B., & Masomtob, M. (2022, March). Impact of Driving Behavior on Power Consumption of Electric Bus: A Case Study on Rama IX Bridge. In *2022 International Electrical Engineering Congress (iEECON)* (pp. 1-4). IEEE.